1-1-2016

Molecular and Cellular Approaches Toward Understanding Dynein-Driven Motility

Swathi Ayloo
University of Pennsylvania, sayloo@sas.upenn.edu

Molecular and Cellular Approaches Toward Understanding Dynein-Driven Motility

Abstract
Active transport is integral to organelle localization and their distribution within the cell. Kinesins, myosins and dynein are the molecular motors that drive this long range transport on the actin and microtubule cytoskeleton. Although several families of kinesins and myosins have evolved, there is only one form of cytoplasmic dynein driving active retrograde transport in cells. While dynactin is an essential co-factor for most cellular functions of dynein, the mechanistic basis for this evolutionarily well conserved interaction remains unclear. Here, I use single molecule approaches with purified dynein to reconstitute processes in vitro, and implement an optogenetic tool in neurons to further dissect regulatory mechanisms of dynein-driven transport in cells. I demonstrate for the first time, at the single molecule level, that dynactin functions as a tether to enhance the initial recruitment of dynein onto microtubules but also acts as a brake to slow the motor. I then extend this work in neurons to understand regulation of the dynein motor at the cellular level. Neurons are particulary dependent on long-range transport as organelles and macromolecules must be efficiently moved over the extended length of the axon and further, have mechanisms in place for the compartment-specific regulation of trafficking in axons and dendrites. I use a light-inducible dimerization tool to recruit motor proteins or motor adaptors to organelles in real time to examine downstream effects of organelle motility and compartment-specific regulation of motors. I find that while dynein works efficiently in both axons and dendrites, kinesins are differentially regulated in a compartment-specific manner. I further demonstrate that dynein-driven motility in neurons is largely governed by microtubule orientation and requires microtubule dynamics for efficient navigation in axons and dendrites. Together, this work sheds light on the molecular and cellular mechanisms of dynein function both in vitro and in vivo using a combination of approaches. My findings converge to a model wherein dynactin enhances the recruitment of dynein onto microtubule plus ends, leading to efficient minus-end directed motility of dynein. This becomes especially critical in neuronal growth cones and dendrites owing to the large number of highly dynamic microtubules in these compartments.

Degree Type
Dissertation

Degree Name
Doctor of Philosophy (PhD)

Graduate Group
Biology

First Advisor
Erika L. Holzbaur

Subject Categories
Biophysics | Cell Biology | Molecular Biology

MOLECULAR AND CELLULAR APPROACHES TOWARD UNDERSTANDING DYNEIN-DRIVEN MOTILITY

Swathi Ayloo

A DISSERTATION

in

Biology

Presented to the Faculties of the University of Pennsylvania

In Partial Fulfillment of the Requirements for the

Degree of Doctor of Philosophy

2016

Supervisor of Dissertation

_____

Erika L.F. Holzbaur, PhD, Professor of Physiology

Graduate Group Chairperson

_____

Michael A. Lampson, PhD, Associate Professor of Biology

Dissertation Committee

Erfei Bi, PhD, Professor of Cell and Developmental Biology

E. Michael Ostap, PhD, Professor of Physiology

Tatyana Svitkina, PhD, Professor of Biology

Michael A. Lampson, PhD, Associate Professor of Biology

MOLECULAR AND CELLULAR APPROACHES TOWARD UNDERSTANDING DYNEIN-DRIVEN MOTILITY

ACKNOWLEDGMENT

This work would not have been possible without the support and help from several people. I would first like to acknowledge my advisor, Erika Holzbaur for her wonderful mentorship. She has always held me to high standards and constantly challenged me to think deeply about my science. She has always encouraged me and I greatly appreciate all the opportunities she provided me with, ensuring my success. Thank you, Erika, for your faith in me and teaching me several things throughout my graduate training. I would also like to thank my thesis committee members: Erfei Bi, Mike Ostap, Tanya Svitkina and Mike Lampson for their insights and advice. Special thanks to Mike Ostap and Mike Lampson for terrific collaborations on both my projects. Both of them were instrumental in providing key reagents and scientific advice which made this thesis work possible.

I would especially like to thank all the past and current members of the Holzbaur lab: Mariko Tokito for making DNA constructs and for all the endless conversations she had with me about protein purification and several other biochemical assays; Karen Wallace for her assistance with mouse work; Adam Hendricks who first introduced me to single molecule assays and was my go-to person for all things biophysics; Meredith Wilson, Betsy McIntosh, Alison Twelvetrees, Amy Ghiretti, Mara Olenick and Eva Klinman for their friendship and for putting up with several of my random bouts of craziness.

Special thanks to Sandra Maday who has been a great friend and has made this journey a lot more fun. I have learned so much from Sandy about data analysis, giving talks and scientific writing. Besides the scientific stuff, I thoroughly enjoyed our late-night working sessions motivating each other, hour-long conversations about random things, sometimes even as late as 3 am and more recently our tea breaks. Thank you Sandy for being there for me through everything and I will truly miss you.

I would also like to thank Aditya Dodda and Ed Ballister for their fantastic collaborations. Aditya spent several hours and days looking at my data to develop new ways to analyze it. What started out with Aditya fixing errors in the basic code I wrote, turned into him developing new algorithms and simulations for my data. Ed Ballister developed the light-inducible dimerization system and was the first one to think about applying it to motors. Working with him was a lot of fun and without him, my second project would never exist.

I would also like to acknowledge the Pennsylvania Muscle Institute (PMI) at Penn, especially Mike Ostap, Yale Goldman, Katya Grishchuck and their lab members. Being part of the PMI gave me access to several key resources and opportunities. I always enjoyed our journal clubs and learned how to think about science through these meetings. The PMI community made me feel at home and inculcated a sense of belonging in me.

Big thanks to all my friends in Boston who was my family away from home. Needless to say, I am quite excited to be surrounded by them the next few years. Their friendship through the years, since my undergrad days has been invaluable. I had a lot of fun with you guys!

I am grateful to all my family members – parents, uncle and aunt, my siblings and my cousins. They were always there for me and made everything possible for me. I would not be where I am today without them. Thank you for believing in me and giving me the freedom to pursue what I wanted.

Finally, I would like to thank Rama, my strength and my pillar of support.

ABSTRACT

MOLECULAR AND CELLULAR APPROACHES TOWARD UNDERSTANDING DYNEIN-DRIVEN MOTILITY

Swathi Ayloo

Erika L.F. Holzbaur

Active transport is integral to organelle localization and their distribution within the cell. Kinesins, myosins and dynein are the molecular motors that drive this long range transport on the actin and microtubule cytoskeleton. Although several families of kinesins and myosins have evolved, there is only one form of cytoplasmic dynein driving active retrograde transport in cells. While dynactin is an essential co-factor for most cellular functions of dynein, the mechanistic basis for this evolutionarily well conserved interaction remains unclear. Here, I use single molecule approaches with purified dynein to reconstitute processes *in vitro*, and implement an optogenetic tool in neurons to further dissect regulatory mechanisms of dynein-driven transport in cells. I demonstrate for the first time, at the single molecule level, that dynactin functions as a tether to enhance the initial recruitment of dynein onto microtubules but also acts as a brake to slow the motor. I then extend this work in neurons to understand regulation of the dynein motor at the cellular level. Neurons are particulary dependent on long-range transport as organelles and macromolecules must be efficiently moved over the extended length of the axon and further, have mechanisms in place for the compartment-specific regulation of trafficking in axons and dendrites. I use a light-inducible dimerization tool to recruit motor proteins or motor adaptors to organelles in real time to examine downstream effects of organelle motility and compartment-specific regulation of motors. I find that while dynein works efficiently in both axons and dendrites,

kinesins are differentially regulated in a compartment-specific manner. I further demonstrate that dynein-driven motility in neurons is largely governed by microtubule orientation and requires microtubule dynamics for efficient navigation in axons and dendrites. Together, this work sheds light on the molecular and cellular mechanisms of dynein function both *in vitro* and *in vivo* using a combination of approaches. My findings converge to a model wherein dynactin enhances the recruitment of dynein onto microtubule plus ends, leading to efficient minus-end directed motility of dynein. This becomes especially critical in neuronal growth cones and dendrites owing to the large number of highly dynamic microtubules in these compartments.

TABLE OF CONTENTS

LIST OF FIGURES

CHAPTER 1: Introduction

I. Intracellular Transport – An Introduction

Cellular organization of macromolecules and organelles in space and time is critical for cellular function. Accurate localization of organelles is often achieved by the process of intracellular transport. Initial experiments by George Palade and colleagues in pancreatic exocrine cells, professional secretory cells, laid the foundation for intracellular transport. This work included pulse-chase experiments *in vivo* (Caro and Palade, 1964) followed by pulse-chase in *in vitro* tissue slices (Jamieson and Palade, 1967a, 1967b) which demonstrated that proteins shuttled from one compartment to another. These experiments also showed that intracellular transport requires energy, as absence of ATP synthesis caused proteins to remain in the endoplasmic reticulum (Jamieson and Palade, 1968), an intriguing finding at the time. Evidence from electron microscopy and other studies in the next few years suggested that the protein transport occurred via vesicular trafficking (Palade, 1975). The discovery of clathrin (Pearse, 1976) followed by elegant work with cell-free systems (Freis and Rothman, 1980) and yeast genetics quickly established the players involved in the secretory trafficking pathway (reviewed in Rothman, 1994).

Although initial work using anti-mitotic agents like colchicine indicated a role for microtubules in intracellular transport (Williams and Wolff, 1972; LeMerchand et al., 1973), it was not until the 1980s, that the evidence for this was fully established (reviewed in section II of this chapter). Following this, molecular motors were discovered (reviewed in section III and IV) which explained the previous results of intracellular trafficking requiring energy.

We now know that molecular motors kinesins and cytoplasmic dynein drive long range transport of vesicles along microtubules. Most kinesins move toward the microtubule plus ends and dynein moves towards the minus ends of microtubules. Further, while several families of kinesins have evolved for specialized functions, there is only form of cytoplasmic dynein driving retrograde transport.

Dynactin (reviewed in section III) is a co-factor that has been shown to be involved in almost every cellular function involving dynein. Although the importance of dynactin is well established, the mechanistic basis for dynein-dynactin interaction has remained controversial. In this thesis, I first focus on dissecting the role of dynactin in dynein-based motility using single molecule approaches (Chapter 2). I then extend this work by studying dynein-based transport in neurons using a recently developed light-inducible dimerization tool (Chapters 3 and 4). Neurons are a great model system to study transport (reviewed in section V) owing to the (i) the large length scale over which transport has to be executed which makes it an attractive system to dissect out regulatory pathways and (ii) compartment-specific mechanisms to regulate trafficking into and within axons and dendrites. Together, using a combination of approaches, this body of work highlights regulatory mechanisms of the dynein motor both *in vitro* and *in vivo*.

II. The Microtubule Cytoskeleton

The cytoskeleton is a dynamic network of cytoplasmic filaments that maintains cell shape, enables cellular motion and plays important roles in intracellular transport and cell division. The cytoskeleton provides a mechanical framework and structural integrity to the cell. The diverse activities of the cytoskeleton depend on three types of protein filaments - actin filaments, microtubules and intermediate filaments. Each type of filament is formed from a different protein subunit: actin for actin filaments, tubulin for microtubules and a family of related fibrous proteins for intermediate filaments. Actin and tubulin have been especially highly conserved throughout the evolution of eukaryotes. Each of these cytoskeletal proteins assemble into distinct linear filaments which serve as tracks for intracellular transport. As the focus of my project is microtubule-based transport, the next set of sections will discuss this in greater detail.

Early work on microtubule structures came from transmission EM studies and aldehyde fixation methods (Fawcett and Porter, 1954; Sabatini et al., 1963). The first physical evidence of these structures was shown by Inoue and co-workers in sea urchin eggs using polarization microscopy (Inoue and Dan, 1951). They also established through a series of experimental perturbations (Inoue and Sato, 1967) that the microtubule structure seen during mitosis was not an artifact of fixation. It was these set of experiments that provided convincing evidence that microtubule polymerization dynamics can indeed pull chromosomes apart, a model which still holds.

Around the same time, pioneering work from Ed Taylor and his students identified the target of colchicine. Colchicine literature at the time was confusing as addition of colchicine not only inhibited mitosis but also prevented intracellular transport (Freed, 1965)

and disrupted the formation of myotubes in chick muscle (Okazaki and Holtzer, 1965). A concern at the time was colchicine had off-target effects. However, elegant biochemistry work established tubulin as the target of colchicine and it was found abundantly in dividing cells, cilia and brain tissue (Borisy and Taylor, 1967a, 1967b). The abundance of this protein made it easy to purify and subsequent biochemical work from various labs identified several properties of these cytoskeletal structures.

Microtubules are composed of heterodimers of α- and β-tubulin. Tubulin heterodimers form linear protofilaments that associate laterally and form 25 nm diameter hollow tubes composed of 10-15 protofilaments (usually 13) arranged in a lattice (Tilney et al., 1973). These individual protofilaments have longitudinal as well as lateral contacts making them rigid structures necessary for their cellular function. Microtubules are polarized filaments with the α-tubulin being the stable minus-end and the β-tubulin end is the dynamic plus-end (Mitchison, 1993). Although 'treadmilling' was proposed as a model to explain microtubule polymerization (Margolis and Wilson, 1978), *in vitro* work described a novel phenomenon of dynamic instability - where microtubules frequently switch between periods of slow growth, called rescue and phases of rapid depolymerization, termed catastrophe (Mitchison and Kirschner, 1984). This was subsequently confirmed in real time by other groups (Horio and Hotani, 1986; Walker et al., 1988).

Dynamic instability is fundamental to the biological functions of microtubules. It is this phenomenon that allows microtubules to rapidly organize its cytoskeletal network both spatially and temporally in response to cellular cues and allows microtubule to search effectively for target sites. Dynamic instability is possible because of the enzymatic activities of the tubulin monomers. Microtubule assembly involves two steps – nucleation and elongation. *In vitro*, tubulin concentration above a certain threshold will promote polymerization via spontaneous nucleation. The elongation of the polymer is dependent on

the nucleotide state of the tubulin subunits. Tubulin heterodimers co-purify with guanine nucleotide (Weisenberg et al., 1968). Both α- and β-tubulin monomers bind guanosine triphosphate (GTP) in solution. Upon incorporation into the polymer, the GTP in the β-tubulin is hydrolyzed to guanosine diphosphate (GDP) while the GTP in the α-tubulin is not (Spiegelman et al., 1977). Soluble tubulin has a very slow rate of GTP hydrolysis. However, upon incorporation into the polymer, this rate is very high which likely leads to disassembly of the polymer (David-Pfeuty et al., 1977). Thus, the hydrolysis of GTP to GDP at the plus-end of microtubule is thought to promote depolymerization of the filament while the subunits when in GTP state resist depolymerization. Pioneering work from Walker et al., 1988 established that polymerization was dependent on tubulin concentration while depolymerization was independent of tubulin concentration. Although this work laid the foundation for several other experiments and models to explain each step in dynamic instability, we lack a unified understanding of this process (reviewed in Gardner et al., 2008).

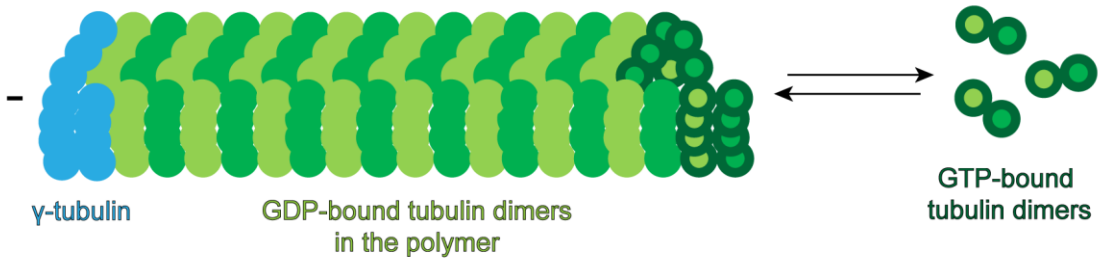

Figure 1.1 Schematic illustrating dynamic instability of microtubules

Interestingly, rates of microtubule dynamics for individual microtubules can be significantly different (O'Brien et al., 1990; Drechsel et al., 1992) and cells have no slow nucleation phases owing to the specialized structures evolved in animal cells called centrosomes. Centrosomes or the microtubule organizing center (MTOC) which is generally located near the nucleus is the site of microtubule nucleation. In most cells, microtubules emanate from the MTOC in a radial fashion with the plus-ends oriented toward the cell

periphery. The MTOC is composed of several proteins including γ-tubulin, pericentrin and ninein (reviewed in Kollman et al., 2011).

A growing body of work has now identified and investigated the roles of several proteins (motor proteins, microtubule associated proteins, severing proteins, nucleating proteins, reviewed in next sections) that regulate the properties of microtubules *in vivo*. Microtubules are constantly remodeled in the cell by the action of several proteins and this is necessary for the diverse cellular functions they are involved in. Some of these concepts will be reviewed in the next set of sections.

III. Kinesin Motors

Studies in early 1980s using extruded axoplasm of giant squid axons established that microtubules provided the tracks for bidirectional vesicle movement along the axon between the neuronal cell body and synaptic termini (Allen et al., 1982; Brady et al., 1982). Shortly thereafter, kinesin-1 was identified as an ATPase that moves along the microtubule plus-ends (Vale et al., 1985a, 1985b, 1985c). Since this initial discovery, the kinesin family now has expanded to include 45 different kinesins (Hirokawa et al., 2009) classified into 14 different classes with commonly agreed nomenclature (Lawrence et al., 2004).

Structurally, kinesins have a motor domain that binds to microtubules and also hydrolyzes ATP (adenosine triphosphate), neck-linker which co-ordinates the two motor heads and a tail which binds to cargos and adaptors (Hirokawa, et al., 1989). Based on their structure, kinesins are generally classified into three types: N-terminal kinesins which have the motor domain at the N-terminus and are generally plus-end directed; C-terminal kinesins which move toward the microtubule minus-end and function in mitosis and M-kinesins which have the motor domain in the middle as in kinesin-13 family which are known to depolymerize microtubules. Functionally, kinesins can be categorized into three broad classes: kinesin that power organelle transport, mitotic kinesins and kinesins that alter microtubule dynamics.

Kinesin-1 motors are heterodimers consisting of two kinesin heavy chains (KHC) and two kinesin light chains (KLC). The KHC of kinesin-1 exists in three forms, KIF5A, KIF5B and KIF5C. While KIF5B is ubiquitous, KIF5A and KIF5C are unique to neurons (Kanai et al., 2000). The motor domain across kinesins is generally conserved and differences in cellular function are largely due to structure outside of the motor domain. Some kinesin-2 motors can

form heterotrimers composed of KIF3A, KIF3B and a kinesin-associated protein, Kap3 (Cole et al., 1993). Kinesin-3 family motors do not dimerize efficiently (Okada et al., 1995) but when dimerized artificially *in vitro*, are processive motors (Okada and Hirokawa, 1999; Tomishige et al., 2003) and it is now thought that they undergo cargo-mediated dimerization *in vivo* (Soppina et al., 2014). Kinesin-5 family motors are homotetrameric (Kashina et al., 1996) that can cross-link and slide anti-parallel microtubules (Kapitein et al., 2005). MCAK and other kinesin-13 familiy proteins do not move processivley on microtubules. Rather, they diffuse along the length of the microtubule and remove tubulin subunits from the ends acting as depolymerases (Hunter et al., 2003). In contrast, Ncd which is a kinesin-14 family member, diffuses along microtubules in a tail-dependent manner and slides anti-parallel microtubules (Fink et al., 2009).

Much of our understanding of the mechanochemical properties of kinesins comes from the conventional kinesin, kinesin-1. Kinesin-1 has been shown to walk in a hand-over-hand motion along the length of the microtubule protofilament in 8 nm steps (which is the length of the tubulin heterodimer), going through one hydrolysis cycle per step (Svoboda et al., 1993; Schnitzer and Block; 1997; Yildiz et al., 2004). This stepping mechanism indicates regulated co-ordination of the biochemical cycles of both motor heads which allows the front head to remain bound to the microtubule while the rear head detaches. Single molecule studies have demonstrated that kinesin-1 has high velocities ranging from 0.5-1.0 μm/s and high stall forces of about 5-7 pN (Visscher et al., 1999), properties which make it an efficient motor for long-range transport. Consistent with this, recent studies have shown that cellular cargo are driven by relatively small teams of kinesin motors (Hendricks et al., 2012; Rai et al., 2013).

The acitivity of kinesins is tightly regulated in cells via an autoinhibition mechanism. Initial *in vitro* experiments with full length KHC showed little to no motility. However,

truncated versions of the KHC with deleted tail exhibited robust motility (Freidman and Vale, 1999). This hinted at an autoinhibitory mechanism which in fact was consistent with the initial micrographs of kinesin structure where in some cases, the tail folded back onto the motor domain (Hirokawa et al., 1989). A short basic motif, IAK in the KHC tail is sufficient to bind to the motor domain (Stock et al., 1999) and subsequently it was shown that full length KHC had several fold lower ATPase activity than the truncated KHC lacking the IAK motif (Hackney and Stock, 2009). This led to the suggestion that the tail of KHC could be folding back onto the ATPase site of the motor, preventing its binding to microtubules (Dietrich et al., 2008). Crystal structures of the kinesin-1 motor domain with and without the tail domain indicated that the tail cross-links the motor domain which potentially inhibits ADP release, thus preventing movement of the motor heads (Kaan et al., 2011). K560, constituting the first 560 amino acids of the kinesin heavy chain is now routinely used as a constitutively active form of the kinesin-1 motor. It is now thought that several kinesins are autoinhibited which serves as a general regulatory mechanism for kinesins (reviewed in Verhey and Hammond, 2009).

In cells, a simple mechanism which relieves autoinhibition is binding of the motor to cargos via adaptors and scaffolding proteins. Several adaptors have now been shown to bind to the tail of kinesin-1 which confers cargo-selectivity (reviewed in Fu and Holzbaur, 2014). Another form of regulation of motors is tubulin modifications (which will be reviewed in section IV) which alter the binding capacities and processivity of kinesin motors. Thus, the fundamental structural differences between the different kinesin families as described above in conjunction with these regulatory mechanisms provide the cell with the specificity required for kinesin-driven transport.

IV. Cytoplasmic dynein

Long before the discovery of kinesins, dynein was first discovered in the cilia of *Tetrahymena* (Gibbons, 1963). It was quickly shown that dynein is an ATPase that drives microtubule sliding in the cilia (Gibbons and Rowe, 1965). Very quickly, sixteen genes were identified encoding the dynein heavy chain with fourteen of them functioning in the axoneme driving cilia beating, one of them is involved in the intraflagellar transport and another one that encodes for the cytoplasmic dynein that drives retrograde transport in cells (Wickstead and Gull, 2007).

Cytoplasmic dynein (referred to as dynein from now on) was initially identified as MAP1C, a microtubule-ATPase which translocated microtubules in the direction opposite to that of kinesin (Paschal et al., 1987; Paschal and Vallee, 1987). Following these initial observations, it was quickly established that MAP1C was infact, the cytoplasmic analogue of axonemal dynein (Vallee et al., 1988). Although kinesins and myosins are structurally similar, dynein has a much more complicated structure (Vale and Milligan, 2000). Dynein is a ~1.6 MDa protein complex with several subunits. The dynein heavy chain constitutes the motor domain, linker, tail and microtubule binding stalk. The tail is required for dimerization and acts as a scaffold for the other subunits of dynein – intermediate chains, light intermediate chains.

Dynein is a AAA protein which are proteins with large hexamers of ATPase domains (Neuwald et al., 1999). Only AAA1-4 of the motor domain have been shown to bind nucleotide with AAA1 being the predominant site for functional hydrolysis (Kon et al., 2004). AAA5 and AAA6 are thought to serve a structural role in the motor domain (Cho et al., 2008; Schmidt et al., 2012). Dynein's microtubule binding site is a 15 nm stalk projecting from the

AAA4 (Gee et al., 1997). Recently, it has been shown that nucleotide binding to AAA1 and microtubule binding by the stalk are allosterically coupled explaining how hydrolysis at AAA1 affects the binding and unbinding of the stalk to microtubules (Carter et al., 2008; Kon et al., 2009).

Single molecule studies in the last decade have begun to elucidate the biophysical properties of dynein. Studies with recombinant yeast dynein showed that dimerization is necessary for processive movement (Reck-Peterson et al., 2006). Further, unlike kinesin, dynein can take variable step sizes of 8-32 nm with sideways stepping on adjacent protofilaments as well as steps toward the microtubule plus-end (Mallik et al., 2004; Ross et al., 2006; DeWitt et al., 2012; Qiu et al., 2012). While the heads of kinesins and myosins are usually tightly co-ordinated, these studies indicate that dynein stepping is not as co-ordinated between its heads. It is likely that this un-coordinated stepping mechanism makes dynein efficient in navigating obstacles such as microtubule associated proteins (MAPs) on the microtubule tracks (Dixit et al., 2008).

Mammalian dynein has a stall force of 1 pN (Mallik et al., 2004; Schroeder et al., 2010) and moves on average at 500-1000 nm/s with a run length of about 1 μm (Mallik et al., 2005; Ross et al., 2006; Ayloo et al., 2014). On the other hand, yeast dynein is a slower and a stronger motor producing stall forces as high as 7 pN (Gennerich et al., 2007). The large forces of yeast dynein are not surprising given that cortical dynein interacts with microtubules to orient the nucleus and promote nuclear migration (Carminati and Stearns, 1997; Moore et al., 2009). Structure studies indicate that the C-terminal domain following AAA6 is smaller in size in the yeast dynein (Carter et al., 2011; Kon et al., 2011). Interestingly, it is now reported that truncation of this C-terminal domain in the mammalian dynein converts it to a motor that can produce large forces (Nicholas et al., 2015) suggesting a mechanism that explains the differences in the yeast dynein and mammalian dynein.

In contrast to single molecule motion of dynein, studies have shown that beads coated with dynein are processive indicating dynein works efficiently in teams (King and Schroer, 2000; Mallik et al., 2005; Ross et al., 2006). More recently, optical trapping of endogenous cargos has demonstrated that dynein molecules work in teams generating large forces that increase linearly with motor number (Hendricks et al., 2012; Rai et al., 2013). This capacity of dynein to work effectively in teams likely enables it to perform the diverse cellular functions it has been implicated in (reviewed in Mallik et al., 2013).

As the major minus-end directed motor in cells, dynein has been shown to transport several organelles including endosomes, lysosomes, mitochondria, lipid droplets. (reviewed in Allan, 2011). Other functions include neuronal migration (reviewed in Vallee et al., 2009), mRNA localization (reviewed in Holt and Bullock, 2009), Golgi positioning (reviewed in Yadav and Lindstedt, 2011) and also in orientation of the mitotic spindle and cell division (reviewed in Siller and Doe, 2009). To perform these various tasks and to achieve specificity, dynein relies on several adaptors that regulate its motility and function. One such ubiquitous adaptor is the dynactin complex highlighted in the next section.

Dynactin

Dynactin was first discovered as a soluble factor that co-purified with dynein by velocity sedimentation but could be separated from dynein by ion exchange (Schroer and Sheetz, 1991). The addition of this soluble factor to dynein enhanced dynein-driven vesicle motility and was suggested to be an activator of dynein motility, hence the name dynactin (Gill et al., 1991). Following these initial observations, several studies quickly established the structural details of this complex.

Dynactin is a 1.2 MDa complex with 11 subunits and based on its structure can be divided into two parts, the projecting side-arm and the Arp1 rod. The Arp1 rod is a 40 nm polymer made of Arp1 subunits and is flanked by CapZ on one end and p62 on the other (Schafer et al., 1994). The Arp1 filament was subsequently shown to be the domain of dynactin that interacted with most cargoes (Holleran et al., 1996; Holleran et al., 2001). The rest of the components making up the Arp1 rod were identified in the next few years (reviewed in Schroer, 2004). The flexible, projecting side-arm constitutes the largest subunit of the dynactin complex, $p150^{Glued}$ which is also the site of dynein interaction (Karki and Holzbaur, 1995; Vaughan and Vallee, 1995). Although $p150^{Glued}$ is the protein that binds dynein, the entire dynactin complex is required for dynein function as over-expression of p50, dynamitin which disrupts the two structural parts of dynactin results in impaired dynein function in cells (Echeverri et al., 1996; Burkhardt et al., 1997).

$p150^{Glued}$ can be divided into 3 broad functional domains – the N-terminal domain that binds to microtubules, independent of dynein (Waterman-Storer et al., 1995); the coiled-coil domain in the middle which is the dynein binding site (King et al., 2003); and the C-terminus which binds to Arp1 of the dynactin complex (Waterman-Storer et al., 1995). The N-terminus is the CAP-Gly domain which is a canonical microtubule binding domain followed by a short region of basic residues. *In vitro* studies have shown that dynactin increases the processivity of dynein via this N-terminal domain (King and Schroer, 2000; Culver-Hanlon et al., 2006). Various studies have now shown that the N-terminal domain of $p150^{Glued}$ enables the loading of the dynactin complex onto microtubule plus-ends. With the initial observation of $p150^{Glued}$ co-localizing with CLIP-170 (Dujardin et al., 1998; Vaughan et al., 1999), several labs quickly showed that CLIP-170 localizes dynactin to microtubule plus ends via its interaction with EB1, microtubule plus-end binding protein (Goodson et al., 2003; Lansbergen et al., 2004; Watson and Stephens, 2006).

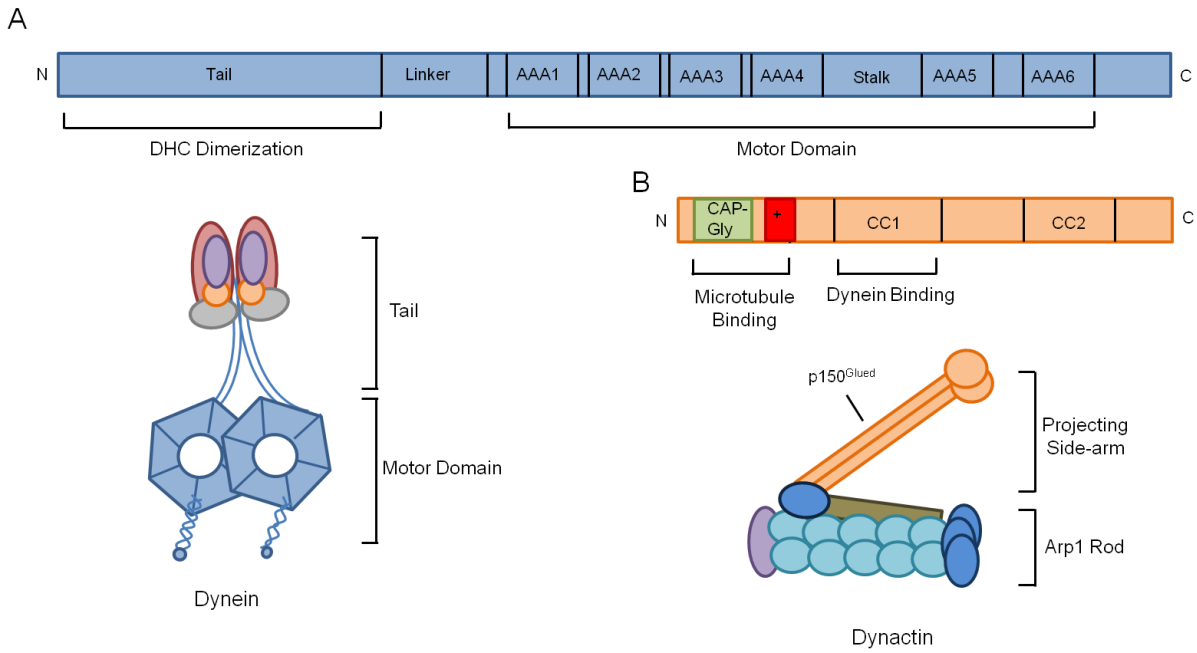

Figure 1.2 Schematic illustrating the dynein and dynactin complexes

Studies in small, non-polarized cell types has indicated that the localization of dynactin at microtubule plus ends is dispensable for dynein-mediated trafficking of organelles (Watson and Stephens, 2006; Kim et al., 2007). This was an intriguing result given that *in vitro* studies indicated that p150^{Glued} increased the processivity of dynein via its N-terminal domain (Culver-Hanlon et al., 2006). On the other hand, mutations in the CAP-Gly domain of dynactin have been shown to cause neurodegenerative disease (Puls et al., 2003; Farrer et al., 2009). Further, studies in mammalian neurons and fly neurons showed that the CAP-Gly domain of dynactin was critical in dynein-mediated trafficking. These studies established that the N-terminus of p150^{Glued} is necessary for enrichment of the dynactin complex at the distal end of axon and this enrichment is essential for efficient initiation of dynein-driven retrograde transport (Moughamian and Holzbaur, 2012; Lloyd et al., 2012). In light of these conflicting results observed in different systems, we set out to elucidate the mechanistic basis of the interaction of dynein with dynactin. This is described in Chapter 2 of this thesis describing results that help put these previous findings in context.

p150^{Glued} has 32 exons (Tokito and Holzbaur, 1998). Several alternatively spliced isoforms of p150^{Glued} with differential exons exist in many tissues (Dixit et al., 2008). An isoform that is unique to the brain tissue is p135 which lacks the N-terminal CAP-Gly and basic domains (Tokito et al., 1996). Although this isoform cannot bind microtubules, it can still bind dynein and distinct dynactin complexes with either p150^{Glued} or p135 exist in the brain tissue. (Tokito et al., 1996). We know very little about this isoform and an attractive hypothesis is that p135 has a specialized function that p150^{Glued} cannot accomplish. The intriguing question of why neurons need this unique isoform still remains an open question.

The first coiled-coil (CC1) domain of p150^{Glued} is the site where the dynein motor binds dynactin (Karki and Holzbaur, 1995; Vaughan and Vallee, 1995; King et al., 2003). CC1 binds the dynein intermediate chain (DIC) and over-expression of this fragment in cells acts as a dominant negative. CC1 competes with endogenous pools of dynactin to bind to endogenous dynein, thus disrupting dynein function in cells (Quintyne et al., 1999). Although CC1 is sufficient to bind the dynein motor, it is not sufficient to increase the processivity of dynein (Culver-Hanlon et al., 2006; Ayloo et al., 2014). More recently, it has been proposed that CC1 could exist as two helices (CC1A and CC1B) instead of one single helix as structure prediction algorithms indicated a break in CC1 between residues 349 through 380 (Siglin et al., 2013; Tripathy et al., 2014). Dynein motility analysis with these individual helices showed that while CC1A had no effect on dynein motility, CC1B stimulated dynein processivity suggesting that when these fragments work together, CC1A inhibits the activity of CC1B (Tripathy et al., 2014). Together, these studies highlight that we still do not fully understand the molecular interactions of dynein with dynactin and only recent structural work has begun to elucidate these interactions at the molecular level (Chowdhury et al., 2015; Urnavicius et al., 2015).

The second coiled-coil (CC2) domain of the C-terminus of p150^{Glued} is the domain that incorporates p150^{Glued} into the rest of the dynactin complex (Waterman-Storer et al., 1995). The rest of the C-terminus acts as a binding site for several cargo adaptors and scaffolding proteins. Few examples include RILP which mediates endosome motility (Jordens et al., 2001), Huntingtin and HAP1 (Engelender, 1997; Li et al., 1998); JIP3 (Cavalli et al., 2005) and JIP1 (Fu and Holzbaur; 2013). All of these proteins have been implicated in regulating motility of various organelles (reviewed in Fu and Holzbaur, 2014). Thus, the C-terminus of p150^{Glued} acts as a hub for several adaptor/scaffolding protein interactions and this is likely a key determinant of cargo specificity for dynein-mediated organelle transport.

Adaptors Regulating Motility of Dynein-Dynactin Complexes

Recent work has shown that addition of certain adaptors to dynein-dynactin complexes converts the weakly processive motor to a highly processive one (McKenney et al., 2014; Schlager et al., 2014). One such adaptor is the Bicaudal D protein (called BICD from here on). BICD was initially identified in Drosophila, where mutations in this gene caused defective embryos (Mohler and Wieschaus, 1986). It was quickly established that BICD was essential for fly oogenesis and played an important role in mRNA localization (Claussen and Suter, 2005). Two orthologs of BICD, BICD1 and BICD2 exist in mammalian cells. Biochemical characterization of BICD2 revealed that it interacted with dynein-dynactin complexes and localized to the Golgi (Hoogenraad et al., 2001). Subsequent work demonstrated that the two N-terminal coiled-coil domains of BICD2 was sufficient to bind to both dynein and dynactin. Recruitment of this N-terminal fragment to organelles in cells induced dynein-mediated transport toward the centrosome (Hoogenraad et al., 2003) and further promoted stable interaction between dynein and dynactin complexes both *in vitro* and *in vivo* (Splinter et al., 2012).

The C-terminal portion of BICD2 has been shown to bind to various proteins that dictate cargo selectivity. Some examples include with Rab6 (Matanis et al., 2002) and Egalatarian which promotes mRNA localization (Mach and Lehmann, 1997). In addition, the C-terminus has also been shown to bind to the N-terminus (Hoogenraad et al., 2003; Splinter et al., 2012) which in turn competes with binding to dynein-dynactin complexes. This suggests a potential autoinhibitory mechanism in cells and indicates that BICD binds to dynein-dynactin only when the C-terminus is bound to cargo adaptors relieving the autoinhibition.

These findings formed the basis of two recent studies which demonstrated that the addition of N-terminal BICD2 to single molecules of dynein-dynactin complexes makes the motor superprocessive *in vitro*, with run lengths as long as seen *in vivo* (McKenney et al., 2014; Schlager et al., 2014). These results are the first to demonstrate superprocessive runs for mammalian dynein at the single molecule level. Few other cargo adaptors have also been been shown to induce superprocessive motility of dynein (McKenney et al., 2014). These include Hook proteins found on edosomes (Bielska et al., 2014; Zhang et al., 2014), spindly found on kinetochores (Griffis et al., 2007) and Rab11-FIP3 found on recycling endosomes (Ullrich et al., 1996; Horgan et al., 2010). The fact that multiple adaptors of dynein induce this robust motility of dynein-dynactin complexes indiactes that this could be a general mechanism for the regulation of dynein in cells and that these adaptors are likely key factors modulating dynein function in a cargo-specific or organelle-dependent manner. Although there is no conserved sequence homology among these various adaptors, a commonality is several coiled-coil domains present in all of them. Thus, an intriguing possibility is that a coiled-coil domain large enough to interact with both dynein and dynactin is sufficient to induce robust motility of the motor. This hypothesis has not been tested yet. Nevertheless, these findings with dynein indicate regulatory mechanisms previously unknown.

Structural Understanding of the Dynein-Dynactin Complexes

The large size and complexity of both dynein and dynactin made structural investigations of these complexes challenging. Although initial structure work provided a framework for our understanding of the dynein motor and dynactin (reviewed earlier in this chapter), it is only now that we are beginning to explore the structural aspects of these protein complexes in part due to technical advancements in electron microscopy (EM).

Two recent studies have now solved structures of dynactin using cryo-EM and both these studies also obtained structures of dynein bound to dynactin and the adaptor protein BICD2 (Chowdhury et al., 2015; Urnavicius et al., 2015). These studies provide some insights into how an adaptor protein can induce such robust motility of the dynein motor when bound to dynactin. Both these reports showed that dynactin and BICD2 bind to the tail of the dynein motor and have overlapping binding sites. Further, this interaction of dynein tail with dynactin seems to be mediated by the N-terminus of BICD2. This explains the need for an adapotor protein facilitating the interaction between dynein and dynactin, thus forming a stable complex.

Chowdhury et al. obtained structures of the dynein tail in complex with BICD2 and dynactin on microtubules and these reveal the two motor domains of dynein aligned in the same direction toward the microtubule minus end. The class averages of EM images obtained by these authors indicate that the dynein motor is poised for unidirectional motility when in a complex with BICD and dynactin. Urnavicius et al. structures indicate that the binding of BICD and dynactin to dynein induces asymmetry in the motor domains of dynein, which could be a mechanism to activate dynein. The authors propose that the binding of adaptor to dynein-dynactin complexes could relieve an auto-inhibited state of the dynein complex consistent with previous report indicating the auto-inhibited state of dynein (Torisawa et al., 2014).

These two studies are the first to demonstrate structural aspects of dynein-dynactin-adaptor complexes both on microtubules (Chowdhury et al., 2015) and off microtubules (Urnavicius et al., 2015). Future studies with higher resolutions structures of dynein-dynactin complexes with other adaptors in conjunction with single molecule motility assays will inform us about the differential modulation of the dynein-dynactin complexes via cargo adaptors.

Dynein-Dynactin in Disease

Mouse mutants generated by chemical mutagenesis experiments were the first dynein mutants that gave us insight into the role of dynein in neuronal development. The initial mouse mutants were Legs at odd angles (Loa), Cramping and Sprawling mice (Duchen, 1974; Hafezparast et al., 2003; Chen et al., 2007), all of them being mutations (point mutations in Loa and Cramping, deletion in Sprawling) in the tail of the dynein heavy chain (*Dync1h1*).

The first dynein mutation to be discovered in humans was in 2010 and the phenotype was developmental delay and intellectual disability (Vissers et al., 2010). A subsequent study identified several mutations in the stalk and microtubule binding domain of dynein in patients with malformations of cortical development (MCD) (Poirier et al., 2013). In the last few years, several mutations have been identified in patients associated with sensory and motor neuropathy (reviewed in Schiavo et al., 2013). While some mutations are located in the motor domain and the stalk, several others are located in the tail highlighting the importance of the several interactions of the dynein tail with adaptors and co-factors.

Mutations in the dynactin complex have also been associated with neurodegenerative diseases. Point mutations in $p150^{Glued}$ of the dynactin complex have been shown to cause hereditary motor neuropathy and Perry syndrome, a form of Parkinsonism

(Puls et al., 2003; Farrer et al., 2009). These mutations are clustered in the CAP-Gly domain of $p150^{Glued}$. Comprehensive characterization of these mutants with biochemical and cellular assays have played an important role in extending our understanding of the dynein complex (Levy et al., 2006; Ori-Mckenney and Vallee, 2011; Moughamian and Holzbaur; 2012). Another important goal would be to understand how a given mutation causes motor deficits but not sensory deficits and vice versa. Further studies are required to explore the selective vulnerability of specific neurons to these mutants, leading to neurodegenerative diseases.

V. Microtubule Modifications and Microtubule Associated Proteins

Microtubules are involved in several cellular processes including intracellular transport, cellular morphogenesis, organelle localization and cell division. Although the fundamental components of microtubules, the heterodimers α- and β-tubulin are the same across all eukaryotic species, microtubules in cells are extensively modified and modulated by various biochemical modifications and interacting proteins respectively. The modifications are post-translation modifications (PTMs) and the interacting proteins are called microtubule associated proteins (MAPs). In the previous sections I reviewed two such MAPs – kinesins and dynein. In this section, I will highlight the various biochemical modifications that microtubules undergo followed by a review of MAPs highlighting the roles PTMs and non-motor MAPs play in establishing and marking the identity of microtubules in cells.

Tubulin Tyrosination

The first observation of tubulin tyrosination came from initial studies that incubated radioactive amino acids with soluble preparations from rat brains (Barra et al., 1973). The incorporation of tyrosine into proteins in the brain extract was several fold higher than other amino acids tested. This process was ATP-dependent and ribosome- and tRNA-independent. These authors quickly found that the factor incorporating tyrosine behaved similar to colchicine binding tubulin in various biochemical assays (Barra et al., 1974). Subsequently, it was shown that the protein incorporating tyrosine was α-tubulin (Arce et al., 1975) and the tyrosine was added at the C-terminus. It is now known that α-tubulin is generally tyrosinated by the enzyme, tubulin tyrosine ligase (TTL) (Schroder et al., 1985; Ersfeld et al., 1993) and acts only on α- and β-tubulin heterodimers (Raybin and Flavin,

1977). Detyrosinating enzymes act predominantly on polymerized microtubules and elegant experiments in cells examining microtubules right after depolymerization indicated that newly made microtubules are generally tyrosinated (Gundersen et al., 1987). Detyrosinated tubulin can be further modified to Δ2-tubulin by the removal of the glutamic acid residue which cannot go back to the tyrosinated form (Paturle-Lafanechere et al., 1991).

Some initial studies that examined the correlation between various microtubule modifications and microtubule stability, suggested that detyrosination of microtubules promoted their stability (Gundersen et al., 1987; Schulze et al., 1987). However, this was not true in all cell types (Schulze et al., 1987) and more recently, it was shown that depolymerizing kinesins MCAK and KIF2, belonging to kinesin-13 family have a preference for tyrosinated microtubules (Peris et al., 2009; Sirajuddin et al., 2014). Thus, detyrosination of microtubules protects them from depolymerizing kinesins which could explain the stability of these microtubules.

Like kinesin-13 motors, KIF5 or the conventional kinesin, kinesin-1 has also been shown to have differential preferences for tyrosinated vs detyrosinated microtubules. Kinesin-1 selectively binds to detyrosinated microtubules (Liao and Gundersen, 1998; Dunn et al., 2008) and this makes the kinesin motor domain preferentially enter the axon enriched with detrysoinated microtubules and hence excluded from the dendrites (Konishi and Setou, 2009). In contrast to kinesin-1, non-motor MAPs such as CLIP-170 and $p150^{Glued}$ that interact with microtubules via their CAP-Gly domain have a preference for tyrosinated microtubules (Peris et al., 2006). These results indicate that tyrosinated microtubules can efficiently recruit microtubule plus-end binding proteins. This result is also consistent with recent studies showing the accumulation of these CAP-Gly proteins at growth cones of axons that are enriched with tyrosinated microtubules (Moughamian and Holzbaur, 2012).

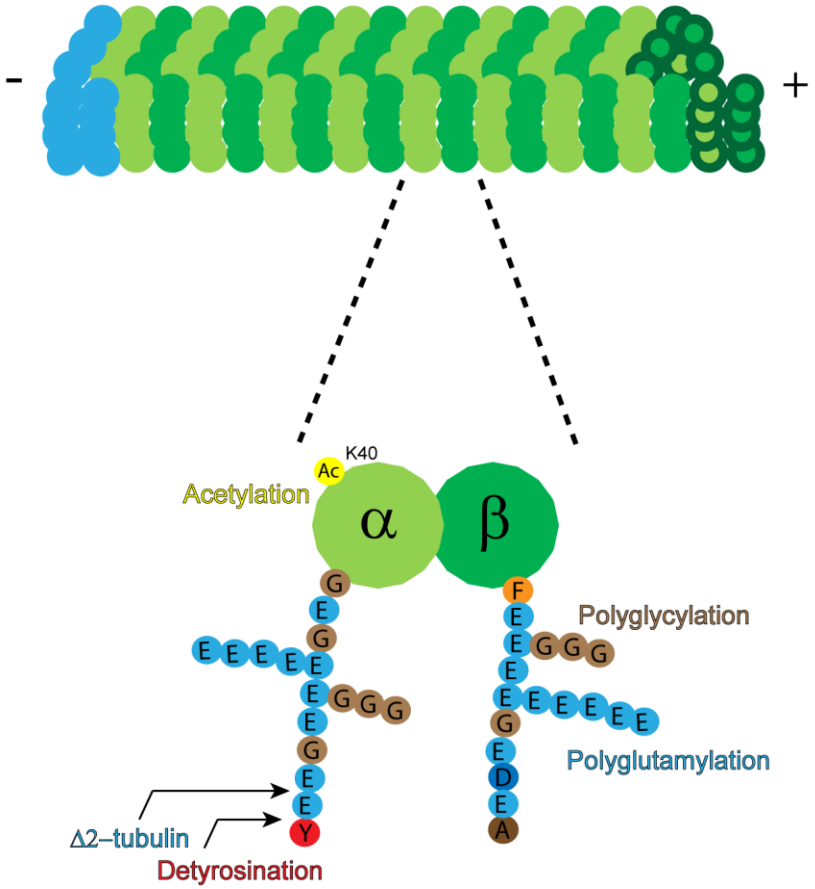

Figure 1.3 Schematic illustrating tubulin post-translational modifications (Adapted from Janke, 2014)

A mouse knockout of the tubulin tyrosine ligase, *Ttl*, was lethal and mice die shortly after birth (Erck et al., 2005). Neurons cultured from these mice have gross alterations in the timeline of axon differentiation and neuronal development *in vitro* highlighting the importance of the detyrosination/tyrosination cycles of tubulin. These findings indicate that these abnormalities could be likely due to the dampened effect of depolymerizing motors and higher affinity of kinesin-1 on detyrosinated microtubules promoting axon extensions longer than the wild-type mice.

Tubulin Acetylation

Acetylation was the second PTM on tubulin to be discovered, first identified in the α-tubulin of *Chlamydomonas* on lysine40 residue (L'Hernault and Rosenbaum, 1985). Lys40 is located in the lumen of the microtubule polymer (Nogales et al., 1998) and hence it is intriguing that acteylation of microtubules can affect the interaction of any motor protein or MAP as these interact with microtubules on the cytoplasmic face of the polymer. Initial functional studies identified HDAC6 (Hubbert et al., 2002) and Sirt2 (North et al., 2003) as microtubule deacetylase enzymes. However, both these enzymes have several substrates besides microtubules alone and hence it is possible that effects downstream of altering these enzymes is not a direct consequence of altered microtubule modification. More recently, tubulin acetyltransferase (TAT) has been discovered as an enzyme that specifically acts on α-tubulin (Akella et al., 2010). Recent work using X-ray crystallography and single molecule assays demonstrated that TAT does indeed enter the microtubule lumen and acetylates from the inside. Further, acetylation marking stable microtubules can be explained by the slow catalytic rate of the enzyme compared to its diffusion rate (Szyk et al., 2014).

Similar to detyrosinated microtubules, tubulin acetylation is predominant on stable microtubules (Schulze et al., 1987). Neuronal studies have indicated that kinesin-1 has a higher affinity for acetylated microtubules (Reed et al., 2006). However, *in vitro* studies with purified components did not observe this preference for kinesin-1 (Walter et al., 2012; Kaul et al., 2014) suggesting that the intracellular trafficking of kinesin-1 to acetylated microtubules is via other interactions. Moreover, increasing the overal acetyation levels of tubulin in neurons did not alter the selectivity of kinesin-1 (Hammond et al., 2010). In contrast to detyrosination/tyrosination of tubulin, it has been harder to establish concrete cellular functions for tubulin acetylation.

Tubulin Polyglutamylation and Polyglycylation

Another modification of tubulin discovered in the early 90s was the covalent addition of chains of glutamate and glycine residues added to the C-terminal tails of tubulin termed as polyglutamylation (Edde et al., 1990) and polyglycylation (Redeker et al., 1994) respectively. In contrast to the other modifications, these modifications are the addition of several amino acids and can occur on both α- and β-tubulin. While glutamylation is found everywhere, glycylation seems restricted to cilia and flagella (Fouquet et al., 1994).

The high levels of polyglutamylation in neurons made possible the discovery of the first polyglutamylase enzyme (Janke et al., 2005). This is a multi-subunit protein complex with its catalytic subunit similar to the tubulin tyrosine ligase enzyme (Janke et al., 2005). Subsequently several other glutamylating and glycylating enzymes have been identified and more recently a deglutamylase enzyme has been discovered which removes the Glu side chains from tubulin (Rogowski et al., 2010). Although several enzymes responsible for glutamylation and glycylation have been identified in recent years, the spatial and temporal localization and function of these enzymes is still unclear.

Biochemical studies have indicated preferential binding of Tau, a microtubule MAP and the kinesin-1 motor domain to polyglutamylated tubulin (Boucher et al., 1994; Larcher et al., 1996). Alteration of synaptic activity in neurons increased overall levels of microtubule polyglutamylation and affected the trafficking of kinesin-1 to neurites (Maas et al., 2009). Polyglutamylation has also been shown to promote microtubule severing by katanin and spastin, microtubule severing enzymes (Sharma et al., 2007; Lacroix et al., 2010). Interestingly, microtubules with long glutamyl side chains were more prone to spastin-mediated severing *in vitro* (Lacroix et al., 2010) and it is possible that cells have mechanisms to prevent such severing of polyglutamylated microtubules. Consistent with this, the

preferential binding of Tau to polyglutamylated tubulin (Boucher et al., 1994) could be one such mechanism as Tau has been shown to protect microtubules from severing (Qiang et al., 2006). It is clear that polyglutamylation and polyglycylation can generate microtubules with varying complexity levels as these are the only modifications that can occur on any residue of either α- or β-tubulin and also the length of the glutamine and glycine chains can be modulated. However, we do not fully understand the cellular cues that dictate these changes and if there are specific tubulin residues that are targeted more often than others.

Other Tubulin PTMs

Several other modifications of tubulin have been reported like arginylation, methylation (reviewed in Janke 2014) and more recently polyamination (Song et al., 2013). It is clear that we are only beginning to understand the several modifications that tubulin can undergo and further studies are needed to gain insights into their functional importance.

Besides these several PTMs of microtubules, there are several other proteins that interact with microtubules and modulate them in cells called MAPs (microtubule associated proteins). Broadly speaking, these include all proteins that bind to microtubules and diverse classes of MAPs have been identified in eukaryotic cells – structural MAPs such as MAP1, MAP2 and tau; microtubule plus-end binding proteins or +TIPs such as EB1, CLIP-170, CLASP; microtubule minus-end binding proteins such as CAMSAPs, microtubule destabilizing enzymes such as spastin, katanin; MAPs that alter microtubule dynamics such as doublecortin (nucleation factor), XMAP215 (polymerase), TPX2 and finally motor MAPs which was reviewed in the earlier sections. This classification is by no means exhaustive (see Lyle et al., 2009 for a complete list) and here, I focus only on structural MAPs and +TIPs which become relevant in Chapter 4 on neuronal transport.

Structural MAPs

MAPs were initially identified as proteins that were enriched in microtubule fractions through repeated cycles of tubulin assembly and disassembly (Shelanski et al., 1973; Borisy et al., 1975). Some of the initial MAPs identified were MAP1, MAP2 (Sloboda et al., 1975) and Tau (Weingarten et al., 1975; Cleveland et al., 1977). While MAP1 consists of polypeptides MAP1A, 1B, 1C; MAP2 consists of 2A and 2B and Tau is the most heterogenous among them ranging from 3-6 polypeptides (reviewed in Olmsted, 1986)

A common feature of all these proteins was the ability to stabilize microtubules and promote tubulin polymerization even at concentrations lower than needed for tubulin alone. These initial studies on MAPs suggested that MAPs could alter microtubule properties in cells. To test this, *in vitro* assays to examine dynamic instability of microtubules were carried out in the presence of purified MAPs. MAPs increase polymerization rates and frequency of rescue, suppress catastrophe rate and frequency of catastrophe (Pryer et al., 1992; Drechsel et al., 1992).

MAPs have traditionally been studied in the brain tissue as the abundance of tubulin in brain extracts facilitated tubulin isolation (Weisenberg, 1972). Antibody staining of adult brain tissue has revealed interesting differences between these MAPs and also striking compartmentalization. MAP1 is present through the neurons and is enriched in white matter relative to grey matter (Vallee, 1982). MAP1 is also 5-fold higher than MAP2 in brain tissue (Vallee, 1982). Immunostaining of MAP2 has revealed that MAP2 is generally found only in dendrites and post-synaptic densities (Matus et al., 1981; Caceres et al., 1984). Tau localization complements that of MAP2 and is found only in axons, excluded from soma and dendrites (Binder et al., 1985). Interestingly, subsequent work demonstrated that the compartmentalization observed with some MAPs is at the messenger RNA level (Garner et al., 1988; Litman et al., 1993).

An attractive hypothesis is that MAPs bound to the microtubule polymer add another layer of regulation to motor proteins. Although this has been explored for Tau with kinesin-1 and dynein (Dixit et al., 2008), we know very little about this regulation with other MAPs and the various ways in which they modulate motor proteins. Besides the role of Tau in microtubule stability and motor transport, Tau is a major protein that is aggregated and modified in several ways in patients with Alzeheimer's disease. This has generated considerable interest in Tau, and Tau dysfunction has now been proposed to be an early marker for neurodegenerative diseases (reviewed in Frost et al., 2015). Future studies focusing on structure-function correlation of these MAPs and the biological implications in neuronal development are needed to further our understanding of their cellular function.

Microtubule Plus-end Binding Proteins

Microtubule plus-end binding proteins or +TIPS are a distinct class of proteins that specifically localize to the plus-ends of growing microtubules. Since the discovery of CLIP-170 (Perez et al., 1999), the first protein shown to localize to microtubule plus-ends, different families of +TIPS have been identified.

EBs or end-binding proteins are one such class initially identified in a yeast two-hybrid screen that interacted with the C-terminus of adenomatous polyposis coli (APC), hence named end-binding (Su et al., 1995). EB proteins are dimers that bind to microtubules via their N-terminal calponin homology (CH) domain and this domain is sufficient for their binding to microtubule plus-ends (Hayashi and Ikura, 2003; Komorova et al., 2009). The C-terminus includes a coiled-coil domain which is essential for dimerization and the rest of the C-terminus is a site for interaction with several other +TIP proteins. Two modes of interaction have been identified so far: (i) through the binding of an SxIP motif with the hydropobic cavity of EBs (Honappa et al., 2009) (ii) CAP-Gly containing proteins that bind to the EEY/F motif in

the C-terminus of EB proteins, CLIP-170 and tubulin itself (Weisbrich et al., 2007). The first class includes proteins like APC, STIM1 and MCAK and the second class includes proteins like CLIP-170 and p150^{Glued} of dynactin. Thus, through these interactions EBs form the core of the +TIP network of proteins.

In vitro studies with EB1 has demonstrated that EB1 does not bind tubulin dimers and its tip tracking behavior on growing microtubules is independent of tubulin concentrations suggesting that EBs do not co-polymerize with tubulin (Bieling et al., 2007). This indicated that EB proteins were recognizing structural features at the microtubule plus-end that was different from the rest of the microtubule lattice. Consistent with this, a recent cryo-EM study showed that the calponin homology domain of EB1 binds to four tubulin subunits in way that it bridges protofilaments except at the seam (Maurer et al., 2012). This suggests that EB1 binds to microtubules in a strategic manner that allows it to sense GTP-hydrolysis induced conformational changes in the microtubule plus-end (Maurer et al., 2012).

Several +TIP proteins undergo auto-inhibition via intramolecular interactions. CLIP-170 which binds to the EEY/F motif of EB1 also has an EEY/F motif at its C-terminus. This allows the CAP-Gly domain of CLIP-170 to interact with its C-terminus (Lansbergen et al., 2004). The autoinhibition can be relieved by proteins containing EEY/F motif like EBs and tubulin which allows the C-terminus of CLIP-170 to bind to p150^{Glued} or Lis1 (Lansbergen et al., 2004; Weisbrich et al., 2007). Further, EB1 itself can be autoinhibited which can be relieved by its binding to tubulin or other +TIPs that bind to its C-terminus (Hayashi et al., 2007).

Another layer of regulation is the tyrosination/detyrosintion cycle that the EEY/F motif of tubulin undergoes in which the tyrosine residue can be removed and added back in cells (reviewed in previous section). Previous work has shown that CAP-Gly containing proteins like CLIP-170 and p150^{Glued} exhibit enhanced binding with tyrosinated microtubules (Peris et

al., 2009). This finding is consistent with structural findings implicating the binding of +TIPs to EEY/F motifs (Weisbrich et al., 2007).

MAPs function in almost all cellular processes where microtubules are involved. It is likely that these proteins are either competing for binding sites or co-operating with each other to regulate binding to microtubule lattice and microtubule plus-ends. Thus, the next challenge is to understand the regulation of these proteins working together. Another aspect of this regulation is to understand how tubulin modification or the 'tubulin code' influences these MAPs as these are the readers of the tubulin code. Further studies are needed to identify broad themes in the regulatory mechanisms cells employ to modulate the activity of the various classes of MAPs.

VI. Neuronal Transport

Ever since Cajal drew out the anatomy of cells in the central nervous system, scientists have always been fascinated with neurons. The polarized and extended morphology of each neuron and the contacts between neurons is integral for propagation of neuronal signals. A key aspect in proper neuronal function is the efficient supply of material synthesized in the cell body to the individual neurites and clearance of misfolded and aggregated proteins from neurites to the soma for their degradation. Thus, neurons employ mechanisms of active transport to constantly supply and clear material to and from neurites, which sometimes can be over a meter away from the cell body.

The first evidence for movement of material in the axon came from observing the effects of nerve constriction of peripheral neurons (Weiss and Hiscoe, 1948). The authors observed disruption in cytoplasmic flow upon nerve constriction which resumed upon relieving the constriction, moving on average at 1 mm per day. This was convincingly demonstrated by subsequent studies using radioactive labeling (Miani, 1960; Droz and Leblond, 1962; Grafstein, 1967). However, besides the slow rate of 1 mm per day, these studies also reported some very fast movements. Quantitative studies reported movements as fast as 100-fold higher than the slow movement initially described by Weiss and Hiscoe (Niemierko and Lubinska, 1967). Around the same time similar experiments with colchicine abolished this movement implicating microtubules playing an important role in axonal transport (Kreutzberg, 1969). Following the development of differential intereference microscopy, fast organelle motility was observed in the extruded axoplasm of giant squid (Allen et al., 1982; Brady et al., 1982). This faster movement in the axon was called fast axonal transport and the slower movement was termed slow axonal transport. The proteins driving the fast movement were quickly identified (reviewed in previous sections) and this

section I will only focus on the fast axonal transport driven by microtubule motors. I will first introduce features of the neuronal cytoskeleton followed by polarized sorting and trafficking highlighting compartment specific differences between axons and dendrites.

Microtubule Organization in Neurons

Initial studies on microtubule organization in axons were done in the early 80s by independent groups showing that microtubules in axons were uniformly polarized (Heidemann et al., 1981; Burton and Paige, 1981). A few years later, examination of mammalian neuronal cultures *in vitro* revealed that dendrites have mixed polarity microtubules while axons have uniformly oriented microtubules (Baas et al., 1988; Burton, 1988). Around the same time, the developmental timing of neuronal growth *in vitro* was documented (Dotti et al., 1988). Neuronal development followed a stereotypical sequence of events – the cells first establish small, immature processes and once one of them becomes the axon, the other processes begin to elongate to become dendrites (Dotti et al., 1988). Initially, microtubules start out uniform in all the processes with their plus-ends out and once processes mature into dendrites, minus-end out microtubules get added, establishing mixed polarity microtubules in dendrites (Baas et al., 1989). These initial findings were subsequently confirmed using live-cell imaging of EB3-GFP which tracks microtubule plus-tips (Stepanova et al., 2003).

A fundamental question in neuronal polarity is what are the cues that dictate the initial specification of the axon and the consequent establishment of the microtubule organization in dendrites. Although a recent study indicated that selective stabilization of microtubules in a given neurite is sufficient to convert it to an axon (Witte et al., 2008), the stabilizing factors are still unclear. As far as the microtubule organization in dendrites is concerned, motors are thought to actively translocate microtubules into dendrites to establish

a mixed polarity pattern. Dynein and certain mitotic kinesins have been implicated in setting up this organization in dendrites (reviewed in Baas and Lin, 2011).

Besides the orientation, axons and dendrites also differ in their microtubule stability, post-translational modifications and the complement of MAPs associated with them in these compartments. Microtubules in axons are known to be enriched in the more stable acetylated and detyrosinated tubulin whereas dendrites and growth cones are enriched in tyrosinated microtubules (Konishi and Setou, 2009; Hammond et al., 2010). Further, structural MAPs localize differentially to axons and dendrites with Tau being axonal only (Binder et al., 1985) and MAP2 marking dendrites (Caceres et al., 1984; see section V for review on tubulin modifications and MAPs). In the section, I will introduce polarized trafficking in neurons and highlight how the underlying microtubule cytoskeleton contributes to the navigation of motor proteins.

Polarized Trafficking in Neurons

Polarized trafficking in neurons was observed as early as in the 1980s and 90s with several proteins shown to have differential localization including mRNA (Davis et al., 1987), ribosomes (Barlett and Banker, 1984), glutamate receptors (Craig et al., 1993), Tau and MAP2 (Dotti et al., 1987). While initial work was using in situ hybridization, later studies were done in cultured neurons *in vitro* revealing the localization of several proteins (reviewed in Craig and Banker, 1994). The polarized distribution itself is not surprising given the extended and polarized morphology of neurons with a distinct axon and dendrites. However, what has been elusive is the mechanisms driving polarized trafficking in neurons.

Sorting Signals

Early work dissecting selective transport of membrane proteins in neurons focused on identifying sorting signals that conferred compartment-specificity. The sorting mechanisms well established in epithelial cell biology (reviewed in Matter and Mellman, 1994; Mellman and Nelson, 2008) provided a foundation for these initial studies. Initial work observed the localization of basolateral marker membrane proteins and apical proteins and demonstrated that basolateral proteins are targeted to dendrites; mutations in the sequences disrupted the dendritic localization (Jareb and Banker, 1998). Interestingly, the apical proteins were targeted uniformly indicating that the sorting signal in apical proteins was not enough to make them axon-specific in neurons (Jareb and Banker, 1998). Although an exciting result at the time, it became apparent very quickly that neurons employ more complicated mechanisms for polarized sorting than just basolateral being equivalent to dendritic targeting. Key examples include identification of somatodendritic targeting signal in the cytoplasmic domain of transferrin receptor which was distinct from the basolateral targeting sequence (West et al., 1997), previously unknown targeting sequences identified in metabotropic glutamate receptors (mGluRs) (Stowell and Craig, 1999).

An earlier study also showed that NgCAM (Neuron-glia Cell Adhesion Molecule), an axonal membrane protein was restricted to the cell surface of axons but the vesicular organelles within the neuron were present throughout the neuron. On the other hand, TfR (Transferrin Receptor), a dendritic protein was restricted to dendritic cell surface and the vesicular organelles also localized only to dendrites (Burack et al., 2000). This study indicated that at least two mechanisms of sorting exist in neurons: one is within the cell which is microtubule-based that establishes selectivity of organelles in neurons via motor proteins (cytoplasmic) and the other is at the plasma membrane level. Further, the commonality among all these studies was that dendritic proteins in vesicular organelles were

excluded from axons but this was not the case for axonal proteins (Jareb and Banker, 1998; Stowell and Craig, 1999; Burack et al., 2000). This suggested that dendritic transport was selective, achieved by motor proteins that selectively entered dendrites while axonal proteins were targeted non-selectively and a downstream step following this initial transport, likely exocytosis made them axon-specific. In the years following these initial studies, selective trafficking of motor proteins in neurons was extensively studied. Several models for how motors drive selective trafficking have been proposed and there seems to be evidence for all of these models. All these models were based on investigations of various kinesins and very little is known about selective transport of dynein-driven cargos. In this section, I will review the models for selective transport with specific examples in each case and conclude with findings from my own work on dynein-driven trafficking in neurons.

(i) Motor-cargo interactions

Kinesin-1 has been shown to be involved in organelle transport in both axons and dendrites (reviewed in Hirokawa et al., 2009). How is a plus-end directed motor able to drive transport in dendrites that have mixed polarity microtubules? One model that explains the polarized trafficking is the ‘cargo-steering’ model. Several lines of evidence have shown that the cargo bound to kinesins determines if the motor-cargo complex is targeted to axons or dendrites. One initial study that supports this model demonstrated that AMPA receptor subunit, GluR2-interacting protein (GRIP1) directly binds to and steers the kinesin heavy chain of kinesin-1 to dendrites (Setou et al., 2002). Over expression of GRIP1 in neurons also caused to localize the KHC predominantly to the somatodendritic compartment, consistent with GRIP1 localization (Setou et al., 2002). On the other hand, JIP1 which is an adaptor for kinesin-1 mediated transport, trafficks kinesin-1 to axons (Verhey et al., 2001). This has also been the case with KIF17, a kinesin-2 motor protein which localizes NMDA

receptor 2B subunit (NR2B) to postsynaptic sites; KIF17 accomplishes this by binding to a PDZ domain of one of the proteins in complex with NR2B (Setou et al., 2000).

More recently, the C-terminus coiled-coil domains and the C-terminal PX domain of KIF16B, kinesin-3 motor have been shown to be important in the accurate localization of KIF16B to somatodendrites (Farkhondeh et al., 2015), implicating the cargo-binding region as domains containing targeting information. Adaptors bound to cargo have also been shown to play a role in targeting the motor-cargo complex to the final destination (van Spronsen et al., 2013). In this study, the authors showed that TRAK/Milton adaptor proteins establish uniform distribution of the mitochondria in neurons with TRAK1 binding to kinesin-1 and dynein which trafficks mitochondria to axons, while TRAK2 binds to dynein-dynactin alone steering these mitochondria to dendrites (van Spronsen et al., 2013).

In all the above examples, the cargo or adaptor protein bound to cargo determine the targeting of the motor-cargo complex. However, there is also evidence that motor-microtubule interactions determine the targeting of the motor, indicating that targeting of motor-cargo complex is intrinsic to the motor-microtubule interactions as reviewed in the examples below.

(ii) Motor-microtubule interactions

Another model explaining differential trafficking of proteins in neuronal transport is the ‘smart-motor’ hypothesis which suggests that motors are capable of navigating to the axon or dendrites solely based on their interactions with axonal and dendritic microtubules. These interactions are modulated by microtubule polarity, post-translational modifications and MAPs associated with microtubules.

One of the initial observations in support of this hypothesis came from studies using

K560, the constitutively active motor domain of kinesin-1. K560 in neurons preferentially accumulated at axon tips (Nakata and Hirokawa, 2003). Further, this preferential accumulation of K560 in axons acts as an early marker for axon specification (Jacobson et al., 2006). Consistent with these initial observations, subsequent work indicated the increased affinity of kinesin with detyrosinated (Konishi and Setou, 2009) and acetylated microtubules (Reed et al., 2006), both of which are enriched in axons. However, it is important to note that correlating motor affinity to tubulin modifications has not been very straightforward due to other conflicting data: study reporting that K560 has no preference for acetylated microtubules *in vitro* (Walter et al., 2012); specifically increasing acetylation levels in neurons did not change the axon-selectivity of kinesin (Hammond et al., 2010). Hence, it is likely that a combination of biochemical cues between motors and microtubules determine the targeting of the motor.

Localization studies with constitutively active motor domains of a subset of kinesin-3 and kinesin-4 motors also lend support to this model – KIF13A and KIF13B, kinesin-3 motors and KIF21A and KIF21B, kinesin-4 motors localize differentially with KIF13A, KIF21A localizing to only axons while KIF13B and KIF21B localize to both axons and dendrites (Huang and Banker, 2012). This study also identified sequences in the loop12 of the motor domain that confer axon selectivity, which when mutated, abolish the selectivity (Huang and Banker, 2012). It is likely that the non-selective kinesins, KIF13B and KIF21B are likely dendritic kinesins as unlike the other kinesins tested these were the only ones that could navigate the dendritic microtubule cytoskeleton and since the motors are constitutively active, axonal accumulation could be a default for all plus-end directed kinesins. Consistent with this idea, full length KIF21B has shown to be enriched in dendrites only (Jenkins et al., 2012) implicating it as a ‘smart-motor’ that can preferentially enter dendrites.

Another model proposed was that the axon initial segment (AIS), a specialized

membrane region in the axon, enriched in Ankyrin G, is the filter that determines which motors are axon-specific (Song et al., 2009). This study used chimeras of KIF5 and KIF17 with the corresponding cargos in different combinations and concluded that the efficacy of the cargo-motor complex determines their ability to navigate through the AIS, thus being targeted to the axon. However, a caveat with this model is that the AIS is set up later in neuronal development and a recent study demonstrated that polarized transport is established early on in neurons, even before the establishment of the AIS (Petersen et al., 2014). The AIS model also does not explain how the same KIF5 motor is axonal when bound to JIP1 for instance (Verhey et al., 2001) and is dendritic when bound to GRIP1 (Setou et al., 2002).

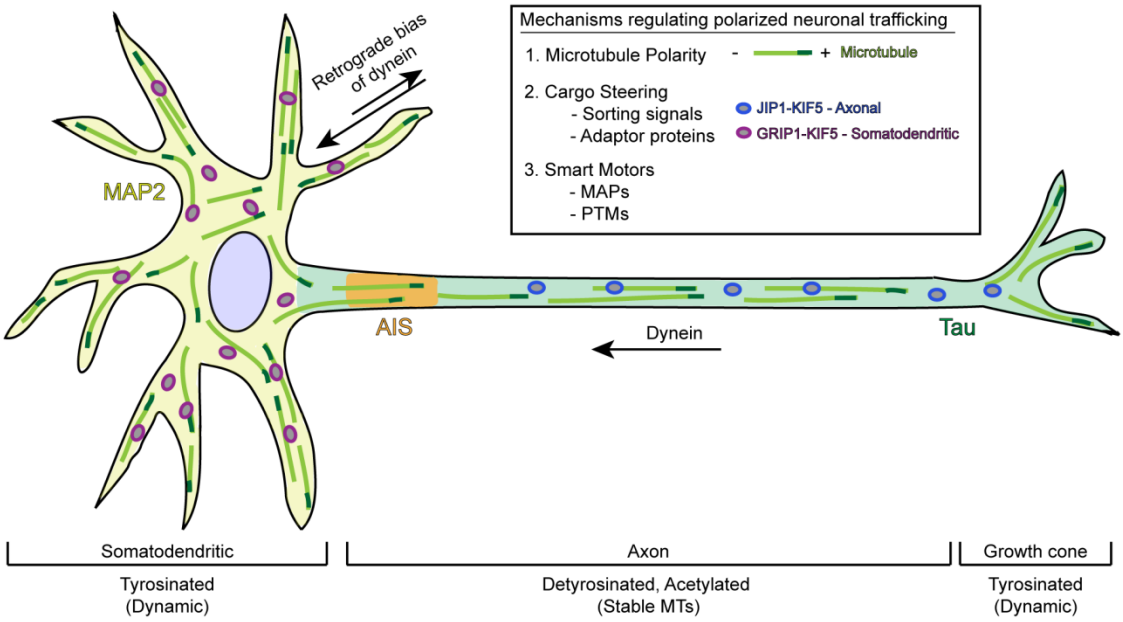

Figure 1.4 Illustration of mechanisms regulating polarized neuronal trafficking

Although a lot of work has been done with kinesins, less is known about dynein-mediated trafficking in dendrites. Although some studies have proposed that dynein could be the major dendritic motor owing to its capacity to move efficiently on mixed microtubules in

dendrites (Black and Baas, 1989; Kapitein et al., 2010), this model does not explain the localization of cargoes that are predominantly dendritic but have kinesins on them (Setou et al., 2000; Setou et al., 2002; Jenkins et al., 2012). In conclusion, it is becoming increasingly clear that polarized trafficking in neurons is regulated at many levels and it is likely that this is controlled via co-ordinated regulation of motor-cargo and motor-microtubule interactions.

In the second half of this thesis, I will present my work on manipulating trafficking in neurons by recruiting various motor proteins to test their ability to navigate axonal and dendritic microtubules. This is one of the few studies exploring dynein-mediated trafficking in dendrites and my work highlights the factors that regulate dynein trafficking in neurons. Together, with my single molecule work of dynein and dynactin *in vitro*, this thesis dissects the functions and regulatory mechanisms of the dynein motor complex using a combination of approaches.

CHAPTER 2: DYNACTIN FUNCTIONS AS BOTH A DYNAMIC TETHER AND BRAKE DURING DYNEIN-DRIVEN MOTILITY

This chapter is adapted from:

Ayloo, S., Lazarus, J.E., Dodda, A., Tokito, M., Ostap, E.M., Holzbaur, E.L.F (2014). Dynactin functions as both a dynamic tether and brake during dynein-driven motility. Nature Communications 5:4807

Contributions: I performed all the experiments, analyzed data and wrote the chapter. Aditya Dodda designed the analysis and performed simulations. Jake Lazarus, Mariko Tokito and Mike Ostap contributed new tools and reagents.

I. Summary

Dynactin is an essential cofactor for most cellular functions of the microtubule motor cytoplasmic dynein, but the mechanism by which dynactin activates dynein remains unclear. Here we use single molecule approaches to investigate dynein regulation by the dynactin subunit $p150^{Glued}$. We investigate the formation and motility motility of a dynein-$p150^{Glued}$ co-complex using dual-color total internal reflection fluorescence microscopy. $p150^{Glued}$ recruits and tethers dynein to the microtubule in a concentration-dependent manner. Single molecule imaging of motility in cell extracts demonstrates that the CAP-Gly domain of $p150^{Glued}$ decreases the detachment rate of the dynein–dynactin complex from the microtubule and also acts as a brake to slow the dynein motor. Consistent with this important role, two neurodegenerative disease-causing mutations in the CAP-Gly domain abrogate these functions in our assays. Together, these observations support a model in which dynactin enhances the initial recruitment of dynein onto microtubules and promotes the sustained engagement of dynein with its cytoskeletal track.

II. Introduction

Cytoplasmic dynein is the major microtubule minus-end directed motor in higher eukaryotes. Dynactin, a large multi-subunit protein complex, interacts with dynein and is essential for a broad range of cellular functions including organelle transport and mitotic spindle assembly (reviewed in Schroer, 2004). Dynactin was first identified as an activator of dynein that increased the ability of dynein to transport organelles (Gill et al., 1991) but the mechanisms involved in dynein activation are not yet understood.

Structurally, dynactin can be divided into two parts—an actin-like Arp1 rod that along with associated subunits forms the base of the complex and a projecting side arm formed from the dimerization of the largest subunit in the complex, $p150^{Glued}$ (Holzbaur et al., 1991; Schafer et al., 1994). $p150^{Glued}$ interacts directly with the dynein intermediate chain (DIC) of the dynein motor (Karki et al., 1995; Vaughan et al., 1995). $p150^{Glued}$ also interacts with microtubules via its Cytoskeletal Associated Protein, Glycine-rich (CAP-Gly) domain at the N terminus (Waterman et al., 1995) which is followed by a highly basic region that has a lower affinity interaction with microtubules (Culver-Hanlon et al., 2004; Lazarus et al., 2013). *In vitro* motility studies using beads coated with purified proteins demonstrated that the microtubule-binding capacity of dynactin increases the processivity of mammalian dynein (King and Schroer, 2000; Culver-Hanlon et al., 2004).

Despite these initial studies, the mechanisms by which dynactin enhances dynein-driven motility have remained controversial. For example, dynactin has been shown to enhance the processivity of yeast dynein, which differs from the mammalian motor in key biophysical properties including velocity and the frequency of backward stepping (Mallik et al., 2013). Surprisingly, however, the dynactin-dependent enhancement of the run lengths of yeast dynein in single molecule assays does not appear to require the CAP-Gly domain

(Kardon et al., 2009), although at the cellular level this highly conserved domain contributes to the initiation and persistence of dynein-dependent nuclear movement (Moore et al., 2009). Studies in higher eukaryotes also suggest that the CAP-Gly domain may be dispensable for some cellular functions, including the trafficking and localization of organelles in S2 and HeLa cells (Kim et al., 2007; Dixit et al., 2008).

In contrast, both cellular and in vivo studies have demonstrated that the CAP-Gly domain of dynactin is essential for dynein function in neurons. In Drosophila and mammalian neurons, the CAP-Gly domain enhances the retrograde flux of cargoes from the distal axon (Lloyd et al., 2012; Moughamian and Holzbaur, 2012). An ordered recruitment pathway has been proposed, in which binding of dynactin to dynamic microtubules enriched in the distal axon leads to the enhanced recruitment of dynein, permitting the efficient initiation of retrograde transport (Moughamian et al., 2013). Importantly, mutations in the CAP-Gly domain of $p150^{Glued}$ cause human disease, including the motor neuron degenerative disease HMN7B and a lethal and rapidly progressive variant of parkinsonism known as Perry syndrome (Puls et al., 2003; Farrer et al., 2009). While the HMN7B-associated G59S mutation induces misfolding and aggregation (Levy et al., 2006), the Perry syndrome mutations cause a loss of CAP-Gly function in cellular assays (Moughamian and Holzbaur, 2012). Together, these genetic findings indicate a key role for the CAP-Gly domain of dynactin in neurons *in vivo*.

In light of these observations, we sought to develop a minimal *in vitro* system to more fully test the mechanisms by which dynactin activates dynein. Our data provide direct evidence that the CAP-Gly domain of dynactin recruits dynein onto microtubules and maintains association of the motor with its track. Our findings demonstrate that dynactin accomplishes this by increasing the landing frequency of dynein and decreasing the likelihood of detachment by functioning as a dynamic tether. Surprisingly, the CAP-Gly

domain also acts as a brake to slow the dynein motor. We propose that these functions of dynactin become essential under specific cellular regimes, such as initiation of organelle transport in regions of the cell with low microtubule density, or maintenance of processive motility for cargos with few dynein motors bound, functions of particular importance in long distance cargo transport in neurons.

III. Results

Dynein-GFP switches between processive and diffusive motion

To study the regulation of dynein by dynactin, we employed single molecule approaches, using a recently established knock-in mouse line (Zhang et al., 2013) to isolate green fluorescent protein (GFP)-tagged dynein. The neuron-specific isoform of dynein intermediate chain, DIC1 is replaced with a DIC1–GFP–3xFLAG transgene under the control of the endogenous promoter (Fig. 2.1A). We purified GFP-labelled dynein from the brain tissue of these mice using microtubule affinity and ATP release followed by sucrose gradient centrifugation. DIC1–GFP incorporates efficiently into the dynein complex and interacts with copurifying dynactin (Fig. 2.1B). Photobleaching analysis indicates the expected stoichiometry of two DIC1–GFP per dynein complex (Fig. 2.1C, D).

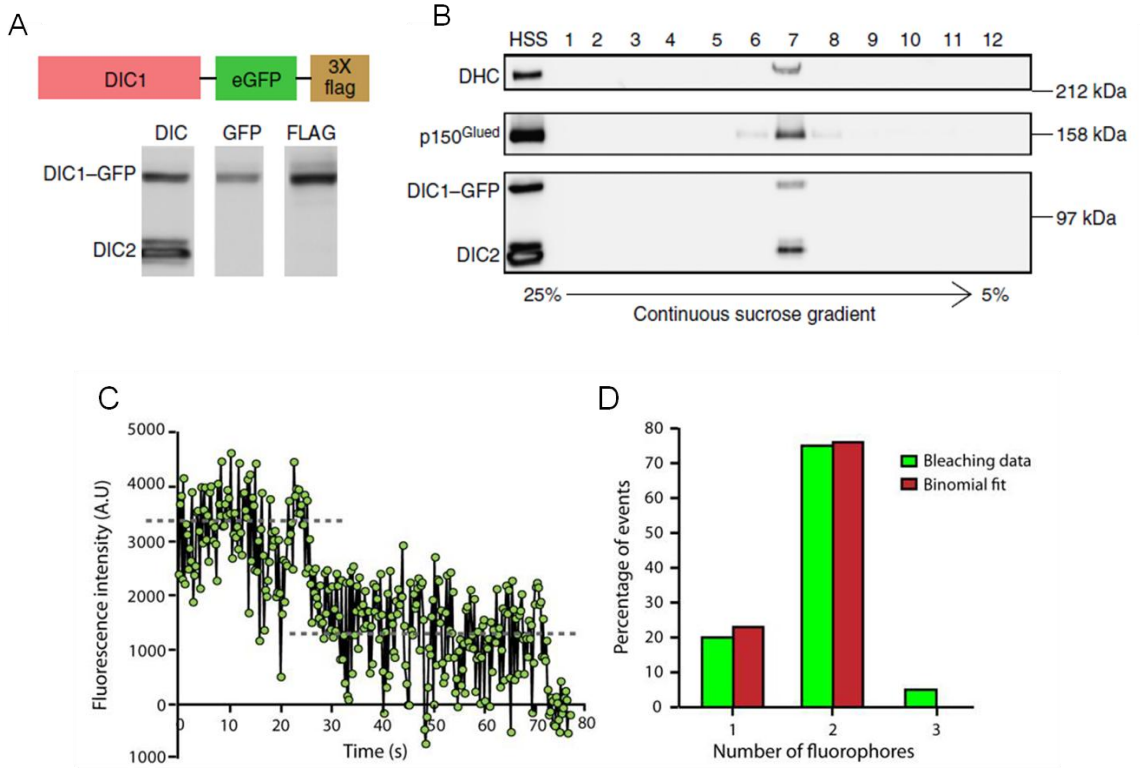

Figure 2.1 DIC1-GFP is efficiently incorporated into the dynein complex.

(A) Schematic of the DIC1–eGFP–FLAG gene knocked into the DIC1 locus. High speed supernatant (HSS) of homogenized mouse brain tissue was probed for DIC, GFP and FLAG. (B) Immunoblot analysis of sucrose gradient purified dynein. DIC1–GFP–FLAG is efficiently incorporated into the dynein complex as indicated by co-sedimentation with dynein heavy chain (DHC) at 20 S. (C) A representative time course of photobleaching showing two steps of decay. Grey lines indicate the steps. (D) Frequency distribution of the photobleaching steps for n=40 particles fit with a binomial distribution.

We performed gliding assays (Fig. 2.2A) and single molecule motility assays (Fig. 2.2B) to confirm that isolated dynein–dynactin complexes are functional. We observed processive, bi-directional ATP-dependent runs along the length of microtubules (Fig. 2.2C). These runs are punctuated by frequent directional switches as well as periods of apparent diffusion. While single dynein motors often diffuse along microtubules, two to three dyneins working together exhibit robust minus-end directed motility (Mallik et al., 2005; Ross et al., 2006) as supported by our gliding assays with isolated dynein–dynactin complexes (Fig. 2.2A). This behaviour may be a functional consequence of the flexible structure of the dynein motor, and may permit multiple dynein motors bound to a single cargo to function effectively in cells (Hendricks et al., 2012; Rai et al., 2013).

To examine the single molecule behaviour of dynein in more detail, we developed an algorithm (Gradient Analysis for Node Detection (GrAND)) to parse out these different states (see Methods). A given trajectory is first split into constant-velocity segments by gradient analysis and then mean-squared displacement (MSD) analysis is performed to classify each segment as processive or diffusive/confined. An example trajectory is shown in Fig. 2.2C. This trajectory was segmented using the GrAND method followed by MSD analysis, which indicated that the particle exhibited uniform processive motion in the first few seconds and

then switched to diffusion for the last few seconds of the track (Fig. 2.2C) We performed this analysis on all the particles tracked and obtained velocities and run lengths from all processive segments. The resulting data are well fit by a Gaussian distribution and a single exponential decay curve (Fig. 2.2D, E).

We also generated a frequency distribution for the fraction of time spent in processive state for all particles tracked (Fig. 2.3A). We observed that ~20% of the particles exhibited processive movement throughout their time bound to the microtubule. For the remainder of the particles, ~60% of their time bound to the microtubule was spent in a processive state; we did not observe a correlation between track duration and fraction of time spent in processive motion. To validate our method of analysis, we simulated particle motion using parameters from our experimental data (see Methods in this chapter) and tested our algorithm in three scenarios - purely diffusive motion, purely processive motion and a mix of diffusive and processive motion with a 50% probability for either type, using concatenated track segments to fully model the stochastic switching observed for dynein (Fig. 2.3B). Analysis of the simulated data indicated that our method was robust for fully processive motion. We observed a false-positive detection rate of ~20% for purely diffusive motion (Fig. 2.3C), that reduced to ~10% if we modeled continuous rather than segmented tracks. However, to more closely represent the motility of dynein, we focused on simulations with track segments (see Methods). Importantly, the intermediate condition of mixed motility was determined to be processive ~70% of the time, which is in close agreement with our experimental data.

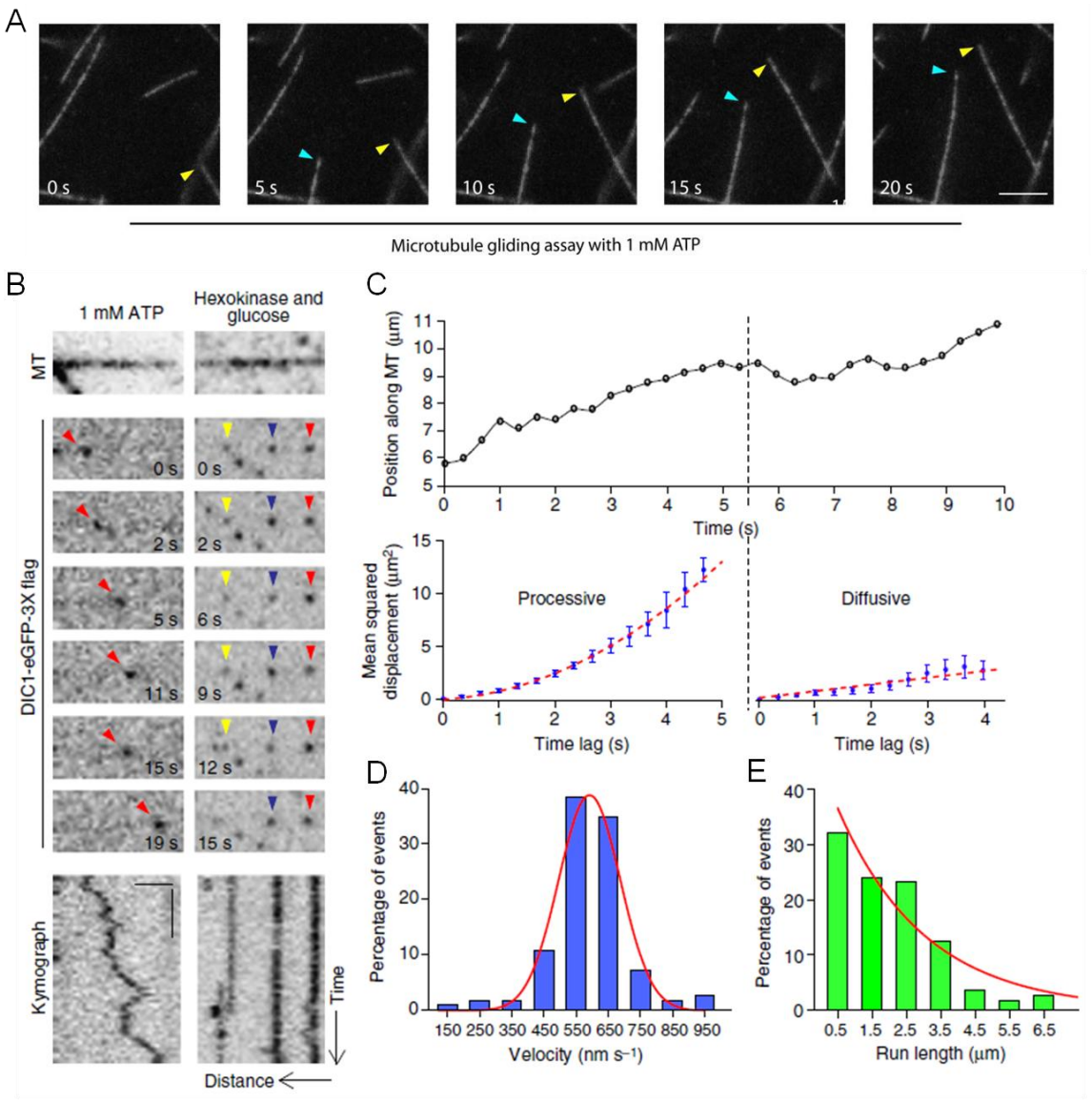

Figure 2.2 Dynein-GFP switches stochastically from processive to diffusive states of motion.

(A) Leading edges of two microtubules marked in a gliding assay with purified dynein. Scale bar, 5 µm. (B) Time series and corresponding kymograph showing projection of the movement of the particle over time for a single dynein–GFP molecule at 1mM Mg-ATP and in the presence of hexokinase and glucose (ATP depletion system). Horizontal bar, 2 µm.

Vertical bar, 5 s. All the images are contrast inverted to represent the signal as black on a white background. (C) A representative trajectory of a dynein–GFP molecule. Following gradient analysis for node detection (see Methods), mean-squared displacement (MSD) analysis shows that the motion switches from processive ($MSD=v^2t^2$) to a diffusive state ($MSD=2Dt$). Error bars indicate SEM. (D, E) Distributions of velocities and run lengths of particles tracked (n=112, three independent experiments). Curves represent a Gaussian distribution and an exponential decay curve respectively.

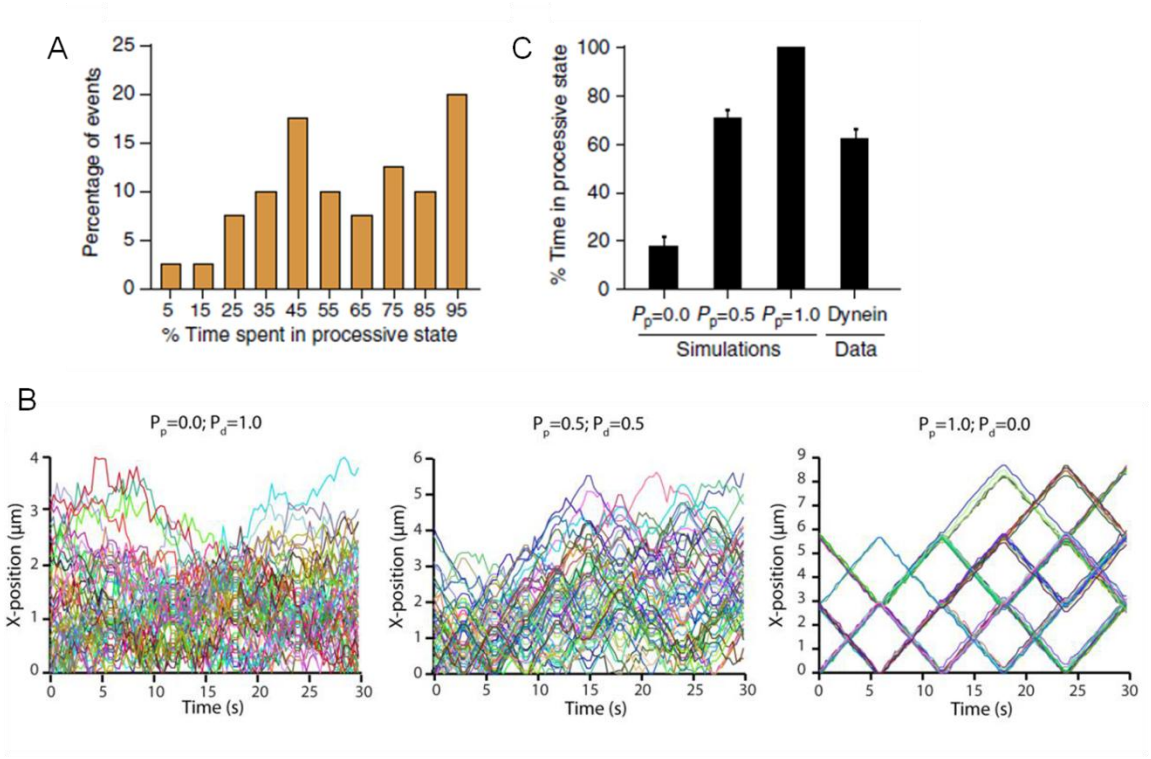

Figure 2.3 Simulations to validate our analysis.

(A) Frequency distribution for the amount of time the particles (n=40, two independent experiments) spent in a processive state. On average, about 60% of the time, the motion is processive. (B) 50 simulated tracks shown for 3 different conditions – purely diffusive motion ($P_p=0$, $P_d=1$), a mix of diffusion and processive motion ($P_p=0.5$, $P_d=0.5$) and fully processive

motion (P_p=1, P_d=0). (C) Quantitation of the per cent time spent in processive state for simulated tracks alongside the average for experimental data obtained from Fig. 2.3A. Mean ± SEM. n=50 for the simulations and n=40 for the experimental data.

p150^{Glued} enhances dynein recruitment onto microtubules

To dissect the role of dynactin in dynein-driven motility, we generated a recombinant human p150^{Glued} 1-CC1 construct fused to C-terminal Halo and FLAG tags, expressed and purified from insect cells. This construct includes the N-terminal tandem CAP-Gly and basic microtubule-binding domains followed by the first coiled-coil (CC1) domain that binds dynein (Fig. 2.4A, B). The 1-CC1 construct lacks the C-terminal domains of p150^{Glued} that mediate association with the Arp1 filament (Waterman et al., 1995) and which are not soluble when expressed recombinantly (Siglin et al., 2013 and our unpublished observations). We purified the construct using FLAG affinity chromatography followed by labelling with a tetramethylrhodamine (TMR) dye that binds irreversibly to the Halo tag (Fig. 2.4C). Single molecule assays on immobilized microtubules demonstrate microtubule-binding activity, with p150^{Glued} 1-CC1-TMR exhibiting lattice diffusion along the length of the microtubule (Fig. 2.4D). The 1-CC1 fragment of p150^{Glued} is sufficient to bind dynein (Fig. 2.4F).

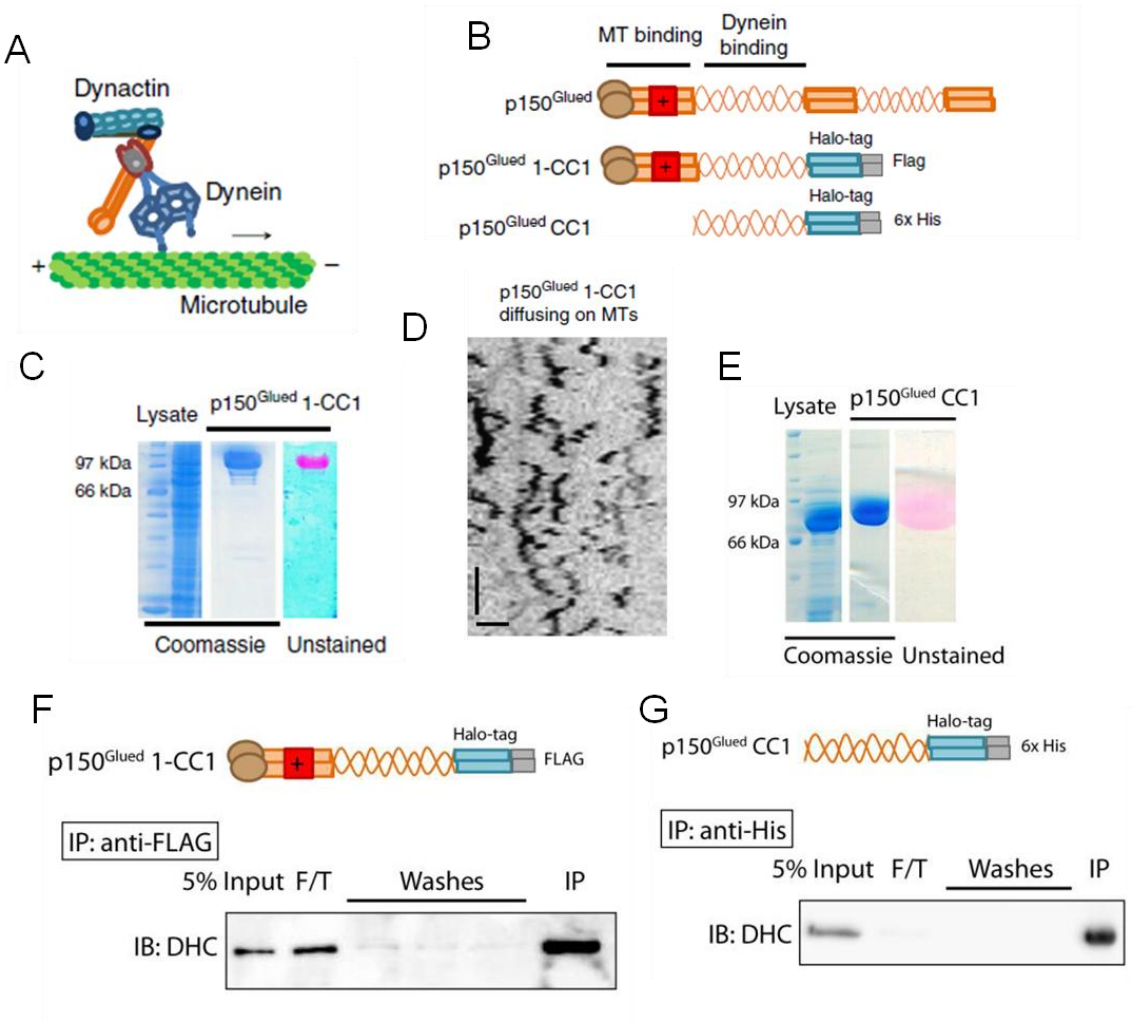

Figure 2.4 Generation of purified recombinant p150^{Glued} constructs.

(A) Schematic illustrating the interaction of dynein with dynactin. (B) Schematic of the recombinant constructs p150^{Glued} 1-CC1 and p150^{Glued} CC1 engineered with a Halo tag and affinity tags at the C terminus. (C) Coomassie-stained gel showing the lysate and the protein p150^{Glued} 1-CC1 after the final purification step. The unstained gel shows the labelling of the protein with TMR. (D) Contrast inverted kymograph of p150^{Glued} 1-CC1 diffusing on microtubules. Horizontal bar, 2 µm. Vertical bar, 5 s. (E) Coomassie stained gel showing the lysate and the protein p150^{Glued} CC1 after the final purification step. (F) Recombinant p150^{Glued} 1-CC1 binds to purified bovine dynein as shown by the immunoblot. The unstained

gel shows the labeling of the protein with TMR. (G) Recombinant p150^{Glued} CC1 binds to purified bovine dynein as shown by the immunoblot.

We next performed dual-colour imaging of dynein–GFP and p150^{Glued} 1-CC1-TMR on microtubules. Although isolated dynein–GFP co-purifies with dynactin (Fig. 2.1B), recombinant exogenously added p150^{Glued} 1-CC1-TMR was added in excess and effectively displaced endogenous dynactin as we observed colocalization (Fig. 2.5A) and co-migration of the co-complex (Fig 2.5B). The double-labelled dynein-GFP and 1-CC1-TMR complex exhibited both processive and diffusive motility along the microtubule, with a mean run length of 2.5 ± 0.13 mm (n=35), consistent with previous reports (Culver-Hanlon et al., 2006; Kardon et al., 2009). Importantly, in the presence of exogenous p150^{Glued} 1-CC1-TMR the recruitment of dynein molecules onto the microtubule was significantly enhanced (Fig. 2.5C), with a greater than 4-fold increase in binding events ($p<0.001$, Fig. 2.5C, D). To test whether the microtubule-binding activity of p150Glued was necessary for this increased recruitment, we generated a recombinant coiled-coil fragment (CC1-TMR) of p150^{Glued} that robustly binds to dynein (Fig. 2.4E, G) but lacks the N-terminal residues encoding both the CAP-Gly and basic domains (Fig. 2.4B). Addition of CC1-TMR did not affect dynein recruitment to the microtubule (Fig. 2.5C, D), indicating that the microtubule-binding domains of p150^{Glued} are required for the enhanced binding observed.

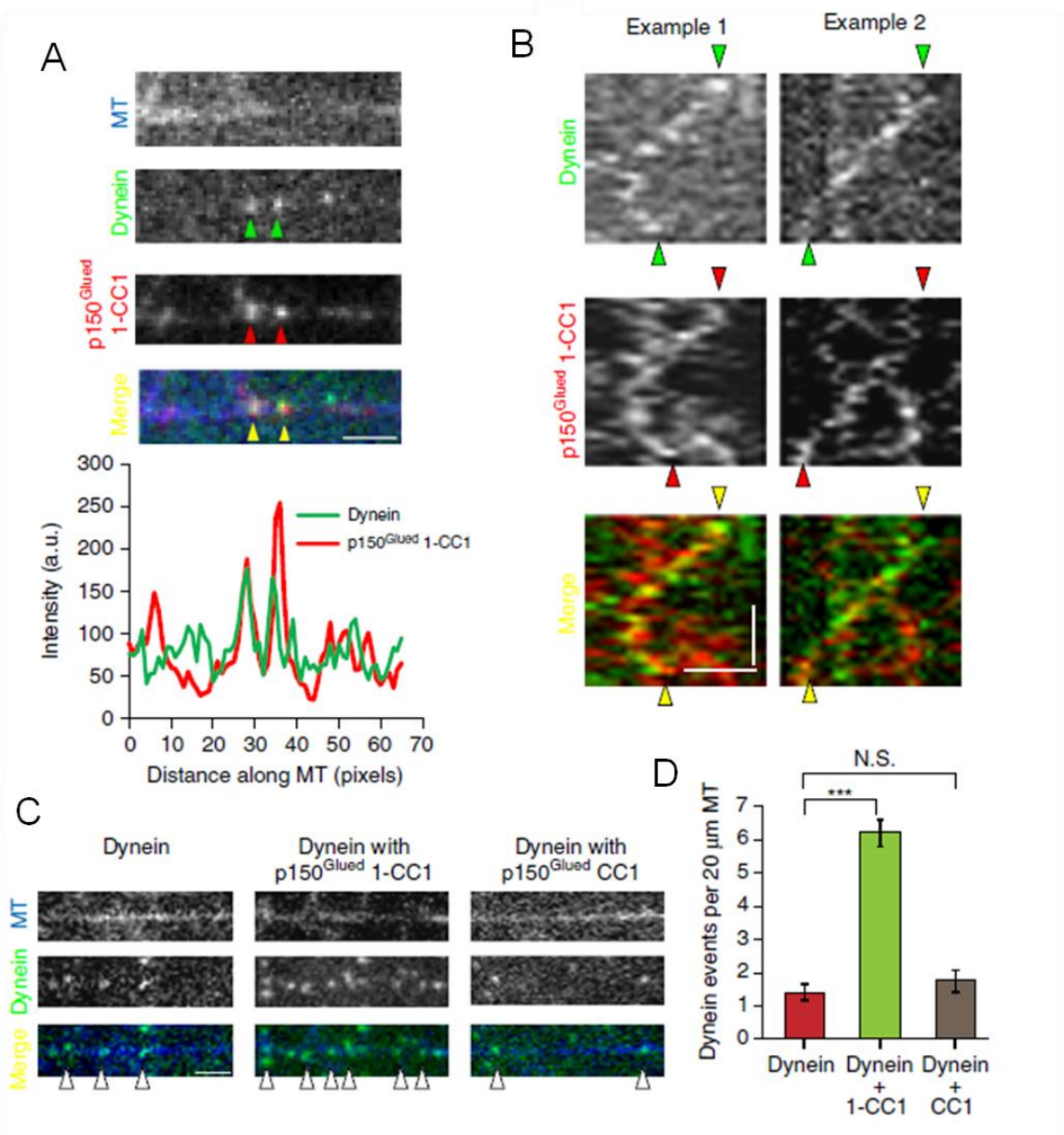

Figure 2.5 p150^{Glued} co-migrates with dynein and enhances its recruitment onto microtubules

(A) Co-localization of dynein and p150^{Glued} 1-CC1 on microtubules and corresponding line scan intensity profile. (B) Representative kymographs of co-migration of dynein with p150^{Glued} 1-CC1. Horizontal bar, 2 µm. Vertical bar, 10 s. (C) Addition of p150^{Glued} 1-CC1 increases the landing events of dynein while p150^{Glued} CC1 has no effect on the recruitment

of dynein. Horizontal bar, 2 μm. (D) Quantitation of the landing events of dynein in each condition shows that p150^{Glued} 1-CC1 increases the landing events greater than fourfold. Mean ± SEM, n=25, two independent experiments, ***p<0.001, one-way analysis of variance with Tukey's post-hoc test. Concentration of the recombinant protein used in each case is 4.5 nM. N.S., not significant.

p150^{Glued} regulates the dynein-microtubule interaction

p150^{Glued} 1-CC1 displayed a concentration-dependent effect on dynein. This is shown in the maximum-intensity projections over time of dynein–GFP motility along the microtubules (Fig. 2.6A). We quantified the per cent length of microtubules decorated by dynein–GFP in these projections and saw a progressive increase with increasing concentrations of p150^{Glued} 1-CC1 (Fig. 2.6B). This effect of p150^{Glued} 1-CC1 could be due to an increase in the landing frequency of dynein or a decrease in the rate of detachment of dynein from microtubules, or both effects could potentially contribute. To address this, we measured the landing frequencies of dynein–GFP in the absence and presence of 1-CC1, and observed a 2.5-fold increase induced by the p150^{Glued} construct (p<0.001, Fig. 2.6C). To test for an effect on detachment, we rigor bound dynein–GFP to microtubules in the absence of ATP, and then flowed 5 mM Mg-ATP into the chamber to release the motors (Huang et al., 2012). In the absence of 1-CC1, we observed rapid detachment of dynein induced by ATP. However, in the presence of p150^{Glued} 1-CC1, the dynein molecules remained bound to the microtubule for longer periods of time, suggesting that the motor is effectively tethered onto the microtubule via the microtubule-binding domains of dynactin at saturating ATP concentrations (Fig. 3D-F). Thus, we conclude that p150^{Glued} effectively recruits and retains dynein motors on microtubules by functioning as a dynamic tether.

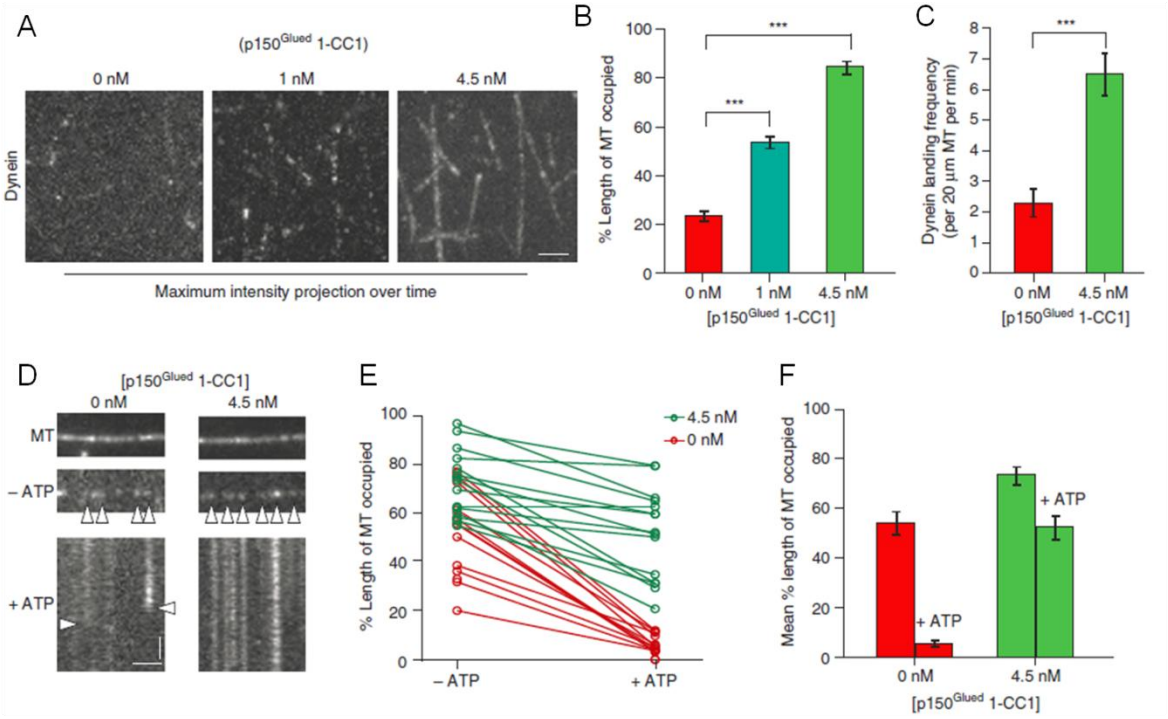

Figure 2.6 p150^{Glued} regulates the association and dissociation of dynein from microtubules.

(A) Maximum-intensity projection over time of dynein motility (movies recorded for 2 min) in the presence of p150^{Glued} 1-CC1. Horizontal bar, 2 µm. (B) Quantitation of the percent occupancy of microtubules using line-scan intensity analysis. Mean ± SEM, n=20, two independent experiments, ***p<0.001, one-way analysis of variance with Tukey's post-hoc test. (C) Addition of p150^{Glued} 1-CC1 increases the landing frequency of dynein. Mean ± SEM, n=20, two independent experiments, ***p<0.001, Student's t-test. (D) Representative images of dynein bound to microtubules in the absence of ATP and kymographs following 5 mM Mg-ATP wash. Horizontal bar, 2 µm. Vertical bar, 10 s. (E) Quantitation of the percent occupancy of microtubules before and after the ATP wash. The corresponding data points for the same microtubules before and after the ATP wash are connected by a line, n=15 for each condition, two independent experiments. (F) Average of the data shown in E. The control had a 10-fold change post ATP wash while the addition of p150^{Glued} 1-CC1 reduced the change to ~1.5-fold. ***P<0.001, Student's t-test.

Motility of p150^{Glued} in cell extracts is dynein-dependent

To further dissect the domains of p150^{Glued} that are critical for the regulation of dynein motility, we sought to develop a more versatile single molecule assay. We performed motility assays using Halo-tagged constructs expressed in cell extracts (Fig. 2.7A). Similar assays have been used extensively to study kinesin motors and their regulation (Blasius et al., 2007; Sun et al., 2011; Fu and Holzbaur; 2013) but have not yet been applied to the dynein motor to test the function of its adaptors and cofactors like dynactin.

We expressed p150^{Glued}-Halo in COS7 cells and co-precipitated extracts with HaloLink resin. p150^{Glued}-Halo was incorporated into dynactin, as assessed by co-precipitation of the endogenously expressed dynactin subunit, dynamitin (p50; Fig. 2.7B). Importantly, Halo-tagged p150^{Glued} co-precipitated both the heavy chain and intermediate chain of cytoplasmic dynein, indicating a robust interaction with endogenous dynein (Fig. 2.7B). Photobleaching analysis of the bound TMR ligand shows two decay steps and is well fit by a binomial distribution, consistent with the efficient dimerization of p150^{Glued} (Fig. 2.7C, D). We generated clarified cell extracts from COS7 cells expressing Halo-tagged p150^{Glued} constructs and performed single molecule assays tracking the motility of dynactin along microtubules (Fig. 2.7E). The observed motility closely resembled that observed for purified dynein–dynactin complexes characterized by frequent switches from processive to diffusive motion. The observed motility is ATP- and dynein-dependent, as it was arrested by depletion of ATP from the flow chamber by hexokinase and glucose (Fig. 2.7E) and significantly reduced by depletion of dynein heavy chain from the cells by siRNA (Fig. 2.7F, G).

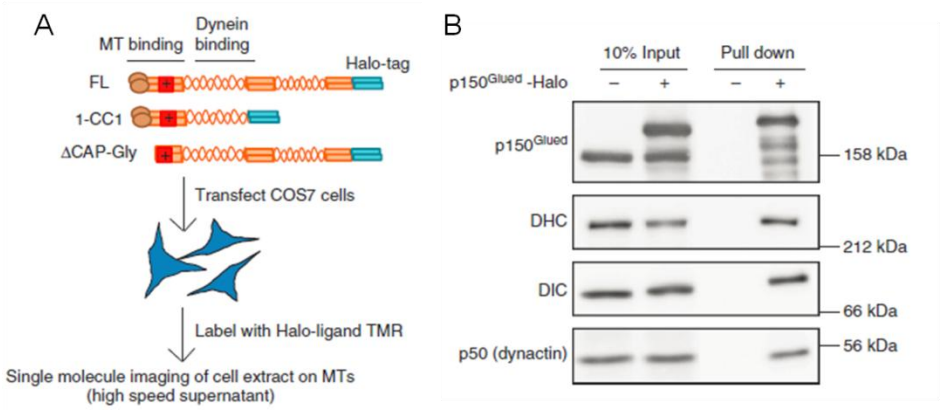
A
MT binding
Dynein binding
Halo-tag
FL
1-CC1
ΔCAP-Gly
Transfect COS7 cells
Label with Halo-ligand TMR
Single molecule imaging of cell extract on MTs (high speed supernatant)
B
10% Input
Pull down
p150Glued -Halo
p150Glued
DHC
DIC
p50 (dynactin)
158 kDa
212 kDa
66 kDa
56 kDa

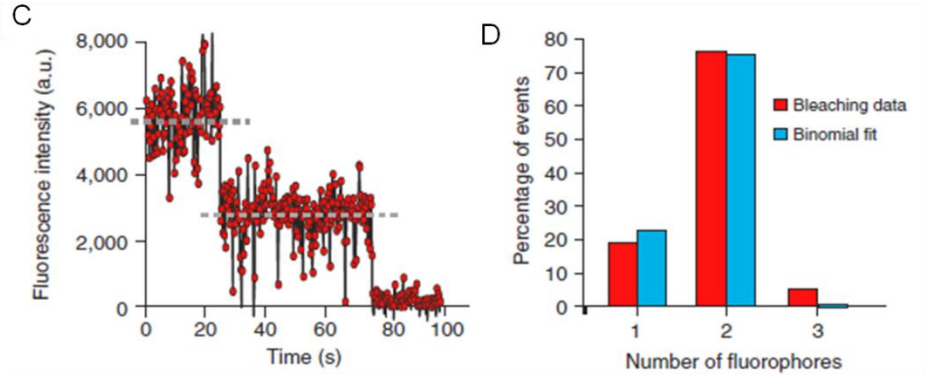
C
Fluorescence intensity (a.u.)
8,000
6,000
4,000
2,000
0
0
20
40
60
80
100
Time (s)
D
Percentage of events
80
70
60
50
40
30
20
10
0
Bleaching data
Binomial fit
1
2
3
Number of fluorophores

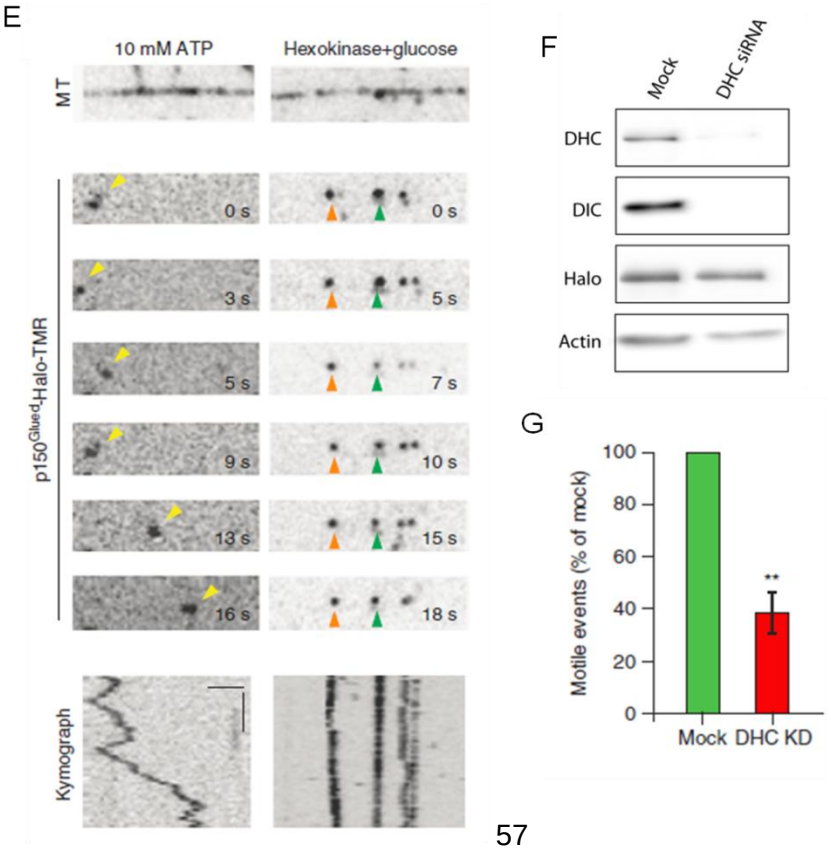
E
10 mM ATP
Hexokinase+glucose
MT
p150Glued-Halo-TMR
0 s
0 s
3 s
5 s
5 s
7 s
9 s
10 s
13 s
15 s
16 s
18 s
Kymograph
F
Mock
DHC siRNA
DHC
DIC
Halo
Actin
G
Motile events (% of mock)
100
80
60
40
20
0
**
Mock
DHC KD

Figure 2.7 The motility of p150^{Glued} in cell extracts is dynein-driven and ATP dependent.

(A) Schematic of the experimental design with an illustration of p150^{Glued} constructs. (B) COS7 cell extracts were precipitated with a HaloLink resin that binds specifically to the Halo tag. Protein complexes bound to the resin were analyzed by immunoblotting. The dynein complex co-precipitates with p150^{Glued}-Halo and the addition of the Halo tag at the C-terminus does not interfere with the incorporation of p150^{Glued} into the dynactin complex (as shown by p50). (C) A representative time course of photobleaching of TMR-labelled p150^{Glued} shows two decay steps. Grey lines indicate the steps. (D) Frequency distribution of the photobleaching steps for n=42 particles fit with a binomial distribution. (E) Representative time series and corresponding kymographs of the motility of p150^{Glued}-Halo in 10mM Mg-ATP and in the presence of hexokinase and glucose (an ATP depletion system). Horizontal bar, 2 µm. Vertical bar, 5 s. All images are contrast inverted. (F) Representative immunoblot of cell extracts from COS7 cells treated with Mock or DHC siRNA followed by transient transfection of p150^{Glued}-Halo. (G) Quantitation of the number of active, motile events of p150^{Glued}-Halo in the mock and dynein knock-down conditions. The number of events was normalized to the length of the microtubules and the expression levels of p150^{Glued}-Halo in extracts (densitometry analysis using ImageJ). DHC knockdown resulted in a reduction in the number of motile events. Mean ± SEM, n=3 experiments, **p<0.01, Student's t-test.

A representative trajectory parsed into segments using GrAND analysis along with the corresponding MSD analysis (Fig. 2.8A) shows that the motion switches from a confined/diffusive state to a processive state. We obtained velocities and run lengths for the processive segments of all particles tracked (Fig. 2.8B, C). The velocities obtained are comparable to those measured for isolated dynein–dynactin complexes (Fig. 2.8B compared to Fig. 2.2D). For particles that had at least one processive segment, we generated a

frequency distribution for the fraction of time spent in a processive state (Fig. 2.8D). In close agreement with the motility characteristics observed for isolated dynein–dynactin complexes (Fig. 2.3A), about ~20% of the p150^{Glued}-Halo-TMR particles tracked were processive throughout their motion along the microtubule while the remainder exhibited stochastic switching between processive and diffusive states. The average diffusion coefficient obtained from the diffusive phases was 0.055 μm^2/s, consistent with previous reports (Mallik et al., 2005; Culver-Hanlon et al., 2006; Ross et al., 2006) Together, these results indicate that we have established a robust assay to study the properties of the dynein motor in complex with its adaptor dynactin; this assay will be useful in exploring the effects of other dynein adaptors in future.

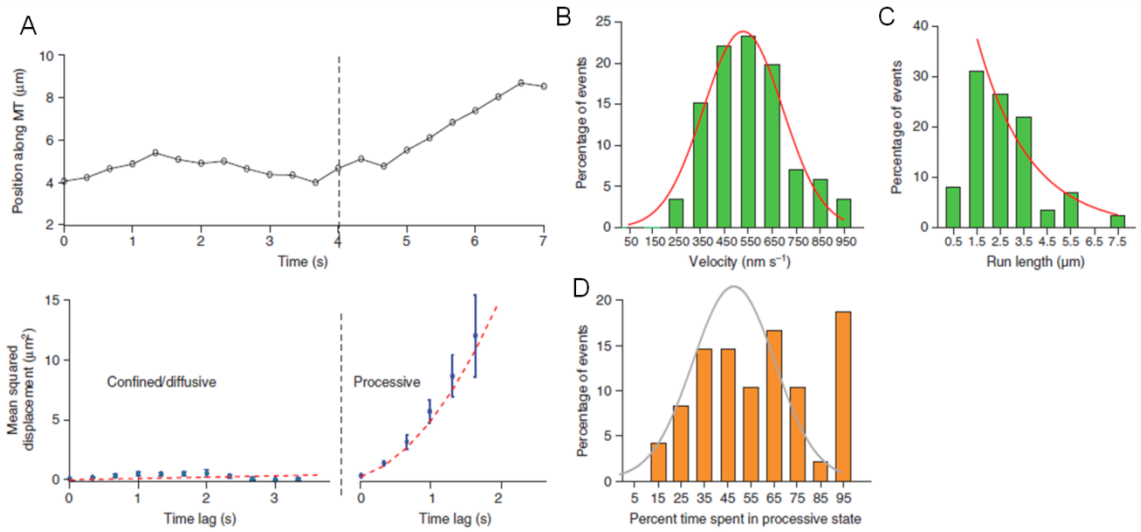

Figure 2.8 The motility of dynactin in cell extracts is similar to *in vitro* motility of purified dynein-GFP.

(A) A representative trajectory of p150^{Glued}-Halo with its corresponding MSD analysis. Error bars indicate SEM. (B, C) Velocity and run length distribution of the tracked p150^{Glued} particles. Tracks (n=60, three independent experiments) were parsed into processive and diffusive states of motion using GrAND and velocities were calculated for the processive

segments only. Curved lines indicate Gaussian and exponential decay fit, respectively. (D) Frequency distribution for the amount of time p150^{Glued}-Halo spent in a processive state. Two populations can be observed—about 20% that are processive throughout the motion along the microtubule and the remaining that display both processive and diffusive phases. A Gaussian fit (shown in grey) excluding the last data point improves the R^2 from 0.45 to 0.81, suggesting there could be two populations.

Using the cell extract assay, we asked whether the entire dynactin complex was required to increase the processivity of mammalian cytoplasmic dynein, as suggested by studies in a yeast strain lacking the Arp1 subunit of dynactin (Kardon et al., 2009), or whether the 1-CC1 construct of p150^{Glued} is sufficient to mediate these effects as suggested by our work with the purified recombinant fragment. p150^{Glued} 1-CC1-Halo expressed in COS7 cells extracts is sufficient to bind to dynein, but does not incorporate into the dynactin complex (Fig. 2.9A). However, the motility we observed with p150^{Glued} 1-CC1-Halo was indistinguishable from that observed with full-length p150^{Glued}, as shown in a representative trajectory in Fig. 2.9B. We observed no significant differences in the velocity or run length distribution (2.6 ± 0.15 µm for p150^{Glued} versus 2.1 ± 0.12 µm for p150^{Glued} 1-CC1) of the two constructs, or in the fraction of time spent in a processive state (Fig. 2.9C-E). These observations suggest that incorporation of p150^{Glued} into the dynactin complex does not affect velocity or further enhance run lengths of the motor complex. Thus, we focused on the specific functions of the microtubule-binding domains of p150^{Glued} in activating dynein using our cell extract assay.

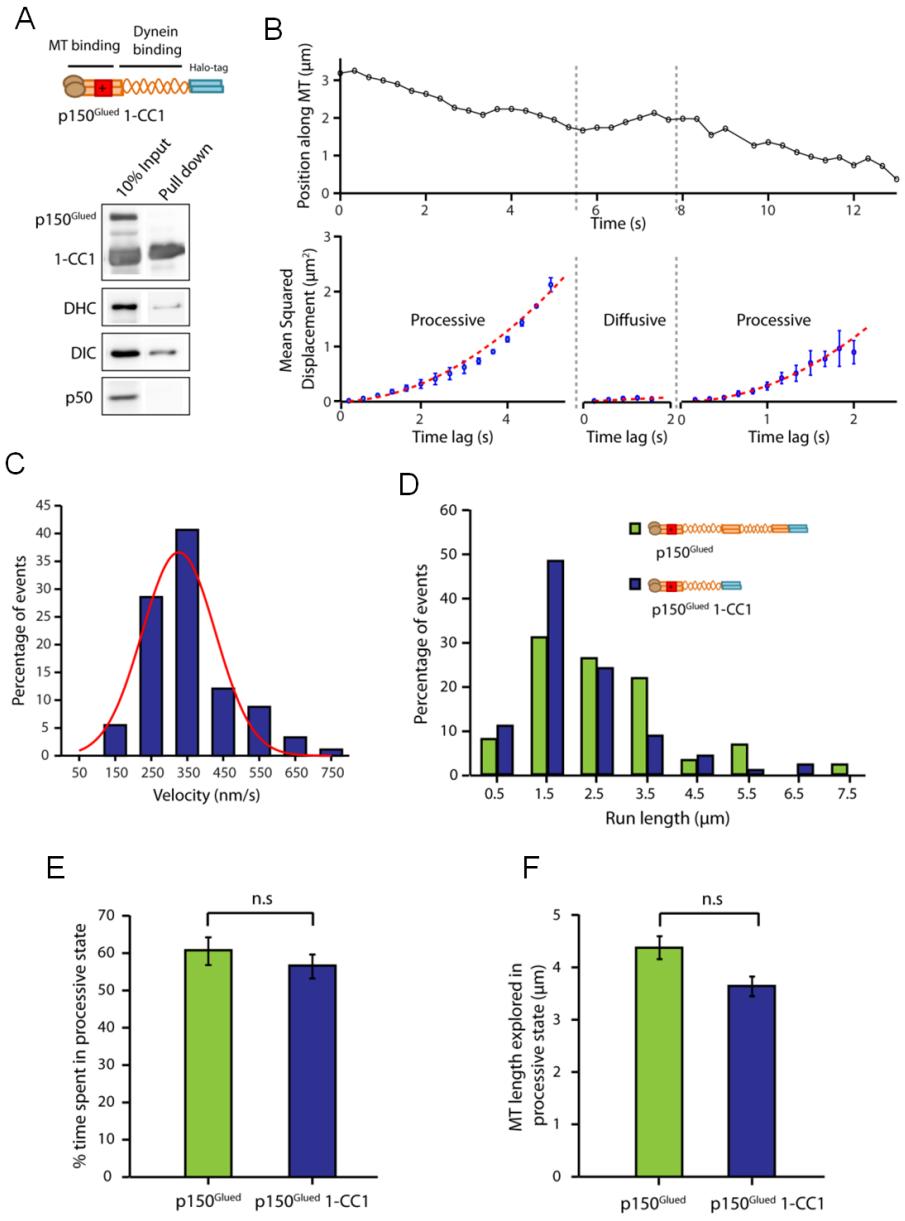

Figure 2.9 p150^{Glued} 1-CC1 shows motility characteristics similar to full length p150^{Glued}.

(A) COS7 extracts expressing p150^{Glued} 1-CC1-Halo were precipitated by the HaloLink resin. Immunoblot analysis shows the truncation does not affect the binding to dynein but inhibits incorporation into the dynactin complex (shown by p50). (B) An example trajectory of this construct and its MSD analysis. Error bars indicate SEM. The particle switches from

processive to diffusive state and switches back to processive again. (C and D) Velocity and run length distributions show no significant differences (Mann-Whitney U-test) between the $p150^{Glued}$ 1-CC1 and $p150^{Glued}$. (n=91 and 87 processive segments respectively obtained from 60 tracked particles each, 3 independent experiments). (E) A slight decrease was observed in the percent time spent in processive state for $p150^{Glued}$ 1-CC1 when compared to the full-length. Mean ± SEM, n.s., not significant, Student's t-test. (F) A similar trend was observed in the microtubule distance explored by the two constructs. Mean ± SEM, n.s., not significant, Student's t-test.

The CAP-Gly domain of dynactin enhances dynein engagement

Both the tandem CAP-Gly and basic domains in the N terminus of $p150^{Glued}$ interact with microtubules (Culver-Hanlon et al., 2006). To independently study the contribution of each of these domains to the motility of dynein, we compared the effects of two constructs—ΔCAP-Gly and Δ5-7. Δ5-7 is a naturally existing isoform of $p150^{Glued}$, which lacks three short exons (5, 6 and 7) and thus has a shorter basic domain compared with full-length $p150^{Glued}$ (Fig. 2.10A). Representative kymographs comparing the motility of the ΔCAP-Gly and Δ5-7 constructs with full-length $p150^{Glued}$ are shown in Fig. 2.10B. We observed no significant differences in the runs of the Δ5-7 isoform as compared with the full-length $p150^{Glued}$ (Fig. 2.10C, D, 2.1 ± 0.14 μm versus 2.6 ± 0.15 μm). In contrast, runs observed with the ΔCAP-Gly construct were significantly faster, approximately 2-fold the rates were observed with the other two constructs ($p<0.001$, Fig. 2.10C, E). Strikingly, binding times for the ΔCAP-Gly construct were extremely short. Histograms of time bound on microtubules for all particles tracked revealed that 70% of the ΔCAP-Gly particles were bound to microtubules for <10 s (Fig. 2.10G). Exponential decay fits to the cumulative frequency distribution curves for binding time of the full length, and ΔCAP-Gly constructs reveal a 3-fold higher detachment

rate in the absence of the CAP-Gly domain (Fig. 2.10F). Together, these data indicate that the CAP-Gly domain may function as an ATP-independent brake, as previously suggested from studies in which the CAP-Gly domain was non-specifically adsorbed to beads (Culver-Hanlon et al., 2006), and that this activity both prolongs the microtubule interaction time of the dynein–dynactin complex and slows the motor during processive motility.

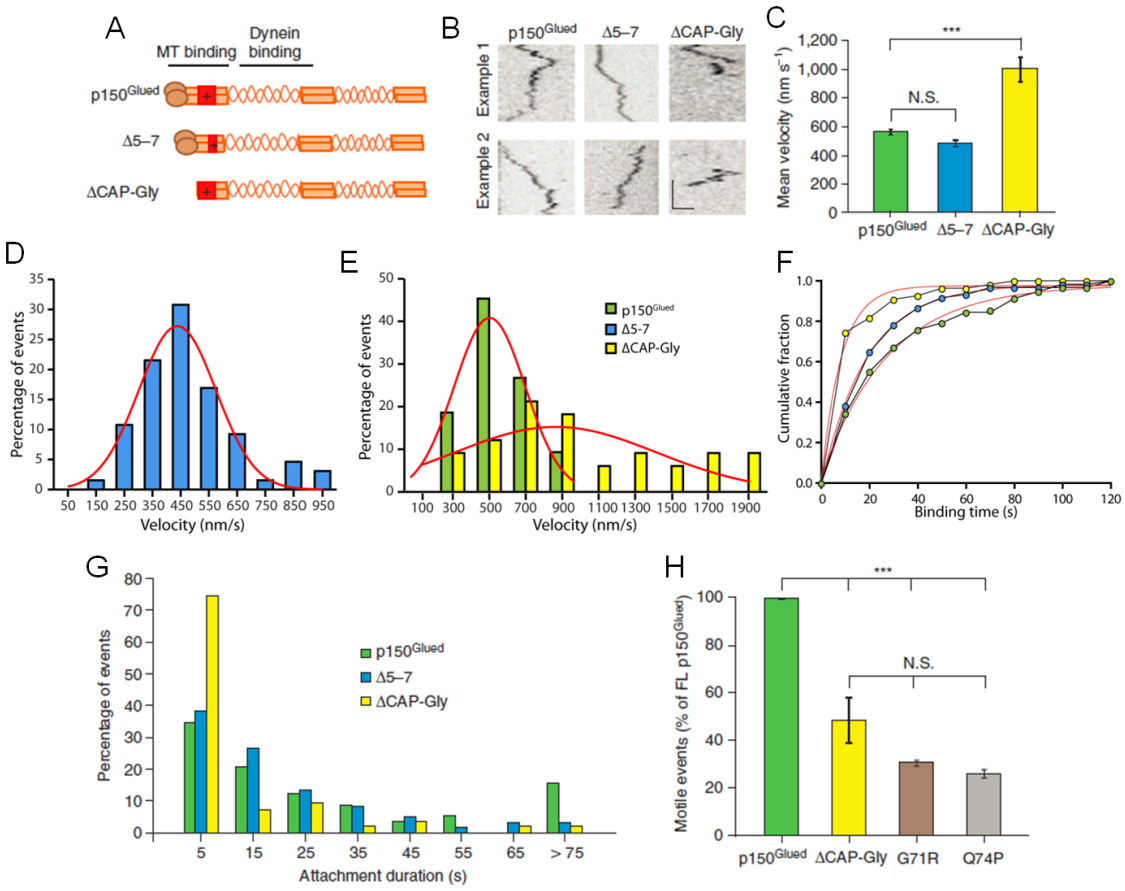

Figure 2.10 The CAP-Gly domain of dynactin enhances the engagement of dynein onto microtubules.

(A) Schematic of the Δ5-7 and Δ CAP-Gly constructs of p150^{Glued}. While the Δ5-7 lacks much of the basic domain, ΔCAP-Gly is a deletion of the CAP-Gly domain. (B) Representative kymographs of the motility of p150^{Glued}, Δ5-7 and ΔCAP-Gly constructs in complex with dynein along microtubules. Horizontal bar, 2 µm. Vertical bar, 5 s. Kymographs are contrast

inverted. (c) Mean velocities of all the particles tracked for $p150^{Glued}$, Δ5-7 and ΔCAP-Gly. Mean ± SEM, n=60 for $p150^{Glued}$ and Δ5-7, n=40 for ΔCAP-Gly, three independent experiments, ***p<0.001, one-way analysis of variance with Tukey's post-hoc test. (D) Velocity distribution of the all the Δ5-7 particles tracked (n=60, 3 independent experiments) (E) Velocity distributions of the ΔCAP-Gly (n=40, 3 independent experiments) in comparison to $p150^{Glued}$ (n=60, 3 independent experiments, same data as in Fig. 2.8B replotted for $p150^{Glued}$). (F) Cumulative frequency plots of the binding time of the 3 constructs. Data points are fit by a one-phase exponential decay (red) with a decay constant of k=0.035 ± 0.003 s-1 for $p150^{Glued}$, k=0.049 ± 0.002 s 1 for Δ5-7 and k=0.11 ± 0.021 s-1 for ΔCAP-Gly. This indicates that the the loss of CAP-Gly increases the detachment rate 3-fold. (G) Frequency distribution of the binding times of Δ5-7 and ΔCAP-Gly in comparison to $p150^{Glued}$ (same data as shown in Fig. 2.10F). Greater than 70% of the ΔCAP-Gly particles have a binding time of less than 10 s (n=60 for each, three independent experiments). (H) Quantitation of the number of active, motile events of the ΔCAP-Gly and the two mutants G71R and Q74P in comparison to the full-length $p150^{Glued}$. The number of events was normalized to the length of the microtubules and the expression levels of constructs in cell extracts (densitometry analysis using ImageJ). Mean ± SEM, n=3 independent experiments, ***p<0.001, one-way analysis of variance with Tukey's post-hoc test.

Multiple mutations in the CAP-Gly domain of $p150^{Glued}$ are causative for neurodegenerative diseases. A G59S mutation that lies at the core of the folded CAP-Gly domain induces misfolding and aggregation, leading to motor neuron-degeneration (Puls et al., 2003; Farrer et al., 2009). A series of nearby mutations that are surface-exposed within the microtubule-binding domain cause a distinct disease - a lethal variant of parkinsonism known as Perry syndrome. We examined two Perry-associated mutations, G71R and Q74P in our assay, and found that both mutations phenocopy the ΔCAP-Gly construct. All

constructs were expressed to a similar degree in our cell extracts but the G71R, Q74P and ΔCAP-Gly constructs all showed significantly decreased motile events as compared with full-length $p150^{Glued}$ (Fig. 2.10H). Together, these results indicate that the CAP-Gly domain has a dual effect. It promotes the sustained engagement of the motor on microtubules by acting as a tether, an activity abrogated by the Perry mutations. However, through its tethering activity, the CAP-Gly domain can induce a drag on dynein, acting as a brake to slow the motor during motility along the microtubule and this function could potentially be regulated in the cell.

IV. Discussion

Dynactin is a key adaptor for the cytoplasmic dynein motor and every organism that has cytoplasmic dynein has dynactin as well (Hammesfahr and Kollmar, 2012). Although a role for dynactin in increasing the processivity of dynein has been previously proposed, the functional significance of the microtubule-binding capacity of dynactin has remained controversial (King and Schroer, 2000; Ross et al., 2006; Kim et al., 2007; Dixit et al., 2008; Moore et al., 2009; Llyod et al., 2012; Moughamian and Holzbaur, 2012).

Here we used single molecule approaches and dual-colour total internal reflection fluorescence microscopy (TIRF) to definitively dissect the functional role that dynactin plays in dynein-driven motility. We isolated GFP tagged dynein from a knock-in mouse line and used purified recombinant $p150^{Glued}$ constructs to examine this problem. We found that dynactin significantly enhances the recruitment of dynein onto microtubules and the microtubule-binding capacity of dynactin is required for this recruitment. Dynactin increases the landing frequency and decreases the detachment rate of dynein from microtubules. We also demonstrate that in contrast to data from yeast (Kardon et al., 2009), the $p150^{Glued}$ C terminus is not required for this activity. Further dissection of the N terminus of $p150^{Glued}$ indicates that the CAP-Gly domain is key in promoting the sustained interaction of the dynein motor with microtubules. Importantly, point mutations in the CAP-Gly domain associated with Perry syndrome phenocopythe deletion of CAP-Gly in our assays. These in vitro observations are in strong agreement with recent studies in Drosophila and mammalian neurons, which demonstrated that the CAP-Gly domain of dynactin is important for the initiation of dynein-driven transport of cargos from the distal end of the axon and suggest that this function is perturbed in neurodegenerative disease (Llyod et al., 2012; Moughamian and Holzbaur, 2012).

Our results are strikingly different from the yeast dynein– dynactin system in that the microtubule-binding capacity of Nip100 (yeast homologue for $p150^{Glued}$ of dynactin) is dispensable in increasing the processivity of dynein (Kardon et al., 2009). There is also evidence for the lack of interaction of Nip100 with microtubules (Kardon et al., 2009), which is in contrast to the robust interaction of $p150^{Glued}$ with microtubules (Lazarus et al., 2013). Further, there is growing evidence that yeast dynein is fundamentally different from the mammalian dynein. Yeast dynein is a slower and stronger motor that takes occasional backward steps, while mammalian dynein is a weaker and faster motor with frequent backward runs and interspersed periods of diffusion (Mallik et al., 2004; Mallik et al., 2005; Reck-Peterson et al., 2006; Ross et al., 2006). Given these important differences, we suggest that the molecular mechanisms of dynactin described here have specifically evolved in higher eukaryotes.

Motor-driven transport involves three key steps—initial recruitment of the motor–cargo complex, transport along cytoskeleton tracks and the off-loading of the cargo at its destination. Thus, the question remains: what is the specific function of dynactin in dynein-driven transport? And is the function of dynactin regime-specific: single motor versus multiple motors; low load versus high load?

In small cells with bundled microtubules, the trafficking defects caused by $p150^{Glued}$ knockdown can be rescued with a construct lacking the microtubule-binding domain (Kim et al., 2007; Dixit et al., 2008). Trafficking of organelles along the stable and densely packed microtubules of the axon shaft also does not require the CAP-Gly domain (Moughamian and Holzbaur, 2012). However, for other cellular functions, the CAP-Gly domain is required (Kim et al., 2007; Moore et al., 2009). Thus, we propose that the CAP-Gly domain of dynactin becomes essential in specific instances of dynein-driven transport (Fig. 2.11). We propose three specific cases where the microtubule-binding capacity of dynactin is necessary to

enhance dynein function: (1) For small cargoes with very few dynein motors, dynactin can actively maintain an interaction with the microtubule during detachment of both dynein heads leading to sustained motility. (2) For large cargoes which generate a high load for the motors, the CAP-Gly domain enhances the ability of dynein to produce movement. (3) Transport of cargos along individual, dynamic microtubules (Lomakin et al., 2009) such as those in the axon terminal as opposed to stable, densely packed or bundled microtubules. Importantly, initial recruitment of dynein motor– cargo complex often occurs near the cell periphery where highly dynamic microtubule plus ends are enriched.

Given the dynamic and crowded cellular environment, all of these are regimes in which the dynein motor must work effectively. Thus, our results converge to a model wherein dynactin is required for the recruitment of the dynein motor onto microtubules for efficient initiation of transport and further, the CAP-Gly domain of dynactin functions as both tether and brake to promote the engagement of dynein on the microtubule.

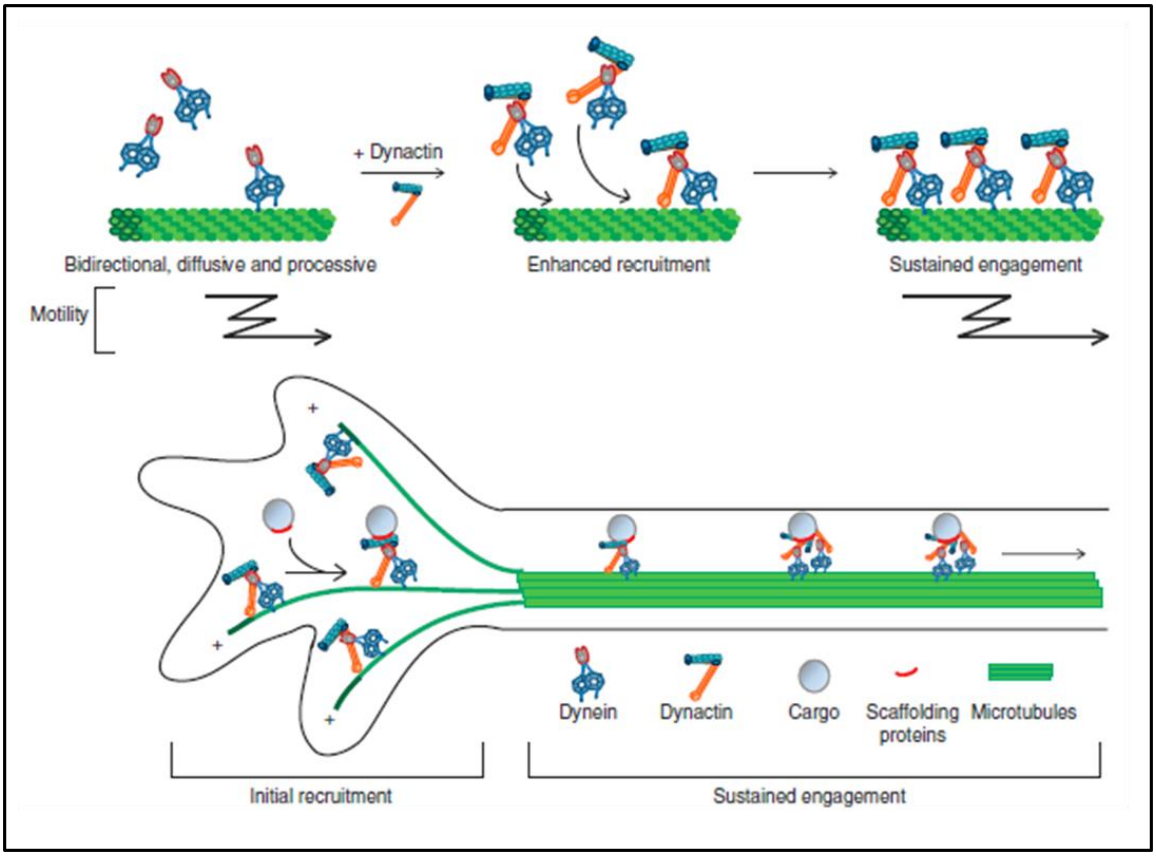

Figure 2.11 Model depicting the roles of dynactin in dynein-driven transport.

Model for the regulation of dynein by dynactin depicting two functions of dynactin—initial recruitment at the start of retrograde transport and sustained engagement of the dynein motor with the cytoskeletal tracks.

V. Material and Methods

Reagents

Cytoplasmic dynein was purified from mice (Mus musculus) that are homozygous knock-in for DIC1 replaced with DIC1–eGFP–3X FLAG. All animal protocols were approved by the Institutional Animal Care and Use Committee (IACUC) at the University of Pennsylvania. Both male and female young adult mice (4–8 months old) were used.

All $p150^{Glued}$ constructs were generated from the human DCTN1 sequence (GenBank accession number NM_004082). The Halo tag from the pHTC Halo tag CMV-neo vector (Promega) was fused in-frame to the C terminus of the $p150^{Glued}$ constructs and cloned into pcDNA3 vector. DNA constructs encoding the Perry syndrome point mutations were obtained from M. Farrer. $p150^{Glued}$ 1-CC1 includes amino acid residues up to Q547 and the ΔCAP-Gly construct starts from K115.

Monoclonal antibodies to p150 (610474, 1:5,000), p50 (611003, 1:1,000) and β-catenin (610153, 1:5,000) were from BD Transduction Laboratories, monoclonal antibodies to actin (1501R, 1:10,000); and DIC (MAB1618, 1:1,000) were from Millipore; and monoclonal antibody to Halo tag (G9211, 1:1,000) was from Promega. A polyclonal antibody to dynein heavy chain (R-325, 1:250) was from Santa Cruz. For binding experiments, monoclonal antibody to FLAG (clone M2, 1:10) from Sigma and monoclonal tetra-His antibody from Qiagen (34670, 1:10) were used. For RNA interference (RNAi) knockdown of dynein, 50nM of the short interfering RNA (siRNA) duplex (Dharmacon) against human dynein heavy chain (GenBank accession number NM_001376; 50-GAGAGGAGGUUAUGUUUAAUU-30) was used.

Protein purification and binding assays

Cytoplasmic dynein was purified from brain tissue from adult mice by microtubule affinity and ATP release, followed by sucrose density gradient centrifugation as described. Briefly, adult mouse brain tissue was homogenized at 1:1 weight/volume in chilled motility assay buffer (10 mM PIPES, 50 mM potassium acetate, 4 mM MgCl2, 1 mM EGTA, pH 7.0 with KOH) with 1 mM dithiothreitol (DTT), 0.5 mM Mg-ATP and protease inhibitors (2 mM phenylmethylsulfonyl fluoride, 0.02 mg/ml Tosyl arginine methyl ester (TAME), 0.02 mg/ml leupeptin, 0.002 mg/ml pepistatin-A). Hexokinase (1Uml/1) and 1mg/ml glucose were used for microtubule affinity and 20 mM Mg-ATP was used for microtubule release. The supernatant from the microtubule release was fractionated on a 5–25% continuous sucrose density gradient and 1ml fractions were collected and analyzed by SDS–PAGE and Western blotting.

$p150^{Glued}$ 1-CC1-Halo-Flag (amino acids 1–547 of DCTN1, NM_004082) was expressed in Sf9 cells using baculovirus following standard methods. After harvest, cells were lysed in Buffer A (Tris-buffered saline supplemented with 200 mM NaCl, 10% glycerol, 0.5% igepal, 0.01 mg/ml TAME, 0.01 mg/ml leupeptin and 1 mM PMSF) in a Dounce homogenizer. After clarification, protein was captured on an M2 agarose column (Sigma), and further purified on a MonoS column (GE Healthcare) with buffer A as above and buffer B as Tris-buffered saline supplemented with 10% glycerol and 1M KCl. Peak fractions were incubated with Halo tag TMR Ligand (Promega) overnight at $4^{o}C$, then separated from unreacted dye on a Superdex column (GE Healthcare) in BRB80 (80 mM PIPES, 1 mM MgCl2, 1 mM EGTA, pH 6.8 with KOH) supplemented with 200 mM KCl and 10% glycerol. Peak fractions were combined, aliquoted and flash frozen and stored in liquid nitrogen.

$p150^{Glued}$ CC1-Halo-6xHis (amino acids 216–547 of DCTN1, NM_004082) was inserted into pET-29b (Novagen). For expression, transformed Rosetta E.coli (Novagen)

were grown in LB at 37^{o}C at 325 r.p.m. under standard kanamycin selection. At OD_{600} ~0.7, cultures were transferred to 25^{o}C and induced with 0.5 mM isopropyl-b-D-thiogalactoside. After 16 h, cells were harvested and resuspended in His-binding buffer (500 mM NaCl, 20 mM Tris-HCl, pH 7.8, 15 mM imidazole, 1 mM Tris (2-carboxyethyl) phosphine hydrochloride (TCEP), 0.01 mg/ ml TAME, 0.01 mg/ml leupeptin, and 1mM PMSF). Cells were then lysed by French press (Thermo) at 18,000 psi followed by DNAse I and RNAse H treatment (Roche). The lysate was clarified at 45,000 g for 20 min at 4^{o}C. The supernatant was filtered and loaded onto a 1 ml HisTrap column (GE Healthcare) by fast protein liquid chromatography. The column was washed with binding buffer and then eluted with binding buffer supplemented with 0.5 M imidazole. The peak fraction was incubated overnight a 4^{o}C with 5 mM TMR ligand. The protein was run on a Superdex column (GE Healthcare) pre-equilibrated with BRB80 supplemented with 200 mM KCl and 10% glycerol. Peak fractions were combined, aliquoted, flash frozen and stored in liquid nitrogen.

Binding assays of purified proteins ($p150^{Glued}$ 1-CC1 and $p150^{Glued}$ CC1) with dynein was performed by first incubating the proteins with protein G dynabeads (Life Technologies) coated with either anti-FLAG antibody or anti-His antibody, followed by the addition of dynein purified from bovine brain supplemented with 1 mg/ml bovine serum albumin. The proteins were eluted off the beads in denaturing buffer and the presence of dynein in the eluate was assayed by Western blot.

Cell culture, transfections and pull downs

COS7 cells (ATCC, CRL-1651) were cultured in DMEM with glutamax and 10% foetal bovine serum. Cells were transiently transfected with Fugene 6 (Roche) according to manufacturer's instructions; cells were harvested 18–24 h post transfection. For RNAi knockdown, cells were transfected with siRNA duplexes using Lipofectamine RNAiMax (Invitrogen) with optimal knockdown obtained between 40 and 48 h. Immunoblots for knock-

down experiments were analyzed by densitometry using ImageJ (NIH). For pull down assays using HaloLink resin (Promega), cells were lysed in 50 mM HEPES, 25 mM NaCl, 1 mM EDTA, 1 mM $MgCl_2$, pH 7.0 with 1 mM DTT, 0.5% triton X-100 and protease inhibitors (1 mM PMSF, 0.01 mg/ml TAME, 0.01 mg/ml leupeptin and 0.001 mg/ml pepistatin-A). Lysates were incubated with the resin for 2 h at 4^{o}C and washed according to the manufacturer's instructions. Precipitated proteins were analyzed by SDS–PAGE and Western Blotting.

Single molecule motility assays

Motility assays were performed in flow chambers made with glass slides and silanized (PlusOne Repel Silane, GE Healthcare) coverslips attached together using adhesive tape, forming a chamber with a volume of 10 ml. There was a 5 min incubation time between each solution that was flowed into the chamber. The chamber was first incubated with 10 ml of 1:50 dilution of the monoclonal anti-tubulin antibody (Sigma), then blocked with two chamber volumes of 5% pluronic F-127 (sigma). Labelled (either Rhodamine or Alexa 488) taxol-stabilized microtubules were flowed into the chamber and allowed to bind to the anti-tubulin antibody. Finally, purified protein or cell extract was flowed in with Mg-ATP (1 mM for purified proteins and 10mM for cell extract), 1mg/ml bovine serum albumin, 1 mg/ ml casein, 20 mM taxol, 1 mM DTT and an oxygen scavenging system (Schroeder et al., 2012). For photobleaching experiments ATP was depleted with 1U/ml hexokinase and 1mg/ml glucose and the oxygen scavenging system was omitted to allow for complete photobleaching. For motility assays with dynein–GFP and purified $p150^{Glued}$ 1-CC1-TMR, dynein was incubated with $p150^{Glued}$ 1-CC1 for 5min at room temperature for co-complex formation before flowing into the chamber. For all co-migration experiments, 7-amino-4-methyl coumarin-3-acetic acid (AMCA)-labelled tubulin (cytoskeleton) was used to prepare taxol-stabilized microtubules.

For motility assays with cell extracts, COS7 cells 18–24 h post transfection were incubated with Halo ligand TMR (Promega) following manufacturer's instructions. The cells were then lysed in 40 mM HEPES, 1 mM EDTA, 120 mM NaCl, 0.1% Triton X-100, 1 mM Mg-ATP supplemented with protease inhibitors (same as above). The lysate was clarified by centrifugation at 1,000 g first and then 100,000 g. The extract was diluted in P12 buffer (12 mM PIPES, 1 mM EGTA, 2 mM $MgCl_2$, pH 6.8) right before perfusion into the flow chamber. For a 70–80% confluent 6 cm plate, cells were lysed in 50 ml lysis buffer, which was then diluted 1:100 for single molecule imaging.

All movies were acquired at room temperature at 3 or 10 frames per second as noted, except for dual-colour co-migration experiments that was imaged at 1 frame per second, using a Nikon TIRF system (Perkin Elmer) on an inverted Ti microscope with the 100X objective and an ImagEM C9100-13 camera (Hamamatsu Photonics) controlled by Volocity software.

Particle tracking and data analysis

Particle tracking was performed using the TrackMate plugin in Fiji (Schindelin et al., 2012). Particles that ran into other adjacent particles, hit the microtubule ends repeatedly or were on microtubule bundles, were excluded from analysis. Only particles with trajectories that could be clearly visualized were tracked and analyzed, and each track detected by TrackMate was confirmed by visual inspection. The tracking resolution was determined to be 36 nm, obtained from the standard deviation of the tracking of stationary particles on microtubules.

As the motility of dynein frequently switches from processive to diffusive states, we developed a new algorithm, GrAND to parse these states within a given track. Each track was split into stationary and non-stationary segments using approximately three times the tracking error (100 nm) as a threshold. The non-stationary segments were then smoothed

using the locally weighted scatterplot smoothing ('lowess') function in MATLAB with the span (smoothing window) set to 20% of the track length. Twenty per cent was determined to be optimum for our acquisition rates and track lengths. The slope at each point of the smoothed track was obtained (gradient analysis) and points of zero slope were identified as nodes. These nodes are points dividing a given trajectory into smaller segments of constant velocity. Smoothing is done only to identify the nodes for a given track and all further analysis is done on raw data. Once the nodes were identified, MSD analysis was performed on the individual segments to classify them as processive or diffusive. Velocity and run length measurements were obtained for the processive segments only.

Simulations

To validate our GrAND method, we simulated tracks using parameters from our experimental data. These parameters include temporal resolution (3 frames per second), track duration (30 s - average track length of the dynein-GFP particles tracked), velocity (550 nm/s), diffusion coefficient (0.055 $\mu m^2/s$) and noise (Gaussian distribution with mean $\mu=0$, standard deviation $\sigma=100$ nm (3x tracking error)).

The inputs to the simulation include probability of diffusion (P_d) and processive (P_p) motions such that $P_d + P_p = 1$. These probabilities indicate the fraction of time spent in diffusive and processive motion, respectively. For example, a particle in a track with a duration of 30 s (90 frames) having $P_d = 2/3$ and $P_p = 1/3$ would spend 20 s (60 frames) and 10 s (30 frames) in diffusive and processive motions, respectively. Since the motion of dynein frequently involves segments of processive motion interspersed with segments of diffusion, we first generated either diffusive or processive segments, which are then concatenated randomly to generate the whole track. In each case, the number of segments was set to five. For processive segments, the particle displacement is given by $x = v \times \Delta t$.

For diffusive segments, the displacements were obtained from a normal distribution with $\mu = 0$, σ = square root (2 x D x Δt) nm.

Photobleaching analysis

To prevent dissociation of the particles from microtubules, data from motility assays in the presence of hexokinase and glucose were used to analyze photobleaching. Only particles bound to microtubules were analyzed. A 5x5 pixel region of interest was drawn around the particle and the intensity was recorded from each frame using the Plot Profile in FIJI. Another 5x5 pixel region of interest was drawn in the vicinity of the particle to record the background intensity. For each frame, the background was subtracted and the intensity was plotted with time to determine the number of bleaching steps.

Landing events

The dynein concentration was kept constant across experiments comparing different conditions (Figs 2.5 and 2.6). To measure the number of landing events for dynein in the presence of $p150^{Glued}$ 1-CC1, microtubules were randomly chosen from the centre of TIRF field and particles on the microtubules were scored by line-scan intensity analysis. Distinct and clear particles on the microtubules showed up as peaks in the intensity profile corrected for background (background intensity was obtained by drawing a line in the vicinity of the microtubule and recording the intensity). Each peak was visually inspected for the presence of a particle. The length of microtubules occupied was determined from the maximumintensity projection over time of dynein in a similar way. Only intensities at least 10% above background were scored as occupied. In each case, the data was normalized to the length of the microtubule. For dynein landing frequency measurements in Fig. 2.6, microtubules in the TIRF field were scored for motile events by kymograph analysis using Multiple Kymograph plugin in FIJI. For Fig. 2.6E, microtubules were randomly chosen in

each condition and for each microtubule the dynein–GFP intensity was recorded before and after the ATP wash. The intensities were recorded by the line-scan intensity analysis in FIJI.

Extracts from cells showing >85% dynein knockdown, as determined by densitometry analysis with ImageJ, were analyzed to test the dependence of $p150^{Glued}$ motility on dynein. To measure landing events (Figs 2.7G and 2.10H), microtubules in the TIRF field were scored for motile events by kymograph analysis using Multiple Kymograph plugin in FIJI. The number of events was normalized to the length of the microtubules and the expression levels of $p150^{Glued}$-Halo were quantified by densitometry analysis using ImageJ (NIH).

Statistical methods

All statistics were performed in GraphPad Prism. Student's t-test was used when comparing two data sets while one-way analysis of variance with Tukey's *post-hoc* test was used with multiple data sets.

CHAPTER 3: OPTOGENETIC CONTROL OF ORGANELLE TRANSPORT USING A PHOTOCAGED CHEMICAL INDUCER OF DIMERIZATION

This chapter is adapted from:

Ballister, E.R., Ayloo, S., Chenoweth, D.M., Lampson, M.A., Holzbaur, E.L.F (2015). Optogenetic control of organelle transport using a photocaged chemical inducer of dimerization

Current Biology 25:R407-R408

Contributions: I performed all the neuronal experiments, Ed Ballister performed all the HeLa cell experiments. Dave Chenoweth provided new reagents. Ed and I analyzed data and wrote the chapter.

I. Summary

Dynamic protein interactions and protein localization are fundamental to several cellular processes. Chemically induced dimerization is a powerful technique to control protein localization. However, chemically induced dimerization does not provide the ability to spatially control protein interactions. More recently, light-induced dimerization systems have been developed which allow cellular perturbations with spatiotemporal precision. In this chapter, we apply a recently developed light-induced dimerization system to recruit motor proteins to specific organelles within the cell to examine effects on motility. We focus on kinesin-1 and dynein and demonstrate that recruitment of either motor induces robust motility of the organelle. In neurons, recruitment of motors to axonal peroxisomes induced robust anterograde motion with kinesin-1 and retrograde motion with dynein. In contrast, recruitment of motors to mitochondria had differential effects from peroxisomes indicating organelle-dependent regulation of motors. Our work highlights the different ways in which we can apply the light-inducible dimerization system to probe biological processes.

II. Introduction

Cell polarity, growth and signaling require organelle transport by cytoskeletal motor proteins that are precisely regulated in time and space. Probing these complex, dynamic processes requires experimental techniques with comparable temporal and spatial precision. Inducible dimerization offers the ability to recruit motor proteins to organelles in living cells. Approaches include rapamycin-induced dimerization of motors and cargo-bound binding partners (Kapitein et al., 2010) or the recent application of the TULIP light-inducible dimerization system (Strickland et al., 2012; van Bergeijk et al., 2015). In the latter system, motor recruitment is activated by blue light, and relaxes to an OFF state in the dark within seconds. While rapid relaxation is desirable for some applications, many experiments require sustained motor recruitment. Here, we use a photocaged chemical dimerizer to achieve sustained, spatially-defined motor recruitment to individual organelles with a single pulse of light. We demonstrate the general applicability of the system by recruiting microtubule plus end-directed kinesin-1 and minus end-directed dynein motors to peroxisomes and mitochondria in HeLa cells and primary neurons, leading to alterations in organelle transport on timescales from <10 seconds to >10 minutes after photoactivation.

III. Results

We recently developed a photoactivatable chemical dimerizer, cTMP–Htag, a synthetic small molecule comprising a Halotag ligand linked to photocaged trimethoprim (TMP). This molecule is designed to heterodimerize Halotag (Halo) and *Escherichia coli* DHFR (eDHFR) fusion proteins (Ballister et al., 2014). Here we use light to recruit eDHFR-tagged molecular motors or motor effectors to specific organelles. cTMP–Htag is cell permeable and covalently binds the Halotag protein, which we localized to the cytosolic surface of either peroxisomes or mitochondria (Kapitein et al., 2010; Ballister et al., 2014). While photocaged, TMP does not bind eDHFR. Uncaging with a pulse of ~400 nm light recruits eDHFR-fusions to the organelle surface (Fig. 3.1A). Photoactivation is spatially restricted to the illuminated organelle since uncaged TMP remains covalently tethered to the Halotag anchor. TMP–eDHFR binding is noncovalent, so individual motor–eDHFR proteins may bind and release, but at steady state the interaction sustains robust motor recruitment. Dimerization can be reversed within minutes by addition of free TMP (Ballister et al., 2014).

We tested three constructs: the constitutively active motor domain of kinesin-1 (amino acids 1–560, K560); an amino-terminal fragment of kinesin light chain 1 (KLC1), which binds and recruits kinesin heavy chain; and an amino-terminal fragment of Bicaudal D2 (BICD), a motor effector that binds and recruits dynein. To localize Halotag protein, we used the peroxisometargeting sequence from human PEX3 or the mitochondrial outer membrane targeting sequence (Mito) from *Listeria monocytogenes* ActA (Fig. 3.1B)

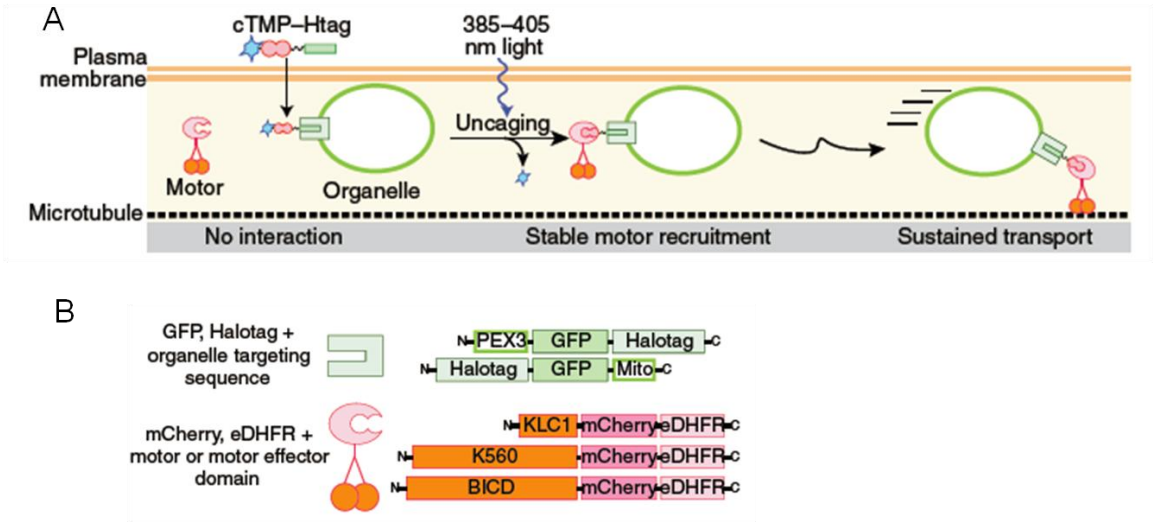

Figure 3.1 Illustration of optogenetic control of organelle transport.

(A) Schematic of experimental approach of light-induced dimerization of motor proteins to organelles. (B) Protein constructs used for this assay.

HeLa cells expressing PEX3-GFP-Halo, together with either KLC1-mCherry-eDHFR or BICD-mCherry-eDHFR, were treated with cTMP-Htag. Before uncaging, peroxisomes localized uniformly (Fig. 3.2A), with motor or effector constructs diffuse throughout the cytosol. In response to a 500 ms widefield pulse of 387 ± 5 nm light, the motor and effector constructs relocalized to peroxisomes within 30 seconds and transported them to the periphery or to the center of the cell, respectively, as predicted for kinesin- or dynein-driven motility Fig. 3.2A). The power of optogenetics is its potential for localized control on subcellular length scales. Using 405 nm light, we photoactivated defined regions within HeLa cells (Fig. 3.2B) Motor or effector recruitment in these cells led to transport of peroxisomes in the predicted directions which is reflected in our quantitation of fluorescence changes in GFP fused to peroxisomes (Fig. 3.2C), while unilluminated organelles in the same cells were unaffected (Fig. 3.2D).

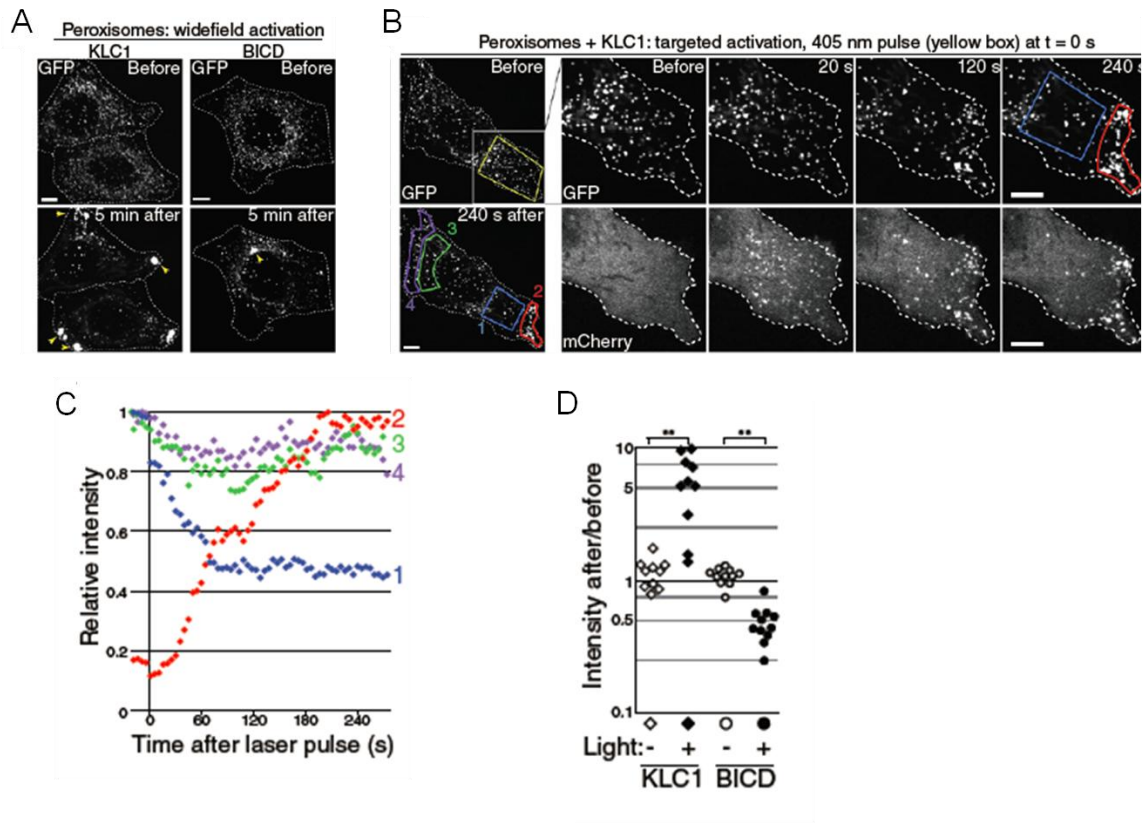

Figure 3.2 Photoactivation of peroxisomes recruits motors and induces motility of peroxisomes.

(A) GFP images show peroxisomes before and after widefield motor recruitment; dashed lines show cell outlines. Peroxisomes accumulated (arrowheads) in the periphery (KLC1), or center (BICD) in 100% of activated cells (n > 15 cells for each, 2 independent experiments). Horizontal bar, 5 µm. (B) KLC1 was recruited to peroxisomes in a defined region (yellow box) at t = 0. Whole-cell images (left) show GFP; insets show area in white square in GFP and mCherry. (C) GFP quantification of regions (1–4) marked in (B) shows peroxisome depletion from the interior of the photoactivated region (1, blue) and accumulation at the nearest edge of the cell (2, red), while unilluminated regions (3, 4, green and purple) are unaffected. Horizontal bar, 5 µm. (D) Following targeted KLC1 or BICD recruitment to peroxisomes (as in panel B), the fold change in average GFP intensity (as a proxy for peroxisome density) was calculated for a photoactivated region (filled symbols) and a comparable unactivated region

(open symbols) in each cell (n ≥ 10 cells each, similar results from 2 independent experiments). **p < 0.002, Student's t-test.

We next performed this assay in axons of hippocampal neurons which have uniformaly polarized microtubules with their plus ends out. In axons, within 5 min of photoactivation, >90% of illuminated peroxisomes moved >5 μm toward microtubule plus ends for K560 (anterograde) or toward microtubule minus ends for BICD (retrograde) (Fig. 3.3A), whereas unilluminated peroxisomes exhibited low-frequency, mixed motility (Fig. 3.3B). K560 recruitment induced peroxisome motility 10 ± 2 s (mean ± SEM) after photoactivation, before a detectable increase in mCherry fluorescence. In contrast, BICD recruitment induced motility 32 ± 6 s (mean ± SEM) after illumination, following a clear increase in mCherry fluorescence (Fig. 3.3C). These observations are consistent with previous findings that intracellular cargo transport requires fewer kinesin than dynein motors, which function in larger teams (Hendricks et al., 2012; Rai et al., 2013).

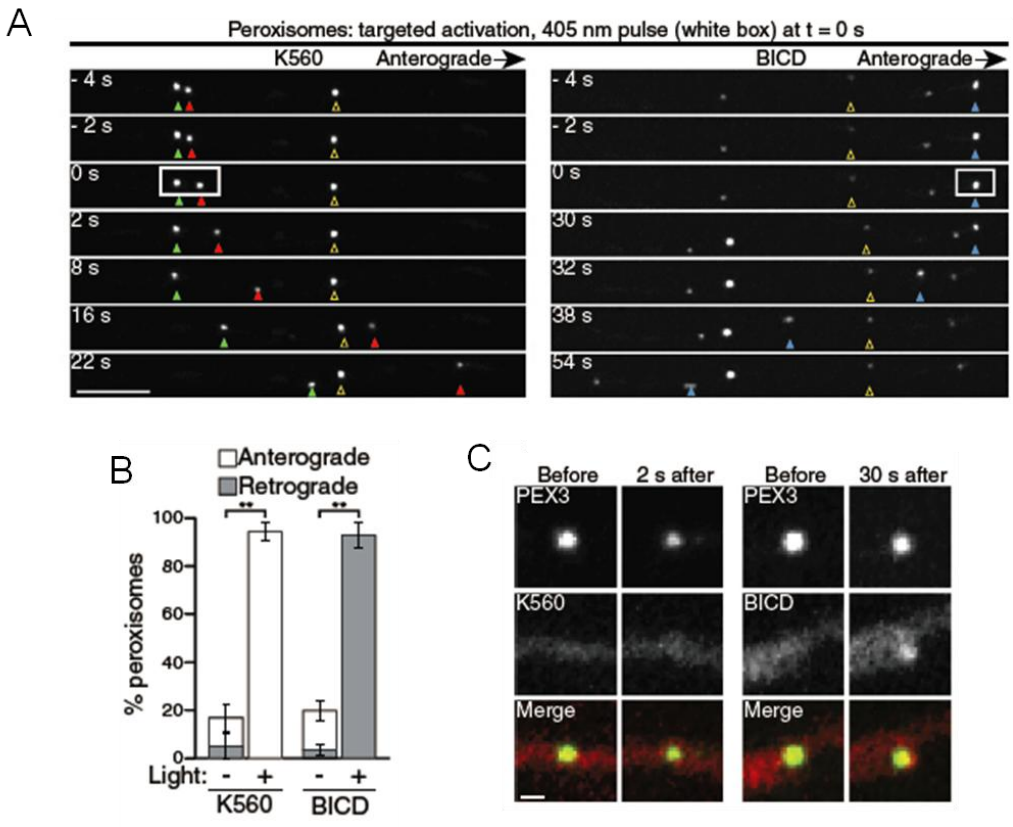

Figure 3.3 Recruitment of motors to peroxisomes in axons induces robust motility.

(A) Peroxisome movement in axons after photoactivation in a defined region (white box) at t = 0. Filled and open arrowheads mark photoactivated and unactivated peroxisomes, respectively. Horizontal bar, 5 µm. (B) Quantification of the percentage of peroxisomes exhibiting anterograde or retrograde movement (mean ± SEM, n = 10 neurons from 3 independent experiments). **p < 0.002, Student's t-test. (C) Representative images of K560 and BICD recruitment to peroxisomes in neurons before photoactivation and immediately prior to motility. Horizontal bar, 500 nm.

We next examined the recruitment of motors to mitochondria in axons of hippocampal neurons. Consistent with our data with peroxisomes, recruitment of either kinesin or dynein induced motility in the predicted direction (Fig. 3.4A). Further, dynein-

induced motion was delayed just like we observed with peroxisomes (Fig. 3.4B). However, while K560 recruitment induced motion in >90% of photoactivated mitochondria, recruitment of dynein induced motility in only ~40% indicating organelle-dependent regulation of motors (Fig. 3.4C).

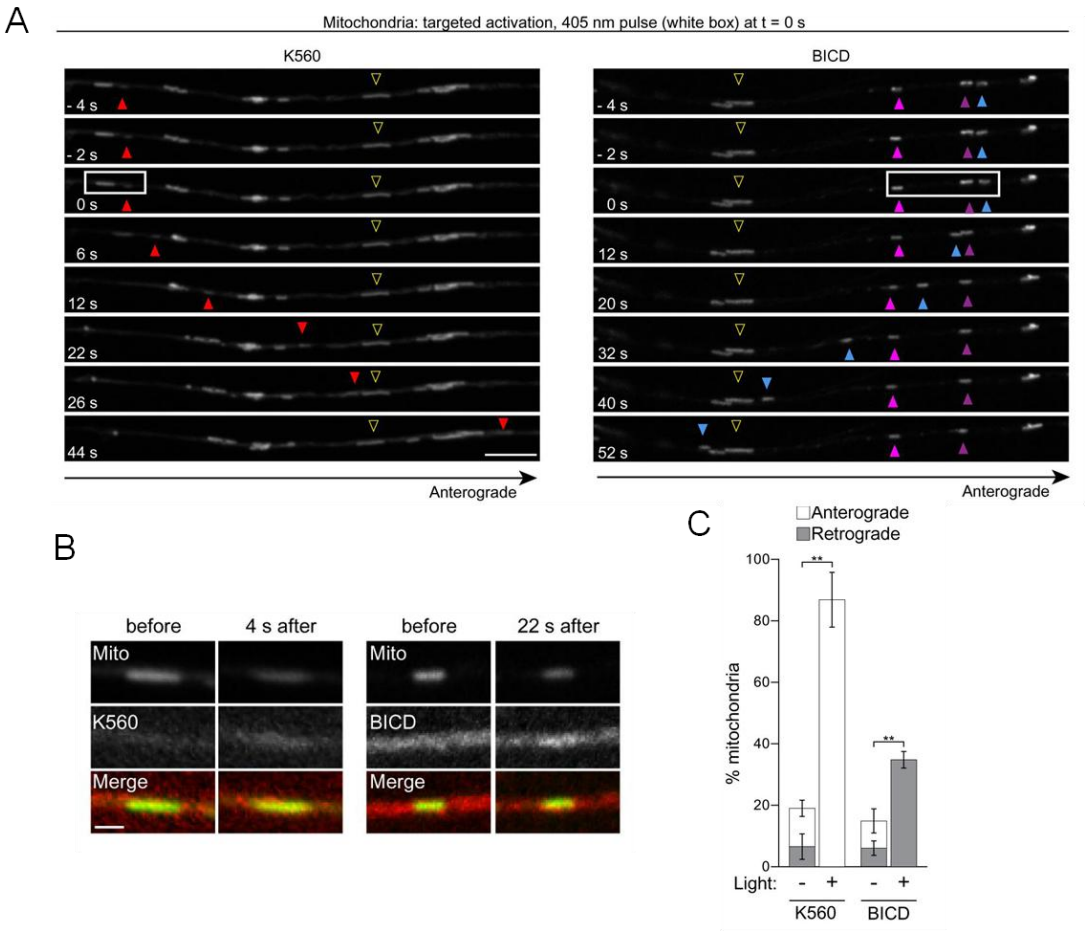

Figure 3.4 Recruitment of motors to mitochondria in axons of neurons.

(A) Time series of mitochondria movement before and after photoactivation. White box indicates the photoactivated region. Filled arrowheads mark positions of photoactivated mitochondria; open yellow arrowheads mark unilluminated mitochondria. Horizontal bar, 5 μm. Note that unlike peroxisomes, not all mitochondria become motile within 5 min after photoactivation. (B) Representative images of recruitment of motor proteins or adaptors

(K560 or BICD) to mitochondria before and after photoactivation. Horizontal bar, 500 nm. (C) Quantitation of the percent of mitochondria exhibiting anterograde or retrograde movement with or without photoactivation in K560 and BICD recruitment experiments in neurons (mean ± SEM, n=10 neurons from 3 independent experiments). **p<0.05 Student's t-test.

IV. Discussion

Our results demonstrate the utility of cTMP-Htag for manipulating organelle transport within living cells with spatial and temporal control. Motor recruitment after uncaging is stable, leading to sustained transport of individual organelles over several minutes after a single pulse of light. Because continuous illumination is not required, we can observe phenomena such as activated organelles bypassing unactivated organelles (Fig. 3.3A, 3.4A). Moreover, cTMP–Htag is insensitive to 488 nm light, allowing GFP imaging without inducing uncaging, and Halotag protein is compatible with both amino- and carboxy-terminal fusion partners. In contrast, the TULIP system, also used for optogenetic control of organelle transport, requires repeated illumination for sustained transport and is sensitive to 488 nm light (Strickland et al., 2012; van Bergeijk et al., 2015). These complementary systems offer the choice of transient (van Bergeijk et al., 2015) or sustained (this study) motor recruitment.

In cells, endogenous motors are tightly regulated by mechanisms including auto-inhibition, effector binding and scaffolding proteins (Fu and Holzbaur, 2014; Hancock, 2014). To better understand intracellular dynamics, multiple approaches must be employed. The use of optogenetics to recruit motors to organelles with temporal and spatial specificity is an exciting addition to the toolkit to dissect motor function within the cell, and to test downstream effects of localized perturbations of organelle transport on cellular physiology.

V. Material and Methods

Reagents

All plasmids in this study are derived from pEM705, which contains a CAG promoter for constitutive expression, obtained from E. V. Makeyev (Khandelia et al., 2011). Halo-GFP-Mito is previously described (Ballister et al., 2014), and includes the C-terminal 47 amino acids of the the *Listeria monocytogenes* ActA gene, which confer mitochondrial outer membrane targeting. PEX3-GFP-Halo includes the N-terminal 42 amino acids of the human Pex3 gene, which confer peroxisome targeting (Kapitein et al., 2010). The mCherry-eDHFR constructs in this study were derived from a previously described mCherry-eDHFR plasmid (Ballister et al., 2014), augmented with motor and motor effector domains described in (Kapitein et al., 2010). BICD-mCherry-eDHFR includes residues 1-572 of mouse BICD2, KLC1-mCherry-eDHFR includes residues 1-175 of rat Kinesin-1 light chain, and K560-mCherry-eDHFR includes residues 1-560 of human Kinesin-1 heavy chain.

HeLa cell culture and transfection

Hela cells (obtained from E. V. Makeyev, Nanyang Technological University) were cultured in growth medium (DME with 10% FBS and penicillin-streptomycin) at 37 °C in a humidified atmosphere with 5% CO2. Peroxisome recruitment experiments in HeLa cells were performed by transiently cotransfecting plasmids expressing PEX3-GFP-Halo and either BICD-mCherry-eDHFR or KLC1-mCherry-eDHFR. Mitochondrial recruitment experiments in HeLa cells were performed by transiently transfecting BICD-mCherry-eDHFR, KLC1-mCherry-eDHFR or K560-mCherry-eDHFR into a stable cell line constitutively expressing Halo-GFP-Mito. The Halo-GFP-Mito stable cell line was created using the Recombinase Mediated Cassette Exchange technique described by Makeyev and coworkers (Khandelia et al., 2011). For single-plasmid transient transfections, cells at ~60% confluency

in a single well of a 6-well plate were transfected with 1 µg of plasmid using 3 µL of Fugene 6 (Promega). Double-plasmid cotransfections were performed similarly, but with 1 µg of each plasmid and 6 µL of Fugene 6. Transient transfections were performed 40 hours prior to experiment.

Neuronal cell culture and transfection

Rat hippocampal neurons obtained from the Neuron Culture Service Center at the University of Pennsylvania were dissected from the hippocampus of rat embryos at embryonic day 18-20 as previously described (Wilcox et al., 1994). Cells were plated at a density of 1,00,000 cells/ml on glass coverslips coated with 0.5 mg/ml poly-L-lysine in 2 ml Neurobasal medium (Gibco) supplemented with 2% B27 (Invitrogen), 1% GlutaMax (Gibco) and cultured at 37°C in a 5% CO2 incubator.

Neuronal experiments were performed after either 8 or 9 DIV (days in vitro) with DNA plasmids transfected on 7 or 8 DIV respectively. Halo-GFP-mito and PEX3-GFP-Halo were co-transfected with either K560-mcherry-eDHFR or BICD-mcherry-eDHFR using Lipofectamine 2000 reagent (Invitrogen). Cells were imaged 12-18 hours post transfection.

Dimerizer treatment

cTMP-Htag was dissolved in DMSO at 10 mM and stored in amber plastic microcentrifuge tubes at -80 °C, then diluted in medium to a final working concentration of 10 µM. Care was taken to minimize incidental exposure of cTMP-Htag or treated cells to light prior to experiment. We found that working quickly in low levels of normal room lighting did not cause any detectable premature uncaging. The low levels of white light necessary for differential interference contrast microscopy also did not cause any detectable cTMP-Htag uncaging. Cells were incubated with 10 µM cTMP-Htag for 5-60 minutes in culture medium, then washed with culture medium for 5-15 minutes prior to experiment. In our hands, 5 minute incubations were as effective as 60 minute incubations.

Image acquisition and photoactivation

For live imaging, HeLa cells were plated on 22 x 22 mm glass coverslips (no. 1.5; Fisher Scientific) coated with poly-D-lysine (Sigma-Aldrich). Coverslips were mounted in magnetic chambers (Chamlide CM-S22-1, LCI). During imaging, cells were maintained in L-15 medium without phenol red (Invitrogen) supplemented with 10% FBS and penicillin/streptomycin. Temperature was maintained at ~35 °C using an environmental chamber (Incubator BL; PeCon GmbH).

For HeLa cell experiments, images were acquired with a spinning disk confocal microscope (DM4000; Leica) with a 100x 1.4 NA objective, an XY Piezo-Z stage (Applied Scientific Instrumentation), a spinning disk (Yokogawa), an electron multiplier charge-coupled device camera (ImageEM; Hamamatsu Photonics), and a laser merge module equipped with 488- and 593-nm lasers (LMM5; Spectral Applied Research) controlled by MetaMorph software (Molecular Devices). Images in Figure 3.2A are maximum-intensity projections of 5 confocal Z-sections, 1 µm spacing.

For whole-cell UV exposure experiments in Figure 1B and Figure S1 A-E, light from a mercury arc lamp (Osram HXP R 120W/45c Vis) was filtered through a 387/11 nm bandpass filter (Semrock part #FF01-387/11 as a component in a DAPI filter cube) and focused through the objective. 5 x 100 ms exposures were used for widefield UV activation. Targeted laser experiments in Figure 3.2B employed an iLas2 illuminator system (Roper Scientific), equipped with a 405 nm laser (CrystaLaser LC model # DL405-050-O, output of 27 mW after fiber coupling) operated at 10% intensity, controlled using the iLas2 software module within Metamorph. Defined areas (2-10 μm^2) were rasterized 2 times over ~100 ms.

Neurons were imaged in low-fluorescence nutrient media (Hibernate E, Brain Bits) supplemented with 2% B27 and 1% GlutaMax. For neuron experiments, all images were acquired on a spinning-disk confocal UltraView VOX (Perkin Elmer) with a 405 nm Ultraview

Photokinesis (Perkin Elmer) unit on an inverted Nikon Ti microscope with apochromat 100X 1.49 NA oil-immersion objective and a C9100-50 EMCCD camera (Hamamatsu) controlled by Volocity software (Perkin Elmer). The Photokinesis module at 25% laser power (0.6 W/cm^2) for 25 cycles was used for localized photoactivation. Only neurons expressing both GFP and mCherry (co-transfected) were imaged and the axons were selected based on morphologic criteria as previously described (Kaech and Banker, 2006). Sequential dual colored images (GFP and mCherry) were acquired for 20 s at 2 s per frame prior to photoactivation and for 5 min at 2 s per frame post photoactivation. There was no evidence of cellular phototoxicity with the photoactivation conditions described here, and we note that these doses of light are less intense than those required for standard FRAP experiments.

Image Processing

All image processing and analysis was performed using ImageJ. For quantification of peroxisome density vs time in Figure 3.2C, average GFP intensity in the indicated regions was measured at each timepoint (cells were imaged every 5 seconds). Background signal was estimated as average intensity in large areas outside the cells and subtracted. To normalize between different regions, the background-subtracted measurements for each region at each timepoint were divided by the maximum intensity observed for each region over the course of the experiment. For the endpoint analysis in Figure 3.2D, 10 cells were analyzed for KLC1 recruitment and 11 cells were analyzed for BICD recruitment. Two regions were defined for each cell: 1 peripheral region contained in the area targeted by the activating 405 nm laser pulse, and one unilluminated peripheral region (on the other side of the cell). Average GFP intensity within these regions was measured before photoactivation (“start”) and at the final timepoint (275 seconds after photoactivation, “end”). Measured values were corrected for background signal and observational photobleaching. The final calculated values are the ratio of end intensity/start intensity for each region.

For analysis of peroxisome (Fig. 3.3B) and mitochondria (Fig. 3.4C) transport in neurons , photoactivated and non-photoactivated organelles within an axon were classified as exhibiting anterograde movement, retrograde movement or no movement. Organelles were considered motile if they moved greater than 5 μm distance in a given direction within a time window of 5 min.

CHAPTER 4: OPTOGENETIC RECRUITMENT OF MOTORS REVEALS DIFFERENTIAL AXO-DENDRITIC REGULATION OF TRAFFICKING IN NEURONS

A version of this chapter has been submitted for publication as a manuscript entitled:

Optogenetic recruitment of motors reveals differential axo-dendritic regulation of trafficking in neurons

Ayloo, S., Holzbaur, E.L.F (2015).

I. Summary

The polarized distribution of proteins in axonal and dendritic compartments is critical for neuronal function. While we have a basic understanding of cargo transport in neurons, much less is known about the differential regulation of transport in axons versus dendrites. We recently developed an optogenetic tool to recruit motors to cellular cargo in real-time. We showed that light-induced recruitment of dynein or kinesin to axonal organelles induced robust retrograde or anterograde motion respectively. Here, we extend this study to report distinct patterns of motor behavior in dendrites. We demonstrate that dynein efficiently navigates the mixed microtubule arrays of dendrites, displaying a retrograde bias consistent with the underlying microtubule polarity. Thus dynein can efficiently drive cargo back to the cell soma. Further, dynein-driven motility depends on microtubule dynamics, suggesting that dynein requires the dynamic plus-ends of microtubules for efficient recruitment onto microtubule tracks. In contrast, while kinesin-1 is a robust motor in the axon, it is not as efficient in dendrites. We further tested this observation by directly comparing the activities of two kinesin-3 family motors, KIF13A and KIF13B that differentially localize to axons and dendrites respectively. Light-induced recruitment of either motor effectively induced motility of axonal organelles, but produced striking differences in dendrites. KIF13B induced robust motion whereas KIF13A failed to move. Collectively, our data highlight the different regulatory mechanisms dynein and kinesins employ in polarized neuronal trafficking. While dynein function is governed by microtubule orientation and dynamics, kinesins show compartment-specific differences likely reflecting preferential tuning to localized cytoskeletal determinants.

II. Introduction

The transport of organelles and proteins within axonal and dendritic compartments is fundamental to neuronal development and is essential to maintain neuronal homeostasis. Accurate trafficking of polarized proteins is important for the formation and maintenance of synapses that are vital for neuronal activity. Previous studies have demonstrated that most dendritic vesicles do not enter the axon (Burack et al., 2000; Silverman et al., 2001) suggesting that microtubule-based transport is selective. More recently, it has been shown that the dendritic vesicles that do enter the axon are typically rerouted back to the cell body (Al-Bassam et al., 2012; Peterson et al., 2014). Thus, an important question in neuronal trafficking involves understanding the mechanisms responsible for polarized transport.

Long-range transport in neurons is a highly regulated process and is primarily mediated by kinesins and dynein moving along the microtubule cytoskeleton. While there are several families of kinesins driving transport towards the microtubule plus-end, dynein is the major minus-end directed motor in cells (Maday et al., 2014). The distinct microtubule cytoskeleton in axons and dendrites of mammalian neurons adds another layer of complexity to this process: whereas axons have uniformly plus-end out microtubules, dendrites have mixed polarity microtubules (Baas et al., 1988; Conde and Caceres, 2009).

How are motor proteins regulated to achieve selective microtubule-based transport in neurons? Several models have been proposed to explain kinesin selectivity in polarized neuronal trafficking. The ‘smart motor’ hypothesis suggests that motors inherently are capable of distinguishing axons from dendrites (Nakata and Hirokawa, 2003; Jacobson et al., 2006; Huang and Banker, 2012). These studies implicate regulation at the motor-microtubule level suggesting that structural elements within motor proteins determine their targeting to

the axon or dendrite. There is also a ‘cargo-steering’ model that postulates that the cargo the motors bind to determines whether the motor-cargo complex is axonal or dendritic (Setou et al., 2002; Song et al., 2009; van Spronsen et al., 2013). These reports suggest that cargo-associated sorting or adaptors influence the targeting of the motor. Collectively, these studies suggest a multi-layered regulation of selective kinesin transport.

Dynein likely employs regulatory mechanisms that are different from kinesins, as a single form of dynein has to perform efficiently in both axons and dendrites. A previous study proposed that dynein establishes the initial sorting of cargo to dendrites (Kapitein et al., 2010) but the factors regulating dynein-driven motility within the dendrite are not known.

In this study, we specifically focused on understanding how motors contribute to differential trafficking in neurons. We applied a novel optogenetic tool (Ballister et al., 2014) to recruit motors to specific organelles and examine their dynamics immediately post recruitment. We demonstrate that recruitment of dynein induces long, bidirectional runs and causes organelles to take more frequent and longer retrograde runs. This retrograde bias reflects the underlying microtubule organization in dendrites and hence dynein can efficiently drive cargo back to the cell soma. Dynein-driven motility also depends on microtubule dynamics suggesting dynein requires the growing ends of microtubules for efficient initiation of minus-end directed transport along microtubules. In contrast, we find that kinesin-1 is not as efficient in dendrites as in axons and is not sensitive to microtubule dynamics. To further explore kinesin motility in dendrites, we investigated two kinesin-3 family motors, KIF13A and KIF13B, and found that both function effectively in axons but only KIF13B induced organelle motility in dendrites. Taken together, our data support a model in which dynein is regulated by microtubule orientation and dynamics while kinesins may be tuned to compartment-specific modifications of the microtubule cytoskeleton.

III. Results

Recruitment of dynein or kinesin to peroxisomes in dendrites induces robust bidirectional motility

In order to recruit motor proteins to organelles, we employed a recently developed light-inducible dimerization tool (Ballister et al., 2014, described in chapter 3). Briefly, in this system the two proteins of interest are tagged with Halo and eDHFR respectively; cTMP-HaloLigand is a caged, membrane permeable dimerizer that dimerizes the Halo and eDHFR tagged proteins following a single pulse of 400 nm (Fig. 1A). In contrast to the recent use of rapalog, an analog of rapamycin used to chemically induce dimerization in the whole cell (Kapitein et al., 2010; Jenkins et al., 2012; Bentley et al., 2015), our light-inducible dimerization system enables us to dimerize proteins locally via photoactivation, recruiting motor proteins to specific organelles (Fig. 4.1A). The ability to spatially control motor recruitment allows us to examine compartment-specific and organelle-dependent regulation of motility. In addition, with this system, we can directly visualize motor recruitment and follow organelle dynamics in real-time.

In initial experiments, this optogenetic tool was used to recruit specific motors to organelles in the axons of hippocampal neurons (Ballister et al., 2015). We used a constitutively active form of the kinesin-1 motor, K560, which includes the first 560 residues of the kinesin heavy chain encoding both the N-terminal motor domain and coiled coil sequences required for dimerization. For dynein recruitment, we used an N-terminal fragment of the adaptor protein Bicaudal D2, which effectively recruits dynein and its activator dynactin (Splinter et al., 2012). In axons, recruitment of either kinesin-1 or dynein motors to peroxisomes induced robust anterograde or retrograde motion, respectively (Ballister et al., 2015). Here, we extend this study to compare and contrast the downstream

effects of motor recruitment to axonal and dendritic organelles. We focused on peroxisomes as these are mostly stationary organelles with a baseline motility of only about ~20% (Ballister et al., 2015) and are enriched in the soma and dendrites of neurons (Kapitein et al., 2010).

While axons have uniformly plus-end out microtubules, dendrites of mature hippocampal neurons have microtubules of mixed polarity (Baas et al., 1988); we verified this organization by examining the directionality of EB3 comets in our cultures (Fig. 4.1B). Quantitation of EB3 comets indicated that microtubules are 64 ± 3.6% plus-end out and 36 ± 3.6% minus-end out (mean ± SEM; n=10 neurons from 2 experiments) in proximal dendrites of our neuronal cultures, similar to previous reports (Baas et al., 1988; Stepanova et al., 2003; Kleele et al., 2014). Consistent with this mixed polarity, recruitment of either K560 or BICD to peroxisomes in dendrites induced long, bidirectional runs as shown in Fig. 4.1C. Dual color imaging enabled us to visualize the specific recruitment of motor proteins or motor adaptors to the photoactivated organelle by an increase in the intensity of mCherry fluorescence as indicated by arrowheads in the time series (Fig. 4.1C). In the corresponding kymographs (Fig. 4.1C), peroxisomes that are initially green-only become yellow post-photoactivation, showing the co-migration of the organelles with the recruited K560 (left) or BICD (right). This induced recruitment is better seen in the stills of peroxisomes pre and post-photoactivation (Fig. 4.1D). Quantitation of the intensity change in mCherry fluorescence pre- and post-photoactivation revealed a ~4 ± 0.4 and ~6 ± 1.2 fold increase (mean ± SEM; n=12 neurons from 3 experiments) with K560 and BICD respectively, indicating successful recruitment of the motors.

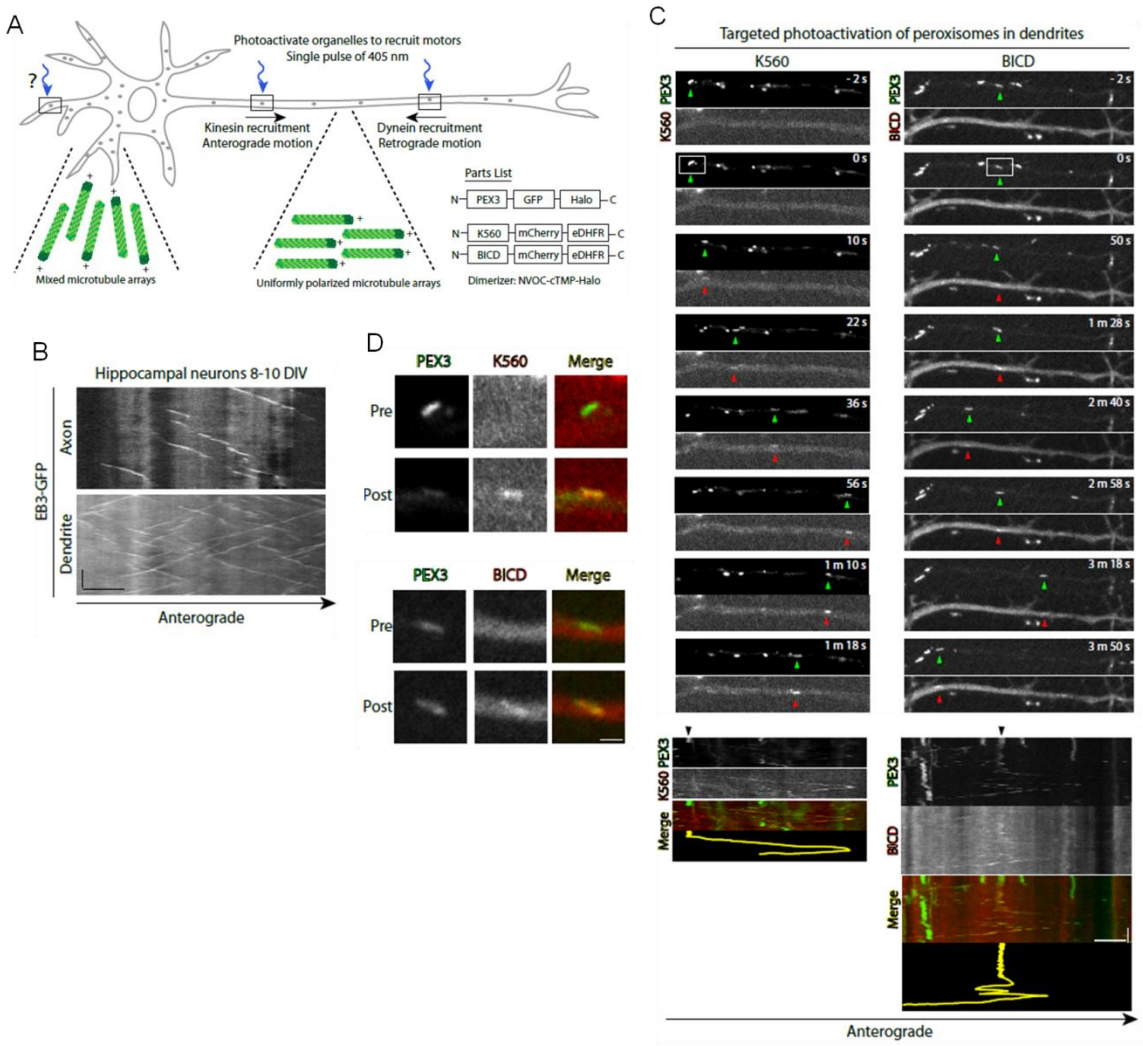

Figure 4.1 Recruitment of dynein or kinesin to peroxisomes in dendrites induces robust bidirectional motility.

(A) Schematic and parts list of the light-inducible dimerization system implemented in mature neurons which have uniformly polarized microtubule arrays in the axon and mixed arrays in dendrites. We previously showed that recruitment of kinesin or dynein motors to peroxisomes in axons induced robust anterograde or retrograde motion, respectively (Ballister et al., 2015). (B) Representative kymographs of EB3 comets in the axon and dendrites of mature hippocampal neurons, 8-10 DIV. Horizontal bar, 5 µm. Vertical bar, 30 s. (C) Time series and corresponding kymographs showing the bidirectional movement of

locally photoactivated peroxisomes (white box). Horizontal bar, 5 µm. Vertical bar, 1 min. (D) Images of motor recruitment to peroxisomes pre and post-photoactivation. Horizontal bar, 1 µm.

Recruitment of dynein induced motility in >90% of the photoactivated organelles (Fig. 4.2A). In contrast, recruitment of K560 induced motility in only ~60% of photoactivated organelles (Fig. 4.2A). Importantly, the lack of motility observed for the remaining ~40% of photoactivated organelles was not due to a lack of recruitment of the K560 motor. This is shown in a representative example of a non-motile peroxisome where there is a clear increase in the fluorescence intensity of mCherry indicating successful K560 recruitment (Fig. 4.2B). With both kinesin and dynein, ~70% of the motile organelles exhibited bidirectional motility with only ~30% moving unidirectionally in either the anterograde or retrograde direction (Fig. 4.2C). These data suggest that dynein efficiently navigates the dendritic cytoskeleton. In contrast, kinesin-1, which functions as a robust motor in axons (Ballister et al., 2015), does not perform as efficiently in dendrites.

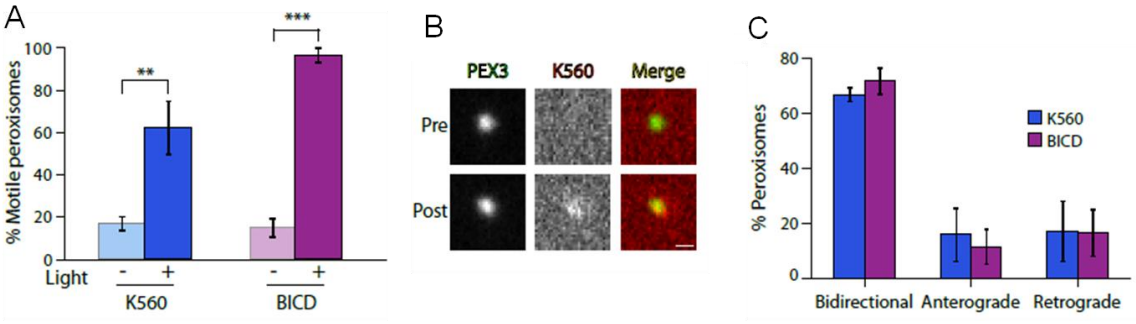

Figure 4.2 Kinesin is not as efficient as dynein in inducing motility in dendrites.

(A) Quantitation of percentange of peroxisomes that are motile. Mean ± SEM, 25 peroxisomes from n=12 neurons and N=3 independent experiments for both K560 and BICD, **p<0.01, ***p<0.001, Student's t-test. (B) Representative stills showing recruitment of K560 even in the case peroxisomes that are immotile post photoactivation. Horizontal bar, 500 nm.

(C) Photoactivated peroxisomes that exhibited movement were further parsed into bidirectional, anterograde or retrograde. Mean ± SEM.

Dynein-driven motility in dendrites has a retrograde bias

Recruitment of dynein to dendritic organelles induced long runs in either direction. However, we noticed that ~50% of these motile organelles eventually entered the cell soma (Fig. 4.3A). Once they enter the soma, these organelles do not re-enter the dendrite during our imaging window. This led us to examine the motor-induced bidirectional movement of the organelles more closely. We first measured velocities of the individual runs of the motile peroxisomes. Photoactivated peroxisomes moved at a speed of 0.49 ± 0.03 μm/s (mean ± SEM) and we observed no significant differences in the velocities induced by either kinesin or dynein recruitment (Fig. 4.3B).

We then measured the run lengths of the motile organelles and found that dynein recruitment caused organelles to take more frequent and longer retrograde runs indicative of a significant retrograde bias (40% anterograde vs 60% retrograde, Fig. 4.3C). Of note, the observation that dynein induced motion of 60% retrograde runs reflects the underlying microtubule organization in dendrites (~65% plus end out microtubules). Similar to the observed run lengths, the run times of dynein-induced motion also exhibited a retrograde bias (Fig. 4.3D). In contrast, K560 did not show any bias when recruited to organelles in dendrites (47% anterograde vs 53% retrograde, difference not-significant, Fig. 4.3E, F). These findings demonstrate that dynein-induced motility has a retrograde bias consistent with the underlying microtubule polarity. These data suggest that microtubule orientation is likely a key determinant of dynein-driven motility in dendrites.

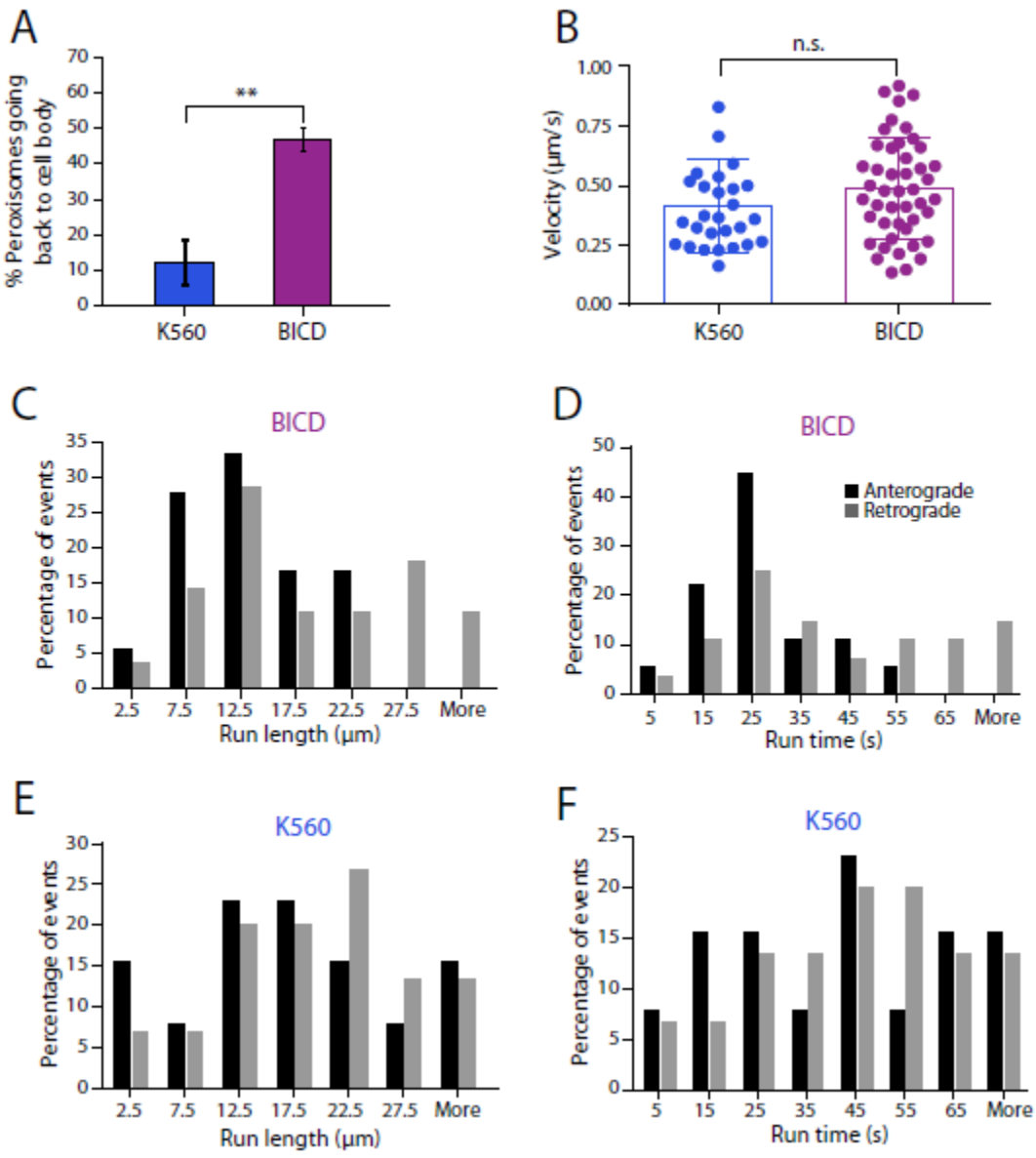

Figure 4.3 Dynein-driven motility in dendrites has a retrograde bias.

(A) Quantitation of percent of peroxiomes going back to the cell body post photoactivation. Mean ± SEM, **p<0.01, Student's t-test. (B) Average velocities of individual runs of peroxisomes that are motile post photoactivation. Mean ± SD, n.s., not significant, Student's t-test. (C-F) Histograms of run length and run time of the individual runs of motile

peroxisomes. Data from 25 peroxisomes from n=12 neurons and N=3 independent experiments.

Dynein requires dynamic microtubules for efficient initiation of transport

Previous work from our lab has established a model wherein dynein is recruited to the dynamic plus-ends of microtubules by dynactin, CLIP-170 and EB1 and this is required for efficient initiation of retrograde transport from the distal axon (Moughamian et al., 2013; Ayloo et al., 2014, Nirschl et al., 2016). We now wanted to ask whether the dynein-induced motility of peroxisomes in neurons would show a similar dependence on dynamic microtubule plus ends. To test this possibility, we performed our photoactivation assay in neurons treated with low dose nocodazole (100 ng/ml), which dampens microtubule dynamics. We incubated neurons with either DMSO or nocodazole for 1.5 hours before imaging; under these conditions, microtubule dynamics are eliminated as shown in the EB3 kymographs from axons and dendrites (Fig. 4.4A).

We first examined kinesin and dynein-driven motility of photoactivated peroxisomes in axons. Dampening microtubule dynamics with nocodazole had no effect on K560-driven motility in axons (Fig. 4.4B, C). Recruitment of kinesin induced robust anterograde motion of the peroxisomes just as in the control case as shown in the kymographs (Fig. 4.4B). In contrast, we observed a significant reduction in dynein-induced motility of peroxisomes in axons (Fig. 4.4B, D). While >90% of the photoactivated peroxisomes moved robustly retrograde upon dynein recruitment in the control case, this went down to ~60% in neurons treated with nocodazole (Fig. 4.4D) with the remaining ~40% of photoactivated peroxisomes showing non-processive motion with frequent pauses and occasional anterograde movements as shown in representative kymographs (Fig. 4.4B). This non-processive movement of peroxisomes is further reflected in the decreased average velocities (Fig. 4.4E)

and the significantly higher number of pauses (Fig. 4.4F) compared to the control peroxisomes. The frequent pauses we observe with dynein motion in the absence of microtubule dynamics may indicate a defect in dynein loading onto plus-ends of microtubules following detachment of the motor from its track.

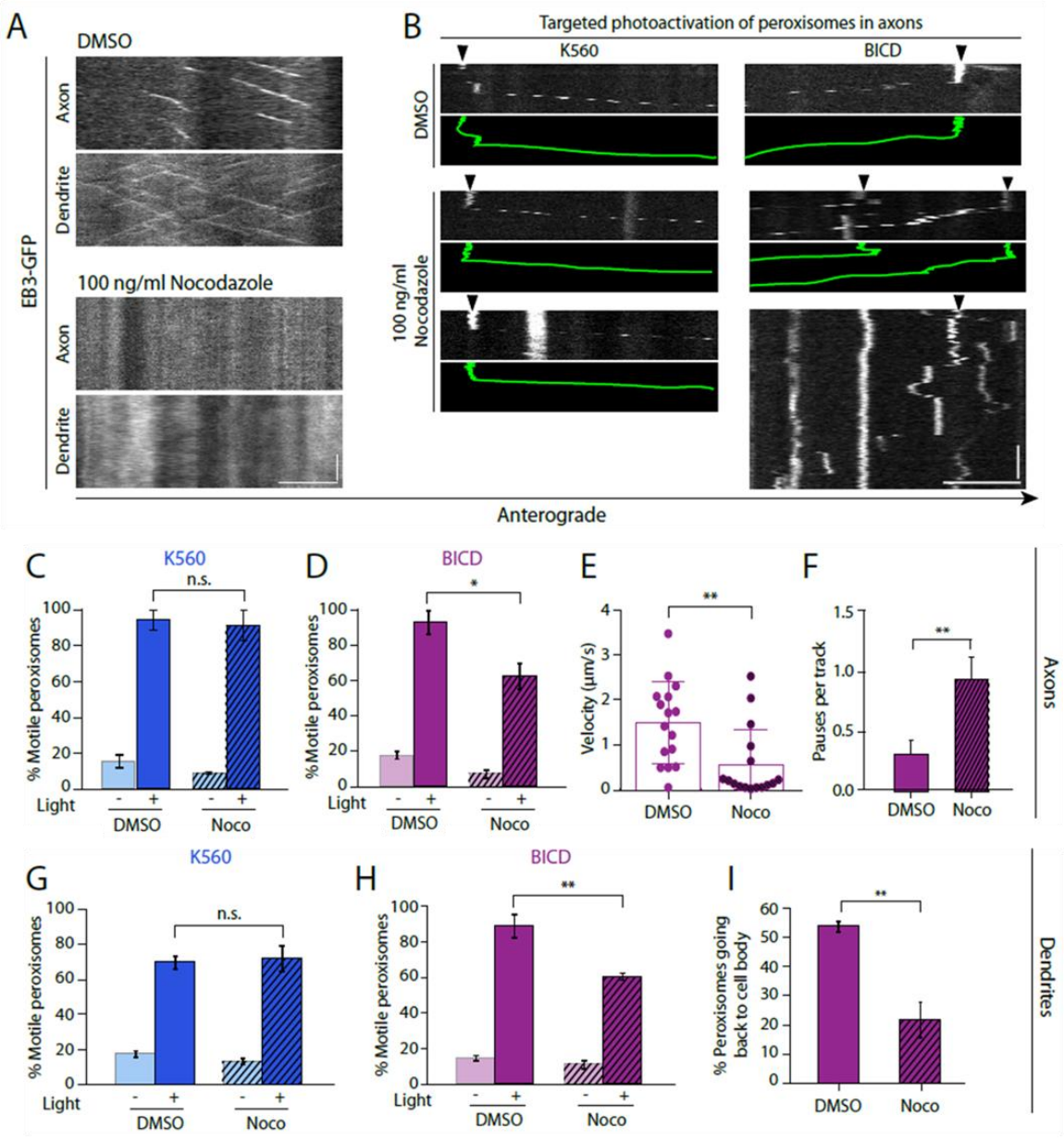

Figure 4.4 Dynein requires dynamic microtubules for efficient initiation of transport.

(A) Representative kymographs of EB3 comets in axons and dendrites of hippocampal neurons treated with DMSO or 100 ng/ml Nocodazole for 1.5 hours at 37^{o}C. Horizontal bar, 5 µm. Vertical bar, 30 s. (B) Representative kymographs showing movement of photoactivated peroxisomes in axons. Horizontal bar, 5 µm. Vertical bar, 1 min. (C) Quantitation of percentage of peroxisomes that are motile in axons of neurons expressing K560, treated with DMSO or Nocodazole. Mean ± SEM. (D) Quantitation of percentage of peroxisomes that are motile in axons of neurons expressing BICD, Mean ± SEM, their average velocities in (E), Mean ± SD and (F) number of pauses per photoactivated peroxisome, Mean ± SEM. (G and H) Quantitation of percentage of peroxisomes that are motile in dendrites of neurons expressing K560 or BICD. Mean ± SEM. (I) With reduced transport in dendrites, there is a concomitant decrease in percentage of peroxisomes going back to the cell body in the case of BICD. Data from 15-20 peroxisomes, n=14 neurons for axons and 25-30 peroxisomes, n=16 neurons for dendrites from N=3 independent experiments, n.s., not significant, *p<0.05, **p<0.01, Student's t-test in E and H, one-way ANOVA with Tukey's post-hoc test in the rest.

We next examined motor-induced motility in the dendrites of neurons treated with nocodazole. Consistent with our observations in axons, kinesin-induced motility was unaffected by nocodazole treatment. In contrast, dynein-induced motility was significantly reduced in nocodazole-treated neurons (Fig. 3G, H). With reduced transport in dendrites, there was also a concomitant decrease in the percentage of peroxisomes going back to the cell soma (Fig. 3I). However, approximately half of the motile organelles eventually reach the cell soma in both control and nocodazole-treated neurons, suggesting that the overall retrograde bias in dynein-induced motility is not affected by the loss of microtubule dynamics.

Collectively, our results indicate that dynein motility is predominantly determined by microtubule polarity, while microtubule dynamics promote efficient dynein-driven transport. In contrast, kinesin-1 shows compartment-specific function, moving organelles robustly in axons but less efficiently when recruited to organelles in dendrites.

Differential regulation of KIF13A and KIF13B in axons and dendrites

To follow up on our observations on the compartment-specific regulation observed for kinesin-1 but not for dynein, we chose to focus on a pair of motors from the kinesin-3 family. Kinesin-3 motors KIF13A and KIF13B show distinct localization preferences in neurons with KIF13A enriched in axons and KIF13B in dendrites (Jenkins et al., 2012; Huang and Banker, 2012). We used our optogenetic assay to ask how these motors perform when specifically recruited to axonal or dendritic organelles. We used motor domain constructs of KIF13A and KIF13B (KIF13A 1-411 ΔP390 and KIF13B 1-412 ΔP391) that have been shown to dimerize efficiently and to function as processive motors in cells and *in vitro* (Soppina et al., 2014); we tagged these constructs with mCherry-eDHFR for our photoactivation assay.

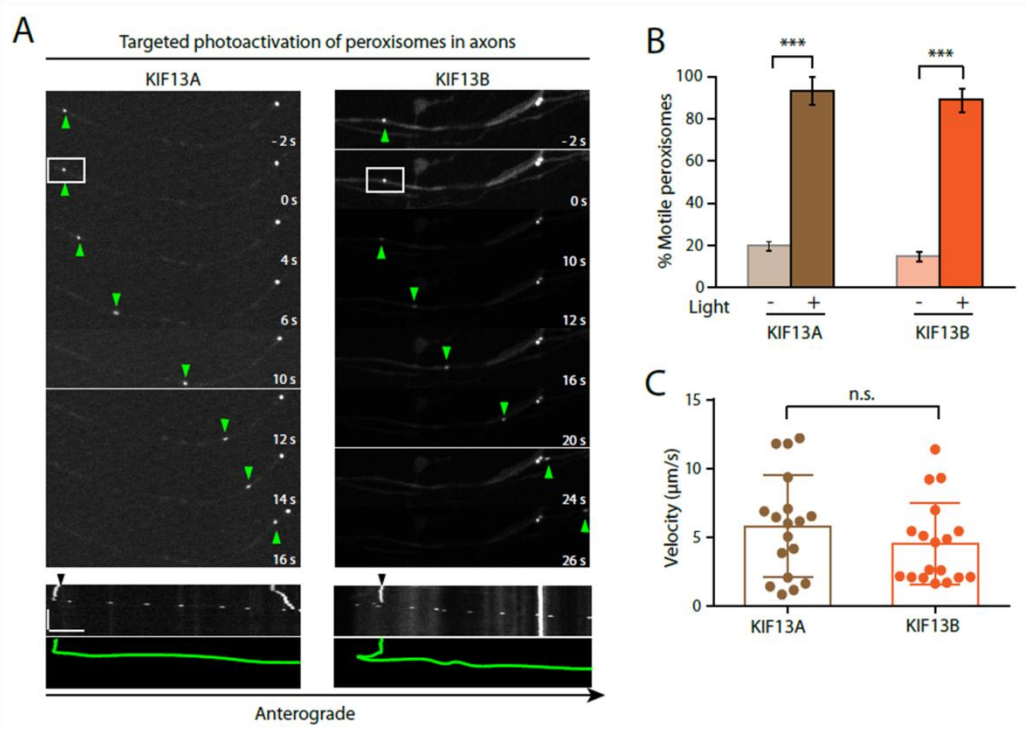

Figure 4.5 Both KIF13A and KIF13B, kinesin-3 family motors are equally efficient in axons

(A) Time series and corresponding kymograph showing movement of photoactivated (white box) peroxisomes in axons. Horizontal bar, 5 µm. Vertical bar, 30 s. (B) Quantitation of percentage of peroxisomes that are motile. Mean ± SEM. ***p<0.001, Student's t-test. (C) Average velocities of peroxisomes that are motile post photoactiavtion. Mean ± SD. n.s., not significant, Student's t-test. Data from 20 peroxisomes from n=14 neurons and N=3 independent experiments.

We first photoactivated peroxisomes in axons and observed that recruitment of either KIF13A or KIF13B induced processive anterograde motion as shown in the time stills and kymographs (Fig. 4.5A). In both cases, >90% of photoactivated peroxisomes moved in the anterograde direction (Fig. 4.5B). Further, velocities of the peroxisomes following photoactivation (Fig 4.5C) were not significantly different between the two motors, indicating that both KIF13A and KIF13B are equally efficient in driving anterograde motion in axons.

This suggests that although KIF13B is a dendritic kinesin, when recruited to axonal organelles, this motor works just as well as an axonally-targeted motor.

In contrast, we observed striking differences between the two motors in dendrites. While KIF13B induced robust bidirectional motility, KIF13A failed to move peroxisomes efficiently (Fig. 4.6A). It is important to note that lack of motion is not due to lack of recruitment of the motor, which was effectively recruited to organelles following photoactivation (see arrow heads in the time stills in Fig. 4.6A). In the corresponding kymographs, peroxisomes that are initially green-only become yellow post-photoactivation, indicative of effective motor recruitment (Fig. 4.6A). In almost all cases, we observed clear recruitment of the motor, as indicated by the increased intensity of mCherry fluorescence at the site of the photoactivated peroxisome. KIF13B induced motion in >85% of photoactivated peroxisomes, whereas KIF13A induced motion in only ~25% of photoactivated organelles (Fig. 4.6B). We also noticed that the few organelles that do move upon recruitment of KIF13A take >200 seconds to begin movement on dendritic microtubules whereas KIF13B recruited organelles generally initiate movement within 30 seconds on average (Fig. 4.6C). This suggests that KIF13A does not interact efficiently with dendritic microtubules. Further analysis of the motile organelles revealed that although the average velocities of KIF13A- and KIF13B-induced motion were similar, KIF13B is predominantly a retrograde motor (Fig. 4.6D-F). On average, the run length of KIF13B-induced motility is 10.8 ± 1.3 μm in the anterograde direction and 21.5 ± 3.8 μm in the retrograde direction (mean ± SEM, n=16 neurons from 3 experiments).

Collectively, these findings indicate that although both KIF13A and KIF13B are equally efficient motors when recruited to axonal organelles, the activities of these motors are differentially regulated in dendrites. While KIF13B induces efficient motility in dendrites in our assays, KIF13A fails to move organelles along dendritic microtubules. Together with our

kinesin-1 data, our results suggest that kinesins may be specifically tuned to function efficiently within their native environments. We propose that this serves as a mechanism to establish compartment-specific regulation of kinesins, contributing to selectivity of trafficking in neurons.

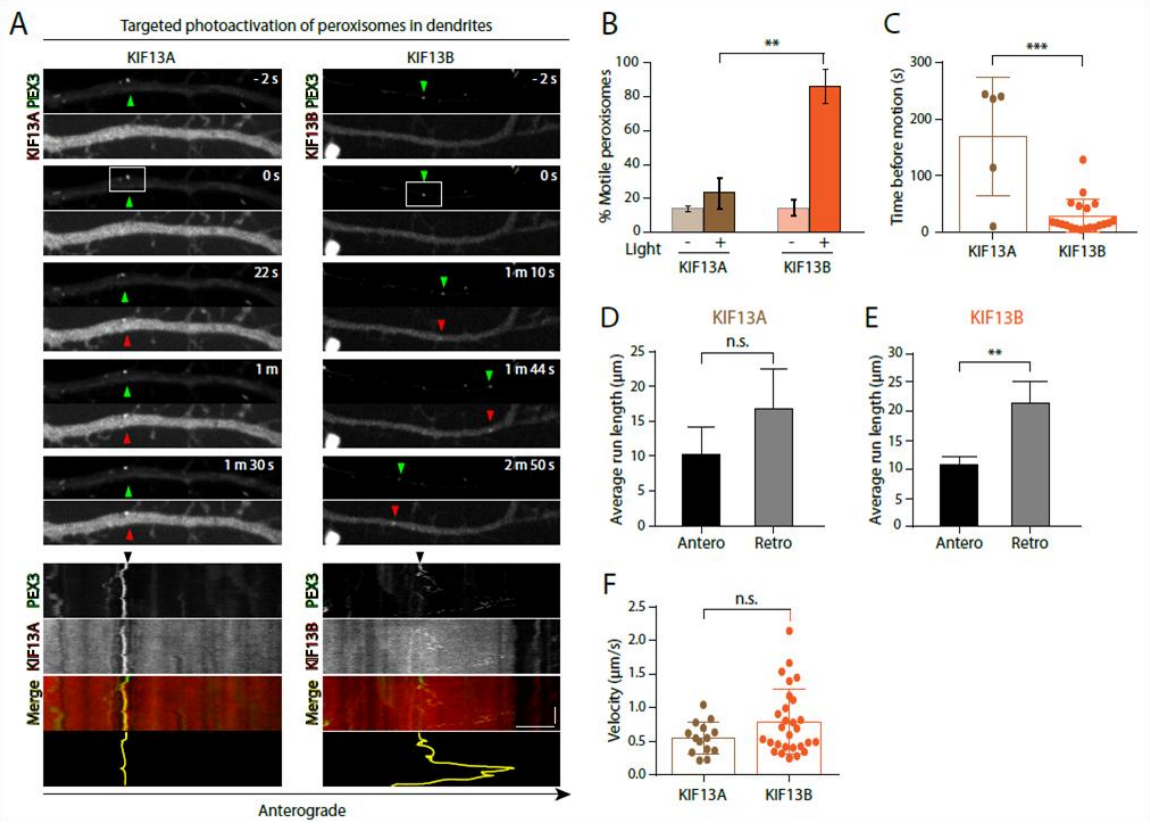

Figure 4.6 Differential regulation of KIF13A and KIF13B in dendrites.

(A) Time series and corresponding kymographs showing movement of photoactivated (white box) peroxisomes upon recruitment of KIF13A and KIF13B in dendrites. Horizontal bar, 5 µm. Vertical bar, 1 min. (B) Quantitation of percentage of dendritic peroxisomes that are motile. Mean ± SEM. **p<0.01, one-way ANOVA with Tukey's post-hoc test. (C) Time taken by peroxisomes to begin movement post photoactivation. Mean ± SD. ***p<0.001, Student's t-test. (D and E) Average run lengths of photoactivated peroxisomes for the two motors in the anterograde and retrograde directions. n.s., not significant, **p<0.01, Student's t-test. (F)

Average velocities of individual runs of peroxisomes that are motile post photoactivation. Mean ± SD, n.s., not significant, Student's t-test. Data from 25 peroxisomes from n=16 neurons and N=3 independent experiments.

IV. Discussion

Using a newly developed optogenetic tool in combination with live-cell imaging, we investigated how selective dendritic transport is regulated in mature neurons. With this approach, we can assess how each motor examined can function in a specific cellular environment. Our findings shed light on the different regulatory mechanisms that cytoplasmic dynein and kinesins employ in neuronal trafficking.

We find that dynein functions as effectively in dendrites as we previously observed in axons (Ballister et al., 2015), with >90% of peroxisomes moving bidirectionally post photoactivation. Dynein motility in dendrites had a retrograde bias that correlated with the bias of ~65% plus-end out microtubules in dendrites, suggesting that dynein motility is predominantly governed by microtubule orientation. While dynein-induced motility caused no observable accumulation of peroxisomes at dendritic tips, ~50% of photoactivated peroxisomes eventually entered the cell soma. This observation is again consistent with the underlying organization of the microtubule cytoskeleton in dendrites, with mixed microtubules in the proximal two-thirds of dendrites and predominantly plus-end out microtubules in distal dendrites (Stepanova et al., 2003; Kleele et al., 2014). Thus, the net bias of dynein-mediated transport in dendrites will be toward the soma, as observed (Fig. 2A).

The microtubule cytoskeleton of mature neurons is organized in a way that prevents dynein-driven cargos in the soma from entering axons, but allows them to enter dendrites. A previous study using a chemical inducible dimerization system showed that bulk recruitment of dynein to peroxisomes in neurons led to a polarized redistribution of these organelles into dendrites (Kapitein et al., 2010). In our assay we find that dynein specifically recruited to dendritic peroxisomes can efficiently navigate these organelles back to the cell soma. Thus,

our results in conjunction with the observations of Kapitein et al. (2010), demonstrate the ability of dynein to transport cargo both *into* and *out of* dendrites. Hence dynein is important for not only establishing the distribution of cargo to post-synaptic sites in dendrites (Kapitein et al., 2010; van Spronsen et al., 2013), but also promotes the efficient retrograde trafficking of cargo within the dendrite (Liot et al., 2013), and from the dendrite back to the cell soma, as shown here.

Regulation of the dynein motor is achieved by interactions with various adaptors (King and Schroer, 2000; Huang et al., 2012; Mckenney et al., 2014; Ayloo et al., 2014). One such ubiquitous adaptor functioning closely with dynein is the dynactin complex. We previously demonstrated that dynactin enriched at the distal end of axons is essential to initiate retrograde transport (Moughamian and Holzbaur, 2012). This observation led us to ask whether dynein motility in dendrites required microtubules to be dynamic. To test this, we performed our photoactivation assay in neurons treated with low dose nocodazole, which eliminates microtubule dynamics without inducing microtubule depolymerization. Consistent with our hypothesis, we observed a significant reduction in dynein-induced motility in both axons and dendrites when microtubule dynamics were inhibited. In particular, we noted a significant increase in the pausing of organelles during active runs. We propose that the decreased transport observed upon nocodazole treatment is a direct consequence of decreased loading of dynein onto the dynamic plus-end of microtubules following detachment of the motor from its track, for example, at a gap between adjacent microtubules. The role of microtubule plus ends in facilitating motor binding may be especially important in dendrites, which have more dynamic microtubules than the mid-axon (Stepanova et al., 2003; Kleele et al., 2014). Collectively, our findings suggest that dynein predominantly responds to microtubule orientation and depends on microtubule dynamics for efficient motility during long distance organelle transport.

Given that cytoplasmic dynein is the major minus end-directed motor in neurons, it is not surprising that dynein works efficiently in both axons and dendrites. In contrast, multiple kinesin motors are expressed in neurons, allowing for specificity, but how is this specificity achieved during polarized trafficking in neurons? Several models have been proposed. Previous work has shown that vesicles containing axonal proteins are trafficked to the axon and those containing dendritic proteins are trafficked to the dendrite (Burack et al., 2000; Setou et al., 2002). This led to the proposal that motor-cargo interactions determine cargo destination, the 'cargo steering' model. There is also work demonstrating that the motors themselves can distinguish between axonal and dendritic microtubules (Nakata and Hirokawa, 2003; Huang and Banker 2012), leading to the 'smart motor' hypothesis. Thus, there are at least two layers of regulation: motor-cargo and motor-microtubule that together determine selective transport in neurons.

Using an optogenetic approach, we can specifically target motor proteins to either axonal or dendritic cargos, allowing us to focus on motor-microtubule interactions. With our assay, we can now examine if the preferential localization of motor domains in a compartment correlates with function – the ability of the motor to actively transport cargos within that compartment. For kinesin-1, previous reports have shown that the constitutively active K560 construct preferentially accumulates in axon tips (Nakata and Hirokawa, 2003). Somewhat surprisingly, we find that although the motility induced by the photoactivated recruitment of K560 to dendritic peroxisomes is not as robust as that observed in axons (~60% in dendrites vs. ~90% in axons), those organelles that do respond exhibit robust motility characterized by long, bidirectional runs. Thus, the kinesin-1 motor is capable of navigating the dendritic microtubule cytoskeleton. This activity is likely to be physiologically relevant, as full length kinesin-1 has been shown to be steered to dendrites by GRIP1, which is predominantly found in the somatodendritic compartment (Setou et al., 2002).

We also examined two KIF13 motor proteins, members of the kinesin-3 family, in our optogenetic assay. Previous work demonstrated that in steady state assays, the motor domain of KIF13A preferentially localizes to axons while KIF13B is dendritic (Huang and Banker, 2012; Jenkins et al., 2012). In our assays, both KIF13A and KIF13B worked robustly in axons, but only KIF13B was effective at moving cargo in dendrites. While recruitment of KIF13B to dendritic peroxisomes resulted in long, bidirectional runs, KIF13A-bound organelles barely moved, suggesting that this motor cannot efficiently interact with dendritic microtubules. Together, these results suggest that the dendritic cytoskeleton is more restrictive for kinesin-driven motility than the axon.

It is likely that the compartment-specific regulation of kinesins observed here and in previous studies is a response to distinct biochemical signatures found on axonal and dendritic microtubules. For example, the decreased efficiency observed for kinesin-1 in dendrites is consistent with the preferential binding of kinesin-1 to acetylated microtubules enriched in axons (Reed et al., 2006). It has also been suggested that the enrichment of detyrosinated tubulin in the axon preferentially steers kinesin-1 to this compartment (Konishi and Setou, 2009). However, the underlying mechanisms are unclear, as increasing tubulin acetylation levels throughout the neuron was not sufficient to alter the selectivity of kinesin-1 mediated trafficking (Hammond et al., 2010). Further, *in vitro* studies indicate that kinesin-1 binds equally well to tyrosinated and detyrosinated microtubules (Nirschl et al., 2016), and detyrosination of tubulin is reported to decrease kinesin-1 processivity (Sirajuddin et al., 2014).

One possibility is that a single signal is not sufficient to mediate specificity, and instead, motor-microtubule interactions are likely to be specified by multiple biochemical cues on microtubules (Hammond et al., 2010). Microtubule-associated proteins, or MAPs, may also contribute to the specificity of localization, as recent work has shown that

doublecortin-like kinase1 (DCLK1) guides KIF1-dependent trafficking of dendritic cargo (Lipka et al., 2016). Further, the microtubule cytoskeleton in neurons undergoes many changes during development, accruing additional post-translational modifications along with changes in the complement of MAPs bound to the cytoskeleton (Janke and Kneussel, 2010). Consistent with this, KIF13A is enriched at axon tips in mature neurons, but fails to accumulate preferentially in immature neurons (Huang and Banker, 2012).

It remains unclear what elements of kinesin motors are responding to compartment-specific differences in the microtubule cytoskeleton. Sequence comparisons of the motor-domains of KIF13A and KIF13B do not reveal any obvious differences that would explain the differential ability of these motors to navigate dendritic microtubules. Konishi and Setou (2009) have previously identified a conserved TERF motif within the motor domain of kinesin-1; when this motif is mutated to the SKLA motif found within the corresponding region of the kinesin-3 motors KIF1A and KIF1B, they report that kinesin-1 is converted to a bi-destination motor with both axonal and dendritic localization. KIF13B shares the SKLA motif found in both KIF1A and KIF1B, while the corresponding motif in KIF13A is SQLA. While it is possible that a single amino acid change could induce specificity of localization, this is unlikely to be sufficient, as engineering the TERF motif from kinesin-1 into KIF1 was not sufficient to restrict the motor to the axonal compartment (Konishi and Setou, 2009).

Other work has focused on the microtubule-binding element loop 12, a lysine-rich K-loop (Okada and Hirokawa, 1999) present in kinesin-3 family motors. Incorporation of this loop into kinesin-1 was sufficient to disrupt axon selectivity (Huang and Banker, 2012), but the converse experiment of engineering the kinesin-1 loop 12 into the kinesin-3 motor KIF1A was not sufficient to induce axonal selectivity. And as noted here, compartment-specific targeting is distinct from the ability of a motor to function within a given compartment. Thus,

further work will be required to dissect the mechanisms providing subcellular specificity of both localization and function.

Polarized sorting in neurons is regulated at multiple levels; here, we focused on one aspect of this regulation, the interaction of motors with their microtubule tracks. Our data converge to a model wherein kinesins achieve specificity via differential interactions with microtubules in axons versus dendrites, while dynein responds to global parameters of microtubules, which are polarity and dynamics (Fig. 4.7). Together, the orchestrated trafficking of organelles by these motors provides the necessary specificity to move organelles to their proper cellular locations.

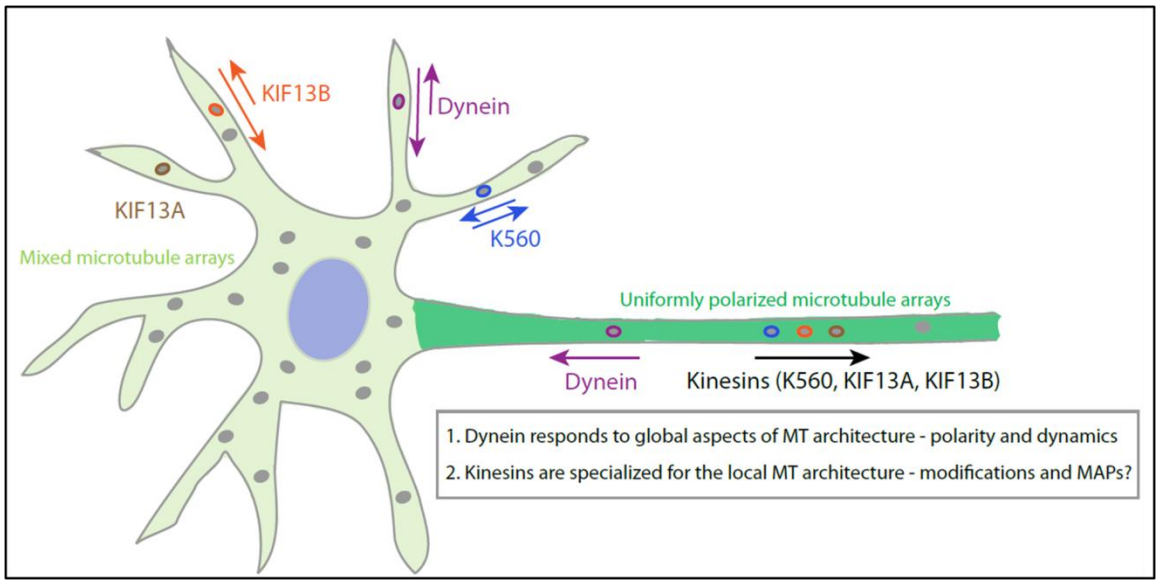

Figure 4.7 Working model for the axo-dendritic regulation of motor proteins.

Axons and dendrites harbor distinct microtubule architecture (shown in shades of green). While both dynein and KIF13B have longer run lengths in the retrograde direction in dendrites, K560 has no bias (as indicated by length of arrows) and KIF13A has very little motility. We propose that kinesins and dynein use distinct mechanisms to navigate the neuronal cytoskeleton. Dynein works efficiently in both axons and dendrites, with motility determined by microtubule orientation and microtubule dynamics. Kinesins are differentially tuned for different compartments and specificity may be achieved by recognizing biochemical modifications and MAPs associated with axonal and dendritic microtubules.

V. Material and Methods

Reagents

DNA constructs for the motor recruitment assay were expressed under the CAG promoter, derived from pEM705, obtained from E.V. Makeyev (Nanyang Technological University). For peroxisome targeting, 1-42 amino acid (aa) residues of the human Pex3 gene were C-terminally fused to GFP-Halo. All the mCherry-eDHFR constructs are derived from the mCherry-eDHFR plasmid previously described in Ballister et al., 2014. BICD-mCherry-eDHFR constitutes residues 1-572 of mouse BICD2 (referred to herein as BICD according to Kapitein et al., 2010) and K560-mCherry-eDHFR includes residues 1-560 of human kinesin-1 heavy chain (Ballister et al., 2015; Kapitein et al., 2010). KIF13A (1-411 ΔP390) and KIF13B (1-412 ΔP391) were obtained from Kristen Verhey (University of Michigan). EB3-GFP under the CMV promoter was recloned from a plasmid provided by Irina Kaverina (Vanderbilt University).

Neuronal cell culture, transfections and drug treatment

Rat hippocampal neurons were dissected from embryos at days 18-20 as described (Wilcox et al., 1984) and obtained in suspension from the Neuron Culture Service Center at the University of Pennsylvania. 1,00,000 cells/ml were plated on 35 mm glass bottomed dishes coated with 0.5 mg/ml poly-L-lysine. Neurons were grown in 2 ml maintenance media (Neurobasal medium supplemented with 2% B-27, 33 mM glucose, 2 mM GlutaMax, 100 units/ml penicillin and 100 µg/ml streptomycin) at 37°C in a 5% CO_2 incubator. Every 3-4 days, 25% of the media was replaced with fresh maintenance media supplemented with 1 µM AraC.

Imaging was done on 8-10 DIV (days in vitro) with DNA plasmids transfected 12-18 hours before imaging. PEX3-GFP-Halo was co-transfected with motor protein construct (either K560-mCherry-eDHFR or BICD-mCherry-eDHFR or KIF13A-mCherry-eDHFR or KIF13B-mCherry-eDHFR) using Lipofectamine 2000 reagent (Invitrogen).

In all experiments, neurons were incubated with 10 µM of the caged dimerizer cTMP-Halo (Ballister et al., 2014) for 30 minutes. The excess ligand was washed away with imaging media prior to imaging. For low dose nocodazole experiments, neurons were treated with 100 ng/ml nocodazole (Sigma) or DMSO control for 1.5 hours at 37°C in a 5% CO_2 incubator. Nocodazole or DMSO was also added to the imaging media.

Image acquisition and photoactivation

Neurons were imaged in low-fluorescence nutrient media (Hibernate E, Brain Bits) supplemented with 2% B27 and 1% GlutaMax. Data were acquired on a spinning-disk confocal UltraView VOX (Perkin Elmer) with a 405 nm Ultraview Photokinesis (Perkin Elmer) unit on an inverted Nikon Ti microscope with apochromat 100X 1.49 NA oil-immersion objective and a C9100-50 EMCCD camera (Hamamatsu) controlled by Volocity software (Perkin Elmer). Only neurons expressing both of the co-transfected GFP and mCherry markers were imaged. Axons and dendrites were identified based on morphologic criteria as outlined (Kaech and Banker, 2006). Localized photoactivation along axons was performed as described (Ballister et al., 2015). At 8-10 DIV, dendrite lengths in our cultures were about ~50-200 µm. Peroxisomes localized approximately to the middle one-third of dendrites were selected for photoactivation. Two-color images (GFP and mCherry) were acquired for 20 s at 2 s per frame prior to photoactivation and for 5 min at 2 s per frame post photoactivation. The green and red signals in the representative two-color movies shown here may appear slightly offset due to delay in acquiring consecutive images. EB3-GFP imaging was recorded at 1 frame per second.

Motility analysis

Photoactivated organelles were classified as motile if they moved greater than a 5 µm distance in our 5 minute imaging window. For axonal data, all velocities reported are average velocities. In dendrites, the motion was considered bidirectional if the organelle moved greater than 5 µm in both the anterograde and retrograde directions at least once during motion. All run length and velocity measurements were made from kymographs drawn using the Kymograph plugin in Fiji (Schindelin et al., 2012). For dendrite data, run length and velocities were obtained for every constant velocity segment in a given trajectory of an organelle. Owing to the depth of the dendrites, only organelles that could clearly be tracked for the entire length of the movie were considered for run length and velocity analysis. Each kymograph was generated in both the GFP and mCherry channels to correlate organelle movement with that of recruited motor.

Fluorescence measurements for recruitment

All intensity measurements for the recruitment analysis were recorded using Fiji. A region of interest (ROI) was drawn enclosing the organelle. Mean intensity of mCherry fluorescence in this ROI was measured one frame prior to photoactivation and one frame before the organelle started to move. In both cases, cytoplasmic background was subtracted. Post-photoactivation intensity was then divided by pre-photoactivation intensity to obtain fold change indicating recruitment of the motor protein or motor adaptor.

Statistical methods

All statistics were performed in GraphPad Prism. Student's t-test was used when comparing two data sets while one-way analysis of variance with Tukey's *post-hoc* test was used with multiple data sets.

CHAPTER 5: Conclusions and Future Directions

In this thesis, I have examined the regulatory mechanisms of dynein using both single-molecule imaging and live-cell imaging of neurons. I used bottom-up approaches reconstituting processes *in vitro*, to dissect dynein function with its co-factor dynactin and I then extended this work using a top-down approach by implementing a dimerization tool to study dynein-mediated transport in polarized neuronal trafficking.

Dynactin was identified in the early 90s but its role in dynein function has been controversial with several conflicting studies, both *in vitro* and *in vivo* (King and Schorer, 2000; Culver-Hanlon et al., 2006; Kim et al., 2007; Kardon et al., 2009; Lloyd et al., 2012; Moughamian and Holzbaur, 2012). Most of the previous *in vitro* studies were done using beads coated with non-specific adsorption of proteins which did not allow for accurate quantification of the stoichiometry of proteins in complex, thus making interpretation at the single molecule level difficult. Part of the reason why this was an attractive method was, it had been difficult to generate recombinant mammalian dynein complex with a fluorescent tag which allowed direct visualization of the protein. Thus, a critical tool which enabled us to undertake this project was the generation of a knock-in mouse line with one of the subunits of dynein fused to GFP (Zhang et al., 2013). Using recombinant $p150^{Glued}$, the subunit of dynactin that interacts with dynein, I was able to examine the co-localization and co-migration of the co-complex for the first time and my experiments reveal that dynactin is sufficient to recruit dynein onto microtubules, increasing the recruitment of dynein greater than 4-fold. My results also indicate that $p150^{Glued}$ both increases the on-rate and decreases the off-rate of dynein from microtubules.

How do adaptor proteins modulate the functioning of dynein-dynactin complexes?

Recent work from other labs has now shown that cargo adaptors like Bicaudal D and Hook proteins increase the processivity of single dynein-dynactin complex several fold (McKenney et al., 2014; Schlager et al., 2014). While previous studies indicated that teams of dynein move robustly *in vitro*, these two studies showed that single molecules of dynein-dynactin move super processively in the presence of adaptor proteins. Thus, these findings highlight a previously unknown regulation of dynein-dynactin complexes; however the mechanistic details of this regulation remain unclear. A fundamental question that arises from these findings is what are the changes the adaptor proteins confer on dynein-dynactin complexes that make them super processive. A hypothesis that has been suggested is that dynein without cargo bound to it exists in an autoinhibited state (Torisawa et al., 2014). Given this, it is likely that adaptor protein binding to dynein, in the presence of dynactin, relieves autoinhibition. High resolution structure studies should provide insight into the structural aspects of how adaptors modulate dynein binding to dynactin.

Another important question these studies raise is the differential modulation of the motility of the dynein-dynactin complexes by the various adaptors. Besides several coiled-coil domains in these proteins, there are no specific common features among these adaptors. Hence the next challenge is to understand adaptor-specific modulation of dynein-dynactin complexes which will inform us about organelle-dependent regulation of dynein motility. An interesting next step in this direction would be to compare and contrast teams of dynein-dynactin molecules with and without the adaptor proteins as organelles in cells have several dynein motors on them (reviewed in Mallik et al., 2013). It is possible that the single molecule behavior of dynein-dynactin-adaptor complexes is the same but when working in teams; dynein could operate in a different regime, shedding light on the differential regulation of dynein-dynactin via adaptors.

Can the CAP-Gly domain function as a switch in vivo, controlled by phosphorylation?

My results from single-molecule imaging of various constructs of $p150^{Glued}$ indicate that the CAP-Gly domain functions to recruit dynein onto microtubules and also acts as an ATP-independent brake to slow down the motor. Based on data from previous reports and my *in vitro* results, we put forth a working model wherein dynactin binding to microtubules becomes important in specific instances of dynein-driven transport, particularly in the efficient initiation of retrograde transport. It is likely that the CAP-Gly domain becomes dispensable once retrograde transport is initiated (consistent with Kim et al., 2007) and given that CAP-Gly domain also slows down the dynein motor, binding of dynactin to microtubules during transport would be inefficient. Hence a key aspect of the regulation of dynactin is a switch that controls the binding of dynactin to microtubules and I hypothesize that phosphorylation is one potential mechanism to achieve this.

Initial metabolic labeling studies identified $p150^{Glued}$ as a phosphoprotein with serine residues being the exclusive phosphorylation sites (Farshori and Holzbaur, 1997). The increased phosphorylation of $p150^{Glued}$ in the presence of activators of protein kinases correlated with increased intracellular transport (Farshori and Holzbaur, 1997). In the context of my working model, this would suggest that phosphorylation of $p150^{Glued}$ prevents its microtubule binding, hence $p150^{Glued}$ can no longer act as a brake to slow down organelle motility. Subsequent work identified S19 in the N-terminus CAP-Gly domain of $p150^{Glued}$ as a phosphorylation site for protein kinase A (Vaughan et al., 2002). This work demonstrated that phosphomimetic version of $p150^{Glued}$, S19E, diminished its microtubule binding both *in vitro* and in cells. A more recent study also identified $p150^{Glued}$ as a substrate for Aurora A (Rome et al., 2010). Dynactin accumulates on microtubules during prophase and disappears from microtubules during nuclear envelope breakdown (Kim et al., 2007). Interestingly, $p150^{Glued}$ that cannot be phosphorylated by Aurora A exhibited high microtubule binding during mitosis

and failed to rescue mitotic defects in cells with knock down of WT p150^{Glued} (Rome et al., 2010). All of these studies are consistent with the idea that phosphorylation of p150^{Glued} in the CAP-Gly domain abolishes its microtubule binding capacity. Hence, it is likely that post initiation of retrograde transport by dynein, phosphorylation of the CAP-Gly of dynactin can indeed act as a switch that gets activated in dynein-driven motility.

A direct follow-up of my *in vitro* data would be to perform single molecule motility assays with phospho-mimetic and phospho-deficient forms of p150^{Glued} and examine the motility aspects and also the capacity of p150^{Glued} to act as a brake which has not been done before. An extension of this work in neurons would be to investigate localization of phosphorylated and non-phosphorylated forms of p150^{Glued} in axons with phosphorylation-specific antibodies (used previously in Vaughan et al., 2002). Observation of gradients of these forms of p150^{Glued} and particularly an enrichment of the non-phosphorylated form of p150^{Glued} at the distal end of the axon will directly test my hypothesis that the microtubule binding function of CAP-Gly becomes important in specific instances of transport, initiation being one such instance.

Why do neurons need a unique isoform of dynactin lacking the CAP-Gly domain?

p135 is an isoform of p150^{Glued} that lacks the CAP-Gly domain and is found only in the brain tissue. This unique isoform was discovered almost 20 years ago (Tokito et al., 1996), yet we know very little about why neurons need this specialized version of dynactin. The recent findings elucidating the importance of CAP-Gly domain in neuronal transport (Moughamian and Holzbaur, 2012; Lloyd et al., 2012) make the presence of this isoform in neurons intriguing. It is known that p150^{Glued} and p135 form distinct dynactin complexes (Tokito et al., 1996) and a key question is when does dynein work with dynactin complexes that have p135 as opposed to p150^{Glued}. Since the CAP-Gly domain slows down the dynein

motor, is p135 containing dynactin preferred under stress conditions or injury when signaling molecules have to be transported over long distances, very quickly for repair? Is p135 containing dynactin enriched in mid-axon while p150 containing dynactin is enriched in the distal axon?

A big challenge in trying to answer some or all of these questions and hypotheses for p135 are the limited tools and reagents that will enable the distinguishing of p135 from $p150^{Glued}$. Currently, there are no siRNAs or antibodies that recognize p135 specifically; the two isoforms have only 4 amino acid residues different with the rest of the protein being the same. Over-expression of either $p150^{Glued}$ or p135 in neurons localizes throughout the neuron with $p150^{Glued}$ enriched at the distal end of axons owing to the CAP-Gly domain binding to microtubules. FRAP analysis of fluorescently tagged $p150^{Glued}$ and p135 revealed no significant differences between the recovery dynamics of the two pools in axons.

One idea to test the functional differences between $p150^{Glued}$ and p135 was to recruit either protein to organelles in neurons and examine the downstream effects on motility of the organelle. Unlike recruitment of adaptor proteins like Bicaudal D, recruitment of $p150^{Glued}$ failed to induce any motility of the organelle. This was the case with both neurons and HeLa cells and similar to this result, recruitment of p135 to organelles also failed to induce motility. An experiment to follow up on this is the ‘anchor-away’ approach that some studies have used to identify the function for proteins that have been implicated in cellular processes but the exact role of the given protein is not known (Robinson et al., 2010; Wong and Munro, 2014). The approach is to deplete proteins from their cellular location by targeting them to other locations (nucleus or mitochondria, for instance) using the inducible dimerization system and examine the processes in which the protein is predicted to play a role. In this case, p135 or $p150^{Glued}$ could be anchored away to the nucleus and motility of endosomes in the axons and dendrites and their flux can be compared in the two cases.

One possibility that remains to be tested is whether p135 is specifically required for dynein-mediated trafficking in dendrites as in all of the experiments mentioned above, only the axons were examined. Interestingly, very little is known about dynein trafficking in dendrites. Neuronal work in *Drosophila melanogaster* has shown that dynein is required for polarized trafficking in dendrites and for the distribution of golgi outposts in dendrites (Zheng et al., 2008). However, a key difference between fly neurons and mammalian neurons is the microtubule orientation in dendrites – mixed polarity in mammalian neurons and all minus-end out organization in flies. Hence it is likely that dendrite trafficking in these two types of neurons differ in several aspects. To this end, I applied the light-inducible dimerization tool in neurons to recruit kinesin and dynein motors to organelles in axons and dendrites to examine effects on organelle motility.

How is organelle-dependent regulation of dynein achieved?

Comparison of the recruitment of motors to peroxisomes and mitochondria in neurons indicated organelle-dependent regulation of the dynein motors. While recruitment of dynein induced robust retrograde motion in >90% of the peroxisomes, this was the case with only about ~40% of mitochondria indicating. One explanation for this difference is that peroxisomes are smaller organelles about 100-200 nm in size while mitochondria are long tubular structures ranging from 0.5–1.0 µm and the forces exerted by dynein are not enough to translocate mitochondria. However, we now know that diverse cellular functions are carried out by teams of dynein that work very efficiently together (reviewed in Mallik et al., 2013); hence it is possible that there are other factors responsiblefor the inability of dynein to move mitochondria in this assay. One such factor could be syntaphilin which has recently been shown to actively dock axonal mitochondria, thus restricting the mobility of these organelles (Kang et al., 2008). It is plausible that syntaphilin docking prevents the motor

activity of dynein that is recruited to mitochondria as has previously been shown with kinesins (Chen and Sheng, 2013). To directly test this hypothesis, syntaphilin could be knocked down and the same recruitment assay can be performed on mitochondria to examine if the absence of syntaphilin can now induce mitochondrial motility when dynein motors are recruited.

Another study examined the motility dynamics of mitochondria in axons and dendrites and identified TRAK1 and TRAK2, adaptors of mitochondrial motility to be differentially distributed in neurons – with TRAK1 enriched in axons and TRAK2 in dendrites (van Spronsen et al., 2013). The authors used *in vitro* biochemical assays to demonstrate that while TRAK1 binds to both kinesin and dynein, TRAK2 predominantly binds to dynein and this can explain the differential localization of the TRAKs as dynein can efficiently navigate the dendrites. However, there also seem to be compensatory effects when either of the TRAK proteins is knocked-down (van Spronsen et al., 2013). A direct way to test the effects of the TRAKs on mitochondria would be to use the light-inducible dimerization assay to specifically recruit either TRAK1 or TRAK2 to mitochondria in the cell soma and examine if they are targeted to the axon or dendrites. This experiment would directly demonstrate that TRAKs acts as steering factors for mitochondria.

Does dynein play a role in conferring a retrograde bias to kinesin motors in dendrites?

Several studies have identified multiple kinesins involved in trafficking in dendrites (reviewed in Hirokawa et al., 2009). Localization studies in mature neurons with constitutively active recombinant proteins revealed that KIF13B, a kinesin-3 motor protein localized to both axonal and dendritic tips while the related proteins, KIF13A localized to only axonal tips (Huang and Banker, 2012). I examined motility of KIF13A and KIF13B by recruiting them to organelles in both axons and dendrites. My results demonstrate that while both KIF13A and

KIF13B function well in axons, KIF13A failed to move in dendrites while KIF13B worked robustly. Interestingly, the motility of KIF13B in dendrites had a retrograde bias with significantly longer run lengths in the retrograde direction.

Given the underlying microtubule polarity in dendrites (~65% plus-end out in proximal dendrites and ~85% plus-end out in distal dendrites) and that KIF13s are plus-end directed motors, this result is surprising. The accumulation at dendritic tips (as seen in Huang and Banker, 2012) is not surprising as the motors that make it through the mixed arrays of microtubules in proximal dendrites, will go only toward the dendritic tips as the microtubules in distal dendrites are mostly plus-end out. However, the retrograde bias seen with KIF13B in dendrites is inconsistent with the underlying microtubule cytoskeleton. An attractive hypothesis is that KIF13B works closely with dynein in dendrites which can confer a retrograde bias to organelles that have KIF13B. The retrograde bias I find with dynein-induced motility of dendritic organelles strengthens this hypothesis. Consistent with this, recent work demonstrated that dynein associates with TrkB positive signaling endosomes and promotes their efficient retrograde trafficking within the dendrites of striatal neurons (Liot et al., 2013). Pull down assays and live-cell imaging of dynein and KIF13B in neurons should reveal if these motor proteins are found together on dendritic organelles. Imaging fluorescent KIF13B in hippocampal neurons dissected from the dynein-GFP knock-in mouse line to examine co-localization and co-migration of these two motors could be the first step toward testing this hypothesis. Interestingly, the retrograde bias seen with KIF13B in dendrites has also been observed with KIF21B (Ghiretti et al, under preparation) which is a kinesin-4 dendritic motor. It is likely that dynein is also involved in KIF21B-mediated trafficking in dendrites indicating that this could be a general principle for dendritic kinesins.

What factors contribute to the differential regulation of KIF13A and KIF13B in neurons

Using the light-inducible dimerization system, I observed striking differences between the motility of KIF13A and KIF13B in dendrites. While KIF13B produced robust motion in both directions, KIF13A failed to move in dendrites. One likely tubulin modification to examine in this context would be tubulin tyrosination. The proximal and mid-axon is generally enriched in detyrosinated tubulin while dendrites and growth cones of axons are enriched in tyrosinated microtubules (Konishi and Setou, 2009; Hammond et al., 2010). One way to test this would be to knock-down the tubulin tyrosine ligase (TTL) enzyme in neurons and perform the same motor recruitment assay to examine if this makes KIF13A a motile motor in dendrites. A more direct way to test this would be to compare the motility of purified KIF13A and KIF13B on tyrosinated and detyrosinated microtubules using single molecule assays (as previously done in Sirajuddin et al., 2014) and tubulin binding assays. An important aspect of tubulin modifications is that it may not necessarily be one modification that is contributing to the specific effects of KIF13A versus KIF13B but a manifestation of a combination of cellular cues and these experiments would be one way to begin to test this.

Previous work identified both KIF13A and KIF13B as kinesins binding to dendritically polarized vesicles containing transferrin (TfR) receptor (Jenkins et al., 2012). Dual color imaging of full length KIF13A or KIF13B with TfR would allow comparing the motility characteristics of these two different populations. Given my observations with the motor domains of KIF13A and KIF13B, I predict that KIF13A associated puncta would be largely stationary. However, it is possible that full length motors could function differently from constitutively active truncated forms as previously observed with the localization of full length and truncated forms of KIF16B (Farkohndeh et al., 2015), in which case the tails of these kinesins and the potential adaptor proteins the tails bind to have to be investigated (as previously done in Jenkins et al., 2012).

Concluding Remarks

In summary, in this thesis, I focused on the regulation of cytoplasmic dynein both *in vitro* and in neurons using a combination of approaches. My work has dissected the role of dynactin in dynein-mediated transport and further regulation of dynein in polarized neuronal transport. Several mutations have been identified in dynein, dynactin and dynein adaptors contributing to diseases associated with trafficking. Important goals for the future include understanding adaptor-specific regulation of dynein, dynein dysfunction in neurodegenerative diseases, selective vulnerability of certain neurons in these diseases and finally cargo-specific regulatory mechanisms in neuronal transport. Research in each one of these areas is required to provide a holistic understanding of our knowledge about dynein-mediated transport.

REFERENCES

Akella JS, Wloga D, Kim J, Starostina NG, Lyons-Abbott S, Morrissette NS, Dougan ST, Kipreos ET, Gaertig J 2010. MEC-17 is an alpha-tubulin acetyltransferase. Nature. 467:218–222

Al-Bassam S, Xu M, Wandless TJ, Arnold DB 2012. Differential trafficking of transport vesicles contributes to the localization of dendritic proteins. Cell Rep 2:89–100

Allan VJ 2011 Cytoplasmic dynein. Biochem. Soc. Trans. 39, 1169–1178.

Arce CA, Rodriguez JA, Barra HS, Caputo R 1975. Incorporation of L-tyrosine, L-phenylalanine and L-3,4-dihydroxyphenylalanine as single units into rat brain tubulin. Eur J Biochem 59:145–149.

Allen RD, Metuzals J, Tasaki I, Brady ST, Gilbert SP 1982. Fast axonal transport in squid giant axon. Science 218:1127-1129

Ayloo S, Lazarus JE, Dodda A, Tokito M, Ostap EM, Holzbaur EL. 2014. Dynactin functions as both a dynamic tether and brake during dynein-driven motility. Nat. Commun. 5:4807

Baas PW, Deitch JS, Black MM, Banker G A 1988. Polarity orientation of microtubules in hippocampal neurons: uniformity in the axon and nonuniformity in the dendrite. Proc Natl Acad Sci U S A 85:8335–8339.

Baas PW, Black MM, Banker GA. Changes in microtubule polarity orientation during the development of hippocampal neurons in culture. J Cell Biol. 1989;109:3085–3094

Baas PW, Lin S 2011. Hooks and comets: the story of microtubule polarity orientation in the neuron. Dev Neurobiol 71:403–418.

Ballister ER, Aonbangkhen C, Mayo AM, Lampson MA, Chenoweth DM 2014. Localized light-induced protein dimerization in living cells using a photocaged dimerizer. Nat Commun 5:5475

Ballister ER, Ayloo S, Chenoweth DM, Lampson MA, Holzbaur ELF 2015. Optogenetic control of organelle transport using a photocaged chemical inducer of dimerization. Curr Biol 25:R407–R408

Barra HS, Rodriguez JA, Arce CA, Caputto R 1973. A soluble preparation from rat brain that incorporates into its own proteins (^{14}C)arginine by a ribonuclease-sensitive system and (^{14}C)tyrosine by a ribonuclease-insensitive system. *J. Neurochem.* 20, 97–108

Barra HS, Arce CA, Rodriguez JA, Caputto R 1974. Some common properties of the protein that incorporates tyrosine as a single unit and the microtubule proteins. Biochem Biophys Res Commun 60:1384–1390.

Bartlett WP, Banker GA 1984a. An electron microscopic study of the development of axons and dendrites by hippocampal neurons in culture. I. Cells which develop without intercellular contacts. J. Neurosci. 4:1 944-53

Bartlett WP, Banker GA 1984b. An electron microscopic study of the development of axons and dendrites by hippocampal neurons in culture . II . Synaptic relationships. J. Neurosci. 4:1954-65

Bentley M, Decker H, Luisi J, Banker G 2015. A novel assay reveals preferential binding between Rabs, kinesins, and specific endosomal subpopulations. J Cell Biol 208:273–281

Bieling P, Laan L, Schek H, Munteanu EL, Sandblad L, Dogterom M, Brunner D, .Surrey T 2007. Reconstitution of a microtubule plus-end tracking system *in vitro*. Nature 450, 1100-1105.

Bielska E, Schuster M, Roger Y, Berepiki A, Soanes DM, et al. 2014. Hook is an adapter that coordinates kinesin-3 and dynein cargo attachment on early endosomes. J. Cell Biol. 204:989–1007

Binder LI, Frankfurter A, Rebhun LI 1985. The distribution of tau polypeptides in the mammalian central nervous system. J. Cell BioI. 101:1371-78

Black MM, Baas PW 1989. The basis of polarity in neurons. Trends Neurosci. 12:211–214

Blasius TL, Cai D, Jih GT, Toret CP, Verhey KJ 2007. Two binding partners cooperate to activate the molecular motor Kinesin-1. J. Cell Biol. 176,11–17

Borisy GG, Taylor EW 1967a. The mechanism of action of colchicine. Binding of colchicine-3H to cellular protein. J. Cell Biol. 34, 525–534

Borisy GG, Taylor EW 1967b. The mechanism of action of colchicine. Colchicine binding to sea urchin eggs and the mitotic apparatus J. Cell Biol. 34:535–548.

Borisy GG, Marcum JM, Olmsted JB, Murphy DB, Johnson KA 1975. Purification of tubulin and of associated high molecular weight proteins from porcine brain and characterization of microtubule assembly *in vitro*. Ann. NY Acad. Sci. 253:107-32

Boucher D, Larcher JC, Gros F, Denoulet P 1994. Polyglutamylation of tubulin as a progressive regulator of *in vitro* interactions between the microtubule-associated protein Tau and tubulin. Biochemistry 33, 12471–12477

Brady ST, Lasek RJ, Allen RD 1982. Fast axonal transport in extruded axoplasm from squid giant axon. Science 218:1129-1131.

Burack MA, Silverman MA, Banker G 2000. The role of selective transport in neuronal protein sorting. Neuron 26:465–472.

Burkhardt JK, Echeverri CJ, Nilsson T, Vallee RB 1997. Overexpression of the dynamitin (p50) subunit of the dynactin complex disrupts dyneindependent maintenance of membrane organelle distribution. J Cell Biol 139:469-484.

Burton PR, Paige JL 1981. Polarity of axoplasmic microtubules in the olfactory nerve of the frog. Proc Natl Acad Sci U S A. 78:3269–3273.

Burton PR 1988. Dendrites of mitral cell neurons contain microtubules of opposite polarity. Brain Res.473:107–115

Caceres A, Banker G, Steward O, Binder L, Payne M 1 984. MAP 2 is localized to the dendrites of hippocampal neurons which develop in culture. Dev. Brain Res. 13:314-18

Carminati J, Stearns T 1997. Microtubules orient the yeast spindle through dynein-dependent interactions with the cell cortex. J. Cell Biol. 138:629-641.

Caro LG, Palade GE 1964. Protein Synthesis, Storage, and Discharge in the Pancreatic Exocrine. J Cell Biol 20:473–495.

Carter AP, Garbarino JE, Wilson-Kubalek EM, Shipley WE, Cho C, et al. 2008. Structure and functional role of dynein's microtubule-binding domain. Science 322:1691–5

Carter AP, Cho C, Jin L, Vale RD. 2011. Crystal structure of the dynein motor domain. Science 331:1159–65

Cavalli V, Kujala P, Klumperman J, Goldstein LSB. 2005. Sunday Driver links axonal transport to damage signaling. J Cell Biol. 168:775-787.

Chen XJ, Levedakou EN, Millen KJ, Wollmann RL, Soliven B, Popko B 2007. Proprioceptive sensory neuropathy in mice with a mutation in the cytoplasmic Dynein heavy chain 1 gene. J Neurosci 27:14515-14524.

Cho C, Reck-Peterson SL, Vale RD. 2008. Regulatory ATPase sites of cytoplasmic dynein affect processivity and force generation. J. Biol. Chem. 283:25839–45

Chowdhury S, Ketcham SA, Schroer TA, Lander GC. 2015. Structural organization of the dynein-dynactin complex bound to microtubules. *Nat. Struct. Mol. Biol.* 22:345–47

Claussen M, Suter B 2005. BicD-dependentlocalization processes: from Drosophila development tohumancellbiology. Ann. Anat. 187, 539–553

Cleveland DW, Hwo SY, Kirschner MW 1977. Purification of tau, a microtubule- associated protein that induces assembly of microtubules from purified tubulin. J. Mol. Biol. 116:207-25

Cole DG, Chin SW, Wedaman KP, Hall K, Vuon T, Scholey, JM 1993. Novel heterotrimeric kinesin-related protein purified from sea urchin eggs. Nature 366, 268-270.

Conde C, Cáceres A 2009. Microtubule assembly, organization and dynamics in axons and dendrites. Nat Rev Neurosci 10:319–332.

Craig AM, Blackstone CD, Huganir RL, Banker G 1993. The distribution of glutamate receptors in cultured rat hippocampal neurons: postsynaptic clustering of AMPA selective subunits. Neuron 10: 1055-68

Craig AM, Banker G 1994. Neuronal polarity. Annu. Rev. Neurosci. 17:267–310.

Culver-Hanlon TL, Lex SA, Stephens AD, Quintyne NJ, King SJ 2006. A microtubule-binding domain in dynactin increases dynein processivity by skating along microtubules. Nat. Cell Biol. *8*, 264-270.

David-Pfeuty T, Erickson HP, Pantaloni D 1977. Guanosinetriphosphatase activity of tubulin associated with microtubule assembly. Proc Natl Acad Sci U S A. 74:5372-6.
Davis L, Banker GA, Steward O 1987. Selective dendritic transport of RNA in hippocampal neurons in culture. Nature 330:477-79

DeWitt MA, Chang AY, Combs PA, Yildiz A. 2012. Cytoplasmic dynein moves through uncoordinated stepping of the AAA+ ring domains. Science 335:221–25

Dietrich KA, Sindelar CV, Brewer PD, Downing KH, Cremo CR, Rice SE 2008. The kinesin-1 motor protein is regulated by a direct interaction of its head and tail. Proc Natl Acad Sci U S A. 105:8938-8943.

Dixit R, Ross JL, Goldman YE, Holzbaur ELF. 2008a. Differential regulation of dynein and kinesin motor proteins by tau. Science. 319:1086-9.

Dixit R, Levy JR, Tokito M, Ligon LA, Holzbaur EL 2008b. Regulation of dynactin through the differential expression of $p150^{Glued}$ isoforms. J Biol Chem 283:33611-33619

Dotti CG, Banker GA, Binder LI 1987. The expression and distribution of the microtubule-associated proteins tau and microtubule- associated protein 2 in hippocampal neurons in situ and in cell culture. Neuroscience 23: 121-30

Dotti CG, Sullivan CA, Banker GA 1988 The establishment of polarity by hippocampal neurons in culture.J Neurosci. 8:1454–1468

Drechsel DN, Hyman AA, Cobb MH, Kirschner MW. 1992. Modulation of the dynamic instability of tubulin assembly by the microtubuleassociated protein tau. *Mol. Biol. Cell* 3: 1141–54

Droz B, Leblond CP 1962 Migration of proteins along the axons of the sciatic nerve. Science 137:1047-1048.

Dunn, S, Morrison EE, Liverpool TB, Molina-Paris C, Cross RA, Alonso MC, Peckham M 2008. Differential trafficking of Kif5c on tyrosinated and detyrosinated microtubules in live cells. Journal of Cell Science. 121:1085-95.

Duchen LW 1974. A dominant hereditary sensory disorder in the mouse with deficiency of muscle spindles: the mutant Sprawling. J. Physiol. (Lond.) 237, 10P–11P

Dujardin D, Wacker UI, Moreau A, Schroer TA, J.E. Rickard JE, De Mey JR. 1998. Evidence for a role of CLIP-170 in the establishment of metaphase chromosome alignment. J. Cell Biol.141:849–862

Echeverri CJ, Paschal BM, Vaughan KT, Vallee RB 1996. Molecular characterization of the 50-kD subunit of dynactin reveals function for the complex in chromosome alignment

Eddé B, Rossier J, Le Caer JP, Desbruyères E, Gros F,Denoulet P 1990. Posttranslational glutamylation of alpha-tubulin. Science. 247:83–85

Engelender S, Sharp AH, Colomer V, Tokito MK, Lanahan A, Worley P, Holzbaur EL, Ross CA 1997. Huntingtin-associated protein 1 (HAP1) interacts with the p150^{Glued} subunit of dynactin. *Hum Mol Genet*. 6:2205-2212

Erck C, Peris L, Andrieux A, Meissirel C, Gruber AD, Vernet M, Schweitzer A, Saoudi Y, Pointu H, Bosc C, et al 2005. A vital role of tubulin-tyrosine-ligase for neuronal organization. Proc. Natl. Acad. Sci. USA. 102:7853 7858.

Ersfeld, K., J. Wehland, U. Plessmann, H. Dodemont, V. Gerke, and K. Weber 1993.Characterization of the tubulin-tyrosine ligase. J. Cell Biol. 120:725–732.

Farkhondeh A, Niwa S, Takei Y, Hirokawa N 2015. Characterizing KIF16B in neurons reveals a novel intramolecular “stalk inhibition” mechanism that regulates its capacity to potentiate the selective somtadendritic localization of early endosomes. The Journal of Neuroscience. 35: 5067-86

Farrer, M. J. et al. 2009. DCTN1 mutations in Perry syndrome. Nat. Genet. 41, 163–165

Farshori P, Holzbaur EL. Dynactin phosphorylation is modulated in response to cellular effectors. Biochem Biophys Res Commun. 1997;232:810–816

Fawcett DW, Porter KR 1954. A study of the fine structure of ciliated epithelia J.Morphol. 94:221–81

Fink G, Hajdo L, Skowronek KJ, Reuther C, Kasprzak AA, Diez S 2009.The mitotic kinesin-14 Ncd drives directional microtubule-microtubule sliding. Nature Cell Biology.11:717–723.

Fouquet JP, Eddé B, Kann ML, Wolff A, Desbruyeres E, Denoulet P 1994. Differential distribution of glutamylated tubulin during spermatogenesis in mammalian testis. Cell Motil. Cytoskeleton. 27:49–58

Freed JJ 1965. Microtubules and saltatory movements of cytoplasmic elements in cultured cells. J. Cell Biol. 27:29A

Friedman DS, Vale RD 1999. Single-molecule analysis of kinesin motility reveals regulation by the cargo-binding tail domain. Nat Cell Biol. 1:293-297.

Fries E, Rothman JE 1980. Transport of vesicular stomatitis virus glycoprotein in a cellfree extract. Proc Natl Acad Sci USA. 77:3870–3874.

Frost B, Götz J, Feany MB 2015. Connecting the dots between tau dysfunction and neurodegeneration Trends Cell Biol., 25, 46–53

Fu MM, Holzbaur EL. 2013. JIP1 regulates the directionality of APP axonal transport by coordinating kinesin and dynein motors. Journal of Cell Biology. 202:495-508.

Fu MM, Holzbaur EL. 2014. Integrated regulation of motor-driven organelle transport by scaffolding proteins. Trends in Cell Biology. 24:564-574.

Gardner MK, Hunt AJ, Goodson HV, Odde DJ 2008. Microtubule assembly dynamics: new insights at the nanoscale. Curr. Opin. Cell Biol. 20 64–70

Garner CC, Tucker RP, Matus A 1988. Selective Localization of messenger RNA for cytoskeletal protein MAP2 in dendrites. Nature 336, 674-677.

Gee MA, Heuser JE, Vallee RB. 1997. An extended microtubule-binding structure within the dynein motor domain. Nature 390:636–9

Gennerich A, Carter AP, Reck-Peterson SL, Vale RD. 2007. Force-induced bidirectional stepping of cytoplasmic dynein. Cell 131:952–65

Gibbons IR 1963. Studies on the Protein Components of Cilia from Tetrahymena Pyriformis. Proceedings of the National Academy of Sciences of the United States of America 50, 1002-1010.

Gibbons IR, Rowe AJ. 1965. Dynein: A Protein with Adenosine Triphosphatase Activity from Cilia. Science. 149: 424-6.

Gill SR, Schroer TA, Szilak I, Steuer ER, Sheetz MP, Cleveland DW. 1991. Dynactin, a conserved, ubiquitously expressed component of an activator of vesicle motility mediated by cytoplasmic dynein. Journal of Cell Biology. 115:1639-50.

Goodson HV, Skube SB, Stalder R, Valetti C, Kreis TE, Morrison EE, Schroer TA 2003. CLIP-170 interacts with dynactin complex and the APC-binding protein EB1 by different mechanisms. Cell Motil. Cytoskeleton.

Grafstein B 1967 Transport of protein by goldfish optic nerve fibers. Science 157:196-198

Griffis ER, Stuurman N, Vale RD 2007. Spindly, a novel protein essential for silencing the spindle assembly checkpoint, recruits dynein to the kinetochore. J. Cell Biol. 177:1005–1015

Gundersen GG, Khawaja S, Bulinski JC 1987. Postpolymerization detyrosination of α-tubulin: a mechanism for subcellular differentiation of microtubules. *J. Cell Biol.* 105, 251–264

Hackney, D.D., and M.F. Stock. 2000. Kinesin's IAK tail domain inhibits initial microtubule-stimulated ADP release. Nat Cell Biol. 2:257-260.

Hafezparast M, et al. 2003. Mutations in dynein link motor neuron degeneration to defects in retrograde transport. Science 300:808-812.

Hammesfahr B, Kollmar M 2012. Evolution of the eukaryotic dynactin complex, the activator of cytoplasmic dynein. BMC Evol. Biol. 12, 95

Hancock WO 2014. Bidirectional cargo transport: moving beyond tug of war. Nat. Rev. Mol. Cell Biol. *9*, 615–628.

Hayashi I, Plevin MJ, Ikura M 2007. CLIP-170 autoinhibition mimics intermolecular interactions with $p150^{Glued}$ or EB1. Nat. Struct. Mol. Biol. 10, 980-981.

Hammond JW, Huang CF, Kaech S, Jacobson C, Banker G, Verhey KJ
2010. Posttranslational modifications of tubulin and the polarized transport of kinesin-1 in neurons. Mol Biol Cell 21:572–583

Heidemann SR, Landers JM, Hamborg MA 1981 Polarity orientation of axonal microtubules. J Cell Biol.91:661–665

Hendricks AG, Holzbaur ELF, Goldman YE 2012. Force measurements on cargoes in living cells reveal collective dynamics of microtubule motors. Proc. Natl. Acad. Sci. USA 109, 18447–18452.

Holleran EA, Tokito MK, Karki S, Holzbaur EL 1996. Centractin (ARP1) associates with spectrin revealing a potential mechanism to link dynactin to intracellular organelles. J Cell Biol 135:1815-1829.

Holleran EA, Ligon LA, Tokito M, Stankewich MC, Morrow JS, Holzbaur EL 2001. beta III spectrin binds to the Arp1 subunit of dynactin. J Biol Chem 276:36598-36605.

Honnappa S, Gouveia SM, Weisbrich A, Damberger FF, Bhavesh NS,
Jawhari H, Grigoriev I, van Rijssel FJ, Buey RM, Lawera A, et al. 2009. An EB1-binding motif acts as a microtubule tip localization signal. Cell 138:366–376.

Hoogenraad CC, Akhmanova A, Howell SA, Dortland BR, De Zeeuw CI,
Willemsen R, Visser P, Grosveld F, Galjart N 2001. Mammalian Golgi-associated Bicaudal-D2 functions in the dynein-dynactin pathway by interacting with these complexes. EMBO J 20:4041–4054

Hoogenraad CC, Wulf P, Schiefermeier N, Stepanova T, Galjart N, Small JV,Grosveld F, de Zeeuw CI, Akhmanova A 2003. Bicaudal D induces selective dynein-mediated microtubule minus end-directed transport. EMBO J22:6004–6015

Horgan CP, Hanscom SR, Jolly RS, Futter CE, McCaffrey MW 2010. Rab11-FIP3 links the Rab11 GTPase and cytoplasmic dynein to mediate transport to the endosomal-recycling compartment. J Cell Sci.123:181–191

Hirokawa N, Pfister KK, Yorifuji H, Wagner MC, Brady ST, and Bloom GS 1989. Submolecular domains of bovine brain kinesin identified by electron microscopy and monoclonal antibody decoration. Cell. 56:867-878.

Hirokawa N, Noda Y, Tanaka Y, and Niwa S 2009. Kinesin superfamily motor proteins and intracellular transport. Nat Rev Mol Cell Biol. 10:682-96.

Holt CE, Bullock SL 2009. Subcellular mRNA localization in animal cells and why it matters. Science. 326(5957):1212–1216.

Horio T, Hotani H 1986. Visualization of the dynamic instability of individualmicrotubules by dark-field microscopy. Nature 321:605-7.

Hubbert C, Guardiola A, Shao R, Kawaguchi Y, Ito A, Nixon A, Yoshida M, Wang X-F, Yao T-P 2002. HDAC6 is a microtubule-associated deacetylase. Nature. 417:455–458.

Huang CF, Banker G 2012. The Translocation selectivity of the kinesins that mediate neuronal organelle transport. Traffic 13:549–564.

Huang J, Roberts AJ, Leschziner AE, Reck-peterson SL 2012. Lis1 acts as a "' Clutch '" between the ATPase and microtubule-binding domains of the dynein motor. Cell:975–986.

Hunter AW, Caplow M, Coy DL, Hancock WO, Diez S, Wordeman L, Howard J 2003. The kinesin-related protein MCAK is a microtubule depolymerase that forms an ATP-hydrolyzing complex at microtubule ends. Mol. Cell 11, 445-457.

Inoue S, Sato H 1967. Cell motility by labile association of molecules. J. Gen. Physiol. 50, S259–S292

Inoue S, Dan K 1951. Birefringence of the dividing cell. J. Morphol. 89:423–56

Jacobson C, Schnapp B, Banker GA 2006. A change in the selective translocation of the kinesin-1 motor domain marks the initial specification of the axon. Neuron 49:797–804.

Jamieson JD, Palade GE 1967a. Intracellular transport of secretory proteins in the pancreatic exocrine cell. II. Transport to condensing vacuoles and zymogen granules. J Cell Biol 34:597–615.

Jamieson JD, Palade GE 1967b. Intracellular Transport of Secretory Proteins in the Pancreatic Exocrine Cell. J Cell Biol 39:589–603.

Jamieson JD, Palade E 1968. Intracellular transport of secretory proteins in the pancreatic exocrine cell IV . Metabolic requirements assay for transport efficiency. J Cell Biol:589–603.

Janke C, Rogowski K, Wloga D, Regnard C, Kajava AV, Strub J-M, Temurak N, van Dijk J, Boucher D, van Dorsselaer A, et al. 2005. Tubulin polyglutamylase enzymes are members of the TTL domain protein family. Science. 308:1758–1762

Janke C, Kneussel M 2010. Tubulin post-translational modifications: Encoding functions on the neuronal microtubule cytoskeleton. Trends Neurosci 33:362–372.

Janke C 2014. The tubulin code: molecular components, readout mechanisms, and functions. J Cell Biol. 206:461–472

Jareb M, Banker G 1998. The polarized sorting of membrane proteins expressed in cultured hippocampal neurons using viral vectors. Neuron. 20:855–867.

Jenkins B, Decker H, Bentley M, Luisi J, Banker G 2012. A novel split kinesin assay identifies motor proteins that interact with distinct vesicle populations. J Cell Biol 198:749–761.

Jordens I, Fernandez-Borja M, Marsman M, Dusseljee S, Janssen L, Calafat J, Janssen H, Wubbolts R, Neefjes J. 2001. The Rab7 effector protein RILP controls lysosomal transport by inducing the recruitment of dynein-dynactin motors. Curr Biol. 11:1680-1685.

Kaan HY, Hackney DD, Kozielski F 2011. The structure of the kinesin-1 motor-tail complex reveals the mechanism of autoinhibition. Science. 333:883-885.

Kaech S, Banker G 2006. Culturing hippocampal neurons. Nat Protoc 1:2406–2415

Kanai Y, Okada Y, Tanaka Y, Harada A, Terada S, Hirokawa N 2000. KIF5C, a novel neuronal kinesin enriched in motor neurons. *J Neurosci*. 20:6374-6384.

Kapitein LC, Peterman EJ, Kwok BJ, Kim JH, Kapoor TM, Schmidt CF 2005. The bipolar mitotic kinesin Eg5 moves on both microtubules that it crosslinks Nature, 435, 114–118

Kapitein LC, Schlager MA, Kuijpers M, Wulf PS, van Spronsen M, MacKintosh FC, Hoogenraad CC 2010a. Mixed Microtubules Steer Dynein-Driven Cargo Transport into Dendrites. Curr Biol 20:290–299

Kapitein LC, Schlager MA, van der Zwan WA, Wulf PS, Keijzer N, Hoogenraad CC 2010b. Probing intracellular motor protein activity using an inducible cargo trafficking assay. Biophys. J. 99, 2143–2152.

Kardon JR, Reck-Peterson SL, Vale RD, R. D. 2009. Regulation of the processivity and intracellular localization of *Saccharomyces cerevisiae* dynein by dynactin. Proc. Natl Acad. Sci. USA 106, 5669–5674

Karki S, Holzbaur EL 1995. Affinity chromatography demonstrates a direct binding between cytoplasmic dynein and the dynactin complex. J Biol Chem 270:28806-28811.

Kashina AS, Baskin RJ, Cole DG, Wedaman KP, Saxton WM, Scholey JM 1996. A bipolar kinesin Nature, 379, 270–272

Kaul N, Soppina V, Verhey KJ 2014. Effects of α-tubulin K40 acetylation and detyrosination on kinesin-1 motility in a purified system. Biophys. J. 106:2636–2643

Kim H, Ling SC, Rogers GC, Kural C, Selvin PR, Rogers SL, Gelfand VI 2007. Microtubule binding by dynactin is required for microtubule organization but not cargo transport. J. Cell Biol. 176, 641-651.

King SJ, Schroer TA 2000. Dynactin increases the processivity of the cytoplasmic dynein motor. Nat. Cell Biol. 2, 20–24

King SJ, Brown CL, Maier KC, Quintyne NJ, Schroer TA, 2003. Analysis of the dynein-dynactin interaction in vitro and in vivo. Mol. Biol. Cell *14*, 5089-5097.

Kleele T, Marinković P, Williams PR, Stern S, Weigand EE, Engerer P, Naumann R, Hartmann J, Karl RM, Bradke F, Bishop D, Herms J, Konnerth A, Kerschensteiner M, Godinho L, Misgeld T 2014. An assay to image neuronal microtubule dynamics in mice. Nat Commun 5:4827

Kollman JM, Merdes A, Mourey L, Agard DA 2011. Microtubule nucleation by gamma-tubulin complexes. Nat. Rev. Mol. Cell Biol. 12, 709–721.

Kon T, Nishiura M, Ohkura R, Toyoshima YY, Sutoh K. 2004. Distinct functions of nucleotide-binding/hydrolysis sites in the four AAA modules of cytoplasmic dynein. Biochemistry. 43:11266-74.

Kon T, Imamula K, Roberts AJ, Ohkura R, Knight PJ, et al. 2009. Helix sliding in the stalk coiled coil of dynein couples ATPase and microtubule binding. Nat. Struct. Mol. Biol. 16:325-33

Kon T, Sutoh K, Kurisu G. 2011. X-ray structure of a functional full-length dynein motor domain. Nat. Struct. Mol. Biol. 18:638–42

Konishi Y, Setou M 2009. Tubulin tyrosination navigates the kinesin-1 motor domain to axons. Nat Neurosci 12:559–567.

Kreutzberg GW 1969. Neuronal dynamics and axonal flow. IV. Blockage of intra-axonal enzyme transport by colchicine. Proceedings of the National Academy of Sciences of the United States of America *62*, 722-728.

Lacroix B, van Dijk J, Gold ND, Guizetti J, Aldrian-Herrada G, Rogowski K, Gerlich DW, Janke C 2010. Tubulin polyglutamylation stimulates spastin-mediated microtubule severing. J. Cell Biol. 189:945–954

Lansbergen G, Komarova Y, Modesti M, Wyman, Hoogenraad CC, Goodson HV, R.P. Lemaitre RP, D.N. Drechsel DN, van Munster E, Gadella Jr TW., et al. 2004. Conformational changes in CLIP-170 regulate its binding to microtubules and dynactin localization. J. Cell Biol. 166:1003–1014.

Larcher, JC, Boucher D, Lazereg S, Gros F, Denoulet P 1996. Interaction of kinesin motor domains with α- and β-tubulin subunits at a tau-independent binding site. Regulation by polyglutamylation. *J. Biol. Chem.* 271, 22117–22124

Lawrence CJ, Dawe RK, Christie KR, Cleveland DW, Dawson SC, Endow SA, Goldstein LS, Goodson HV, N. Hirokawa, Howard J, Malmberg RL, McIntosh JR, Miki H, Mitchison TJ, Okada Y, Reddy AS, Saxton WM, Schliwa M, Scholey JM, Vale RD, Walczak CE, and Wordeman L 2004. A standardized kinesin nomenclature. Journal of Cell Biology. 167:19-22.

Le Marchand Y, Singh A, Assimacopoulos-Jeannet F, Orci L, Rouiller C, Jeanrenaud B 1973. A role for the microtubular system in the release of very low density lipoproteins by perfused mouse livers. J Biol Chem 248:6862–6870.

Levy JR, Sumner CJ, Caviston JP, Tokito MK, Ranganathan S, Ligon LA, Wallace KE, LaMonte BH, Harmison GG, Puls I, Fischbeck KH, Holzbaur EL (2006) A motor neuron disease-associated mutation in $p150^{Glued}$ perturbs dynactin function and induces protein aggregation. J Cell Biol 172:733-745.

L'Hernault SW, Rosenbaum JL 1985. Chlamydomonas alpha-tubulin is posttranslationally modified by acetylation on the epsilon-amino group of a lysine. Biochemistry. 24:473-8.

Li SH, Gutekunst CA, Hersch SM, Li XJ 1998. Interaction of huntingtinassociated protein with dynactin $p150^{Glued}$. J Neurosci 18:1261-1269.

Liao G, Gundersen GG 1998. Kinesin is a candidate for cross-bridging microtubules and intermediate filaments. Selective binding of kinesin to detyrosinated tubulin and vimentin.J. Biol. Chem. 273:9797–9803

Liot G, Zala D, Pla P, Mottet G, Piel M, Saudou F 2013. Mutant Huntingtin alters retrograde transport of TrkB receptors in striatal dendrites. J Neurosci 33:6298–6309
Lipka J, Kapitein LC, Jaworski J, Hoogenraad CC 2016. Microtubule-binding protein doublecortin-like kinase1 (DCLK1) guides kinesin-3-mediated cargo transport to dendrites. EMBO J 1:1–17.

Litman P, Barg J, Rindzooski L, Ginzburg I 1993. Subcellular Localization of Tau mRNA in Differentiating Neumnal Cell Cuhum: Implications for Neumnal Polarity. Neuron 10:627-638.

Lloyd TE et al. 2012. The $p150^{Glued}$ CAP-Gly domain regulates initiation of retrograde transport at synaptic termini. Neuron 74, 344–360

Lomakin, A. J. et al. 2009. CLIP-170-dependent capture of membrane organelles by microtubules initiates minus-end directed transport. Dev. Cell 17, 323–333

Lyle K, Kumar P, Wittmann T 2009a. SnapShot: Microtubule regulators I. Cell 136: 380.

Lyle K, Kumar P, Wittmann T 2009b. SnapShot: Microtubule regulators II. Cell 136: 566.

Maas C, Belgardt D, Lee HK, Heisler FF, Lappe-Siefke C, Magiera MM, van Dijk J, Hausrat TJ, Janke C, Kneussel M 2009. Synaptic activation modifies microtubules underlying transport of postsynaptic cargo. Proc. Natl. Acad. Sci. USA. 106:8731–8736

Mach JM, Lehmann R 1997. AnEgalitarian–BicaudalD complex is essential for oocyte specification and axis determination in Drosophila. Genes Dev. 11, 423–435

Maday S, Twelvetrees AE, Moughamian AJ, Holzbaur ELF 2014. Axonal Transport: Cargo-Specific Mechanisms of Motility and Regulation. Neuron 84:292–309

Mallik R, Carter BC, Lex SA, King SJ, Gross SP. 2004. Cytoplasmic dynein functions as a gear in response to load. Nature 427:649–52

Mallik R, Petrov D, Lex SA, King SJ, Gross SP 2005. Building complexity: an in vitro study of cytoplasmic dynein with in vivo implications. Curr. Biol. 15, 2075–2085

Mallik R, Rai AK, Barak P, Rai A, Kunwar A 2013. Teamwork in microtubule motors. Trends Cell Biol. 23, 575–582

Margolis RL, Wilson L 1981. Microtubule treadmills--possible molecular machinery. Nature 293, 705-711.

Matanis T, Akhmanova A, Wulf P, Del Nery E, Weide T, Stepanova T, Galjart N, Grosveld F, Goud B, De Zeeuw CI, et al. 2002. Bicaudal-D regulates COPI-independent Golgi-ER transport by recruiting the dynein-dynactin motor complex. Nat Cell Biol. 4:986–992.

Matter K, Mellman I 1994. Mechanisms of cell polarity: sorting and transport in epithelial cells. Curr. Opin. Cell Biol. 6:545–554

Matus A, Bernhardt R, Hugh-Jones T 1981. High molecular weight microtubule associated proteins are preferentially associated with dendritic micro tubules in brain. Proc. Natl. Acad. Sci. USA 78:3010-14

Maurer SP, Fourniol FJ, Bohner Gergő, Moores CA, Surrey T. EBs recognize a nucleotide dependent structural cap at growing microtubule ends. Cell. 2012;149:371–382

McKenney RJ, Huynh W, Tanenbaum ME, Bhabha G, Vale RD 2014. Activation of cytoplasmic dynein motility by dynactin-cargo adapter complexes. Science 345:337–41

Miani N 1960. Proximo-distal movement along the axon of protein synthesized in the perikaryon of regenerating neurons. Nature London 189: 541
Mellman I, Nelson WJ 2008. Coordinated protein sorting, targeting and distribution in polarized cells. Nat Rev Mol Cell Biol. 9:833–845

Mitchison T, Kirschner M 1984. Dynamic instability of microtubule growth. Nature 312:237-42.
Mitchison TJ 1993. Localization of an exchangeable GTP binding site at the plus end of microtubules. Science. 261:1044-7.

Mohler J, Wieschaus EF 1986. Dominant maternal-effect mutations of *Drosophila melanogaster* causing the production of double-abdomen embryos. Genetics 112:803–22

Moore JK., Sept D, Cooper JA 2009. Neurodegeneration mutations in dynactin impair dynein-dependent nuclear migration. Proc. Natl Acad. Sci. USA 106, 5147–5152

Moughamian AJ, Holzbaur ELF 2012. Dynactin is required for transport initiation from the distal axon. Neuron 74, 331–343

Nakata T, Hirokawa N 2003. Microtubules provide directional cues for polarized axonal transport through interaction with kinesin motor head. J Cell Biol 162:1045–1055.

Neuwald AF, Aravind L, Spouge JL, Koonin EV 1999. AAA+: A class of chaperone-like ATPases associated with the assembly, operation, and disassembly of protein complexes. Genome research 9, 27-43.

Nicholas MP,Hook P, Brenner S, Wynne CL, Vallee RB, Gennerich A. 2015b. Control of cytoplasmic dynein force production and processivity by its C-terminal domain. Nat. Commun. 6:6206

Niemierko S, Lubinska L 1967. Two fractions of axonal acetylcholinesterase exhibiting different behavior in severed nerves. J. Neurochem. 14: 761-769.

Nirschl JJ, Magiera MM, Lazarus JE, Janke C, Holzbaur ELF 2016. Tubulin tyrosination and CLIP-170 phosphorylation regulate the initiation of dynein-driven transport in neurons (In Press)

Nogales E, Wolf SG, Downing KH 1998. Structure of the αβ tubulin dimer by electron crystallography. Nature 391, 199–203

North BJ, Marshal BL, Borra MT, Denu JM, Verdin E 2003. The human Sir2 ortholog, SIRT2, is an NAD^+-dependent tubulin deacetylase. *Mol. Cell* 11, 437–444

O'Brien ET, Salmon ED, Walker RA, Erickson HP. 1990. Effects of magnesium on the dynamic instability of individual microtubules. *Biochemistry* 29:6648–56

Okada Y, Hirokawa N (1999) A processive single-headed motor: kinesin superfamily protein KIF1A. Science 283:1152–1157.

Okada Y, Yamazaki H, Sekine-Aizawa Y, Hirokawa N (1995) The neuron-specific kinesin superfamily protein KIF1A is a unique monomeric motor for anterograde axonal transport of synaptic vesicle precursors. Cell 81:769–780.

Okazaki K, Holtzer H 1965. An analysis of myogenesis in vitro using fluorescein-labeled antimyosin. J Histochem Cytochem. 13(8):726–739

Olmsted JB 1986. Microtubule-associated proteins. *Annual Review of Cell Biology*. 2:421-57.

Ori-McKenney KM, Valle RB 2011. Neuronal migration defects in the Loa dynein mutant mouse. Neural Dev 6:26

Palade G 1975. Intracellular aspects of the process of protein synthesis. Science. 189:347–358.

Paturle-Lafanechère L, Eddé B, Denoulet P, Van Dorsselaer A, Mazarguil H, Le Caer JP, Wehland J, Job D 1991. Characterization of a major brain tubulin variant which cannot be tyrosinated. Biochemistry. 30:10523–10528. doi:10.1021/bi00107a022

Paschal BM, Shpetner HS, Vallee RB 1987. MAP 1C is a microtubule-activated ATPase which translocates microtubules in vitro and has dynein-like properties. Journal of Cell Biology. 105:1273-82.

Paschal BM, Vallee RB 1987. Retrograde transport by the microtubule-associated protein MAP 1C. Nature. 330:181-3.

Pearse BM 1976. Clathrin: A unique protein associated with intracellular transfer of membrane by coated vesicles. ProcNatl Acad Sci USA 73:1255–1259

Perez F, Diamantopoulos GS, Stalder R, Kreis TE 1999. CLIP‐170 highlights growing microtubule ends *in vivo*. Cell 96, 517–527

Peris L, Thery M, Fauré J, Saoudi Y, Lafanechère L, Chilton JK, Gordon-Weeks P, Galjart N, Bornens M, Wordeman L, Andrieux A 2006. Tubulin tyrosination is a major factor affecting the recruitment of CAP-Gly proteins at microtubule plus ends. J. Cell Biol.174:839–849.

Peris L, Wagenbach M, Lafanechère L, Brocard J, Moore AT, Kozielski F, Job D, Wordeman L, Andrieux A 2009. Motor-dependent microtubule disassembly driven by tubulin tyrosination. J. Cell Biol. 185:1159–1166.

Petersen JD, Kaech S, Banker G 2014. Selective Microtubule-Based Transport of Dendritic Membrane Proteins Arises in Concert with Axon Specification. J Neurosci 34:4135–4147

Poirier K, et al. 2013. Mutations in TUBG1, DYNC1H1, KIF5C and KIF2A cause malformations of cortical development and microcephaly. Nat. Genet. 45, 639–647

Pryer NK, Walker RA, Skeen VP, Bourns BD, Soboeiro MF, Salmon ED. 1992. Brain microtubule-associated proteins modulate microtubule dynamic instability in vitro. Real-time observations using video microscopy. J. Cell Sci. 103:965–76

Puls, I. et al. 2003. Mutant dynactin in motor neuron disease. Nat. Genet. 33, 455–456

Qiang L, Yu W, Andreadis A, Luo M, Baas PW 2006. Tau protects microtubules in the axon from severing by katanin. J. Neurosci. 26, 3120–3129

QiuW, Derr ND, Goodman BS, Villa E, Wu D, et al. 2012. Dynein achieves processive motion using both stochastic and coordinated stepping. Nat. Struct. Mol. Biol. 19:193–200

Quintyne NJ, Gill SR, Eckley DM, Crego CL, Compton DA, Schroer TA. 1999. Dynactin is required for microtubule anchoring at fibroblast centrosomes. J. Cell Biol. 147:321 334.

Rai AK, Rai A, Ramaiya AJ, Jha R, Mallik R 2013. Molecular adaptations allow dynein to generate large collective forces inside cells. Cell *152*, 172–182.

Raybin D, Flavin M 1977. Enzyme which specifically adds tyrosine to the α chain of tubulin. *Biochemistry* 16, 2189–2194

Reck-Peterson SL, Yildiz A, Carter AP, Gennerich A, Zhang N, Vale RD. 2006. Single-molecule analysis of dynein processivity and stepping behavior. Cell 126:335–48

Redeker V, Levilliers N, Schmitter JM, Le Caer JP, Rossier J, Adoutte A, Bré MH 1994. Polyglycylation of tubulin: a posttranslational modification in axonemal microtubules. Science.266:1688–1691

Reed NA, Cai D, Blasius TL, Jih GT, Meyhofer E, Gaertig J, Verhey KJ 2006. Microtubule Acetylation Promotes Kinesin-1 Binding and Transport. Curr Biol 16:2166–2172.

Ross JL,Wallace K, ShumanH,Goldman YE,Holzbaur EL. 2006. Processive bidirectionalmotion of dynein-dynactin complexes in vitro. Nat. Cell Biol. 8:562–70

Ross JL, Dixit R 2010. Multiple color single molecule TIRF imaging and tracking of MAPs and motors. Methods. Cell Biol. 95, 521–542

Robinson MS, Sahlender DA, Foster SD 2010. Rapid Inactivation of Proteins by Rapamycin-Induced Rerouting to Mitochondria. Dev Cell 18:324–331

Romé P, Montembault E, Franck N, Pascal A, Glover DM, Giet R 2010. Aurora A contributes to $p150^{Glued}$ phosphorylation and function during mitosis. J. Cell Biol.189:651–659

Rogowski K, van Dijk J, Magiera MM, Bosc C, Deloulme J-C, Bosson A, Peris L, Gold ND, Lacroix B, Bosch Grau M, et al. 2010. A family of protein-deglutamylating enzymes associated with neurodegeneration. Cell. 143:564–578

Rothman J 1994. Mechanisms of intracellular protein transport. Nature 372:55–63.

Sabatini DD, Bensch K, Barrnett RJ. 1963. Cytochemistry and electron microscopy. The preservation of cellular ultrastructure and enzymatic activity by aldehyde fixation. J. Cell Biol. 17:19–58

Schafer DA, Gill SR, Cooper JA, Heuser JE, Schroer TA. 1994. Ultrastructural analysis of the dynactin complex: an actin-related protein is a component of a filament that resembles F-actin. *Journal of Cell Biology*. 126:403-12.

Schiavo G, Greensmith L, Hafezparast M, Fisher EM 2013. Cytoplasmic dynein heavy chain: the servant of many masters. Trends Neurosci 36:641–651

Schindelin J, Arganda-Carreras I, Frise E, Kaynig V, Longair M, Pietzsch T, Preibisch S, Rueden C, Saalfeld S, Schmid B, Tinevez J-Y, White DJ, Hartenstein V, Eliceiri K, Tomancak P, Cardona A 2012. Fiji: an open-source platform for biological-image analysis. Nat Methods 9:676–682

Schlager MA, Hoang HT, Urnavicius L, Bullock SL, Carter AP. 2014. *In vitro* reconstitution of a highly processive recombinant human dynein complex. EMBO J. 33:1855–68

Schmidt H, Gleave ES, Carter AP. 2012. Insights into dynein motor domain function from a 3.3-A° crystal structure. *Nat. Struct. Mol. Biol.* 19:492–97

Schnitzer MJ, Block SM 1997. Kinesin hydrolyses one ATP per 8-nm step. Nature. 388:386-90.

Schroeder HW, 3rd, Mitchell C, Shuman H, Holzbaur ELF, Goldman YE 2010. Motor number controls cargo switching at actin-microtubule intersections in vitro. Current biology 20, 687-696.

Schroer TA, Sheetz MP 1991. Two activators of microtubule-based vesicle transport. *Journal of Cell Biology*. 115:1309-18.

Schroer TA 2004. Dynactin. Annu Rev Cell Dev Biol 20:759-779.

Schröder HC, Wehland J, Weber K 1985. Purification of brain tubulin-tyrosine ligase by biochemical and immunological methods. J. Cell Biol. 100, 276–281

Schulze E, Asai DJ, Bulinski JC, Kirschner M 1987. Posttranslational modification and microtubule stability. J Cell Biol 105:2167–2177.

Setou M, Nakagawa T, Seog DH, Hirokawa N 2000. Kinesin superfamily motor protein KIF17 and mLin-10 in NMDA receptor-containing vesicle transport. *Science* 288, 1796-1802

Setou M, Seog D-H, Tanaka Y, Kanai Y, Takei Y, Kawagishi M, Hirokawa N 2002. Glutamate-receptor-interacting protein GRIP1 directly steers kinesin to dendrites. Nature 417:83–87.

Sharma N, Bryant J, Wloga D, Donaldson R, Davis RC, Jerka-Dziadosz M, Gaertig J 2007. Katanin regulates dynamics of microtubules and biogenesis of motile cilia J. Cell Biol., 178, 1065–1079

Shelanski ML, Gaskin F, Cantor CR 1973. Assembly of micro tubules in the absence of added nucleotide. Proc. Natl. Acad. Sci. USA 70:765-68

Siglin AE, Sun S, Moore JK, Tan S, Poenie M, et al. 2013. Dynein and dynactin leverage their bivalent character to form a high-affinity interaction. PLOS ONE 8:e59453

Siller KH, Doe CQ 2009. Spindle orientation during asymmetric cell division. Nat Cell Biol. 11:365–374

Silverman MA, Kaech S, Jareb M, Burack MA, Vogt L, Sonderegger P, Banker G 2001. Sorting and directed transport of membrane proteins during development of hippocampal neurons in culture. Proc Natl Acad Sci U S A 98:7051–7057

Sirajuddin M, Rice LM, Vale RD 2014. Regulation of microtubule motors by tubulin isotypes and post-translational modifications. Nat. Cell Biol. 16:335–344.

Sloboda RD, Rudolph SA, Rosenbaum JL, Greengard P 1975. Cyclic AMP-dependent endogenous phosphorylation of a microtubule-associated protein. Proc. Natl. A cad. Sci. USA 72:177-81

Song AH, Wang D, Chen G, Li Y, Luo J, Duan S, PooMM 2009. A selective filter for cytoplasmic transport at the axon initial segment. Cell 136:1148–1160.

Song Y, Kirkpatrick LL, Schilling AB, Helseth DL, Chabot N, Keillor JW, Johnson GVW, Brady ST 2013. Transglutaminase and polyamination of tubulin: posttranslational modification for stabilizing axonal microtubules. Neuron. 78:109-123

Soppina V, Norris SR, Dizaji AS, Kortus M, Veatch S, Peckham M, Verhey KJ (2014) Dimerization of mammalian kinesin-3 motors results in superprocessive motion. Proc Natl Acad Sci U S A 111:5562–5567

Spiegelman BM, Penningroth SM, Kirschner MW. 1977. Turnover of tubulin and the N site GTP in Chinese hamster ovary cells. Cell 12:587–600

SplinterD, RazafskyDS, Schlager MA, Serra-Marques A,Grigoriev I, et al. 2012. BICD2, dynactin, and LIS1 cooperate in regulating dynein recruitment to cellular structures. Mol. Biol. Cell 23:4226–41

Stepanova T et al. 2003.Visualization of microtubule growth in cultured neurons via the use of EB3-GFP (end-binding protein 3-green fluorescent protein). J Neurosci 23:2655–2664.

Stoc MF, Guerrero J, Cobb B, Eggers CT, Huang TG, Li X, Hackney DD 1999. Formation of the compact confomer of kinesin requires a COOH terminal heavy chain domain and inhibits microtubule-stimulated ATPase activity. J Biol Chem. 274:14617-14623.

Stowell JN, Craig AM 1999. Axon/dendrite targeting of metabotropic glutamate receptors by their cytoplasmic carboxy terminal domains Neuron, 22, 525–536

Strickland D, Lin Y, Wagner E, Hope CM, Zayner J, Antoniou C, Sosnick TR, Weiss EL, Glotzer M 2012. TULIPs: tunable, light-controlled interacting protein tags for cell biology. Nat. Methods 9, 379–384.

Su LK, Burrell M, Hill DE, Gyuris J, Brent R, Wiltshire R, Trent J, Vogelstein B, Kinzler KW 1995. APC binds to the novel protein EB1. Cancer Res 55:2972–2977

Sun F, Zhu C, Dixit R, Cavalli V 2011. Sunday Driver/JIP3 binds kinesin heavy chain directly and enhances its motility. EMBO J. 30, 3416–3429

Svoboda K, Schmidt CF, Schnapp BJ, Block SM 1993. Direct observation of kinesin stepping by optical trapping interferometry. Nature. 365:721-7.

Szyk A, Piszczek G, Roll-Mecak A 2013. Tubulin tyrosine ligase and stathmin compete for tubulin binding in vitro. J. Mol. Biol. 425:2412–2414

Tilney LG, Bryan J, Bush DJ, Fujiwara K, Mooseker MS, Murphy DB, Snyder DH 1973. Microtubules: evidence for 13 protofilaments. Journal of Cell Biology 59:267-75.
Tokito MK, Holzbaur EL 1998. The genomic structure of DCTN1, a candidate gene for limb-girdle muscular dystrophy (LGMD2B). Biochim Biophys Acta 1442:432-436.

Tokito MK, Howland DS, Lee VM, Holzbaur EL 1996. Functionally distinct isoforms of dynactin are expressed in human neurons. Mol Biol Cell 7:1167-1180.

Tomishige M, Klopfenstein DR, Vale RD (2002) Conversion of Unc104/KIF1A kinesin into a processive motor after dimerization. Science 297:2263–2267.
Torisawa T, Ichikawa M, Furuta A, Saito K, Oiwa K, et al. 2014. Autoinhibition and cooperative activation mechanisms of cytoplasmic dynein. Nat. Cell Biol. 16:1118–24

Tripathy SK,Weil SJ, Chen C, Anand P, Vallee RB, Gross SP 2014. Autoregulatory mechanism for dynactin control of processive and diffusive dynein transport. Nat. Cell Biol. 16:1192–201

Ullrich O, Reinsch S, Urbé S, Zerial M, Parton RG 1996. Rab11 regulates recycling through the pericentriolar recycling endosome J. Cell Biol., 135, 913–924

Urnavicius L, Zhang K, Diamant AG, Motz C, Schlager MA, et al. 2015. The structure of the dynactin complex and its interaction with dynein. *Science* 347:1441–46

Vale RD, Reese TS, and Sheetz MP 1985a. Identification of a novel force-generating protein, kinesin, involved in microtubule-based motility. Cell. 42:39-50.

Vale RD, Schnapp BJ, Reese TS, and Sheetz MP 1985b. Movement of organelles along filaments dissociated from the axoplasm of the squid giant axon. Cell. 40:449-54.

Vale RD, Schnapp BJ, Reese TS, and Sheetz MP 1985c. Organelle, bead, and microtubule translocations promoted by soluble factors from the squid giant axon. Cell. 40:559-69.

Vale RD, Milligan RD 2000. The way things move: looking under the hood of molecular motors. Science 288: 88-95

Vallee R 1982. A taxol-dependent procedure for the isolation of microtubules and microtubule-associated proteins (MAPs) J. Cell BioI. 92:435-42

Vallee RB, Wall JS, Paschal BM, Shpetner HS 1988. Microtubule-associated protein 1C from brain is a two-headed cytosolic dynein. Nature *332*, 561-563.

Vallee RB, Seale GE Tsai JW 2009. Emerging roles for myosin II and cytoplasmic dynein in migrating neurons and growth cones. *Trends Cell Biol.* 19, 347–355 (2009).

van Bergeijk P, Adrian M, Hoogenraad CC, Kapitein LC 2015. Optogenetic control of organelle transport and positioning. Nature 518, 111–114.

van Spronsen M, Mikhaylova M, Lipka J, Schlager MA, van den Heuvel DJ, Kuijpers M, Wulf PS, Keijzer N, Demmers J, Kapitein LC, Jaarsma D, Gerritsen HC, Akhmanova A, Hoogenraad CC 2013. TRAK/Milton Motor-Adaptor Proteins Steer Mitochondrial Trafficking to Axons and Dendrites. Neuron 77:485–502.

Vaughan KT, Vallee RB 1995. Cytoplasmic dynein binds dynactin through a direct interaction between the intermediate chains and p150Glued. J Cell Biol 131:1507-1516

Vaughan KT, Tynan SH, Faulkner NE, Echeverri CJ, Vallee RB 1999. Colocalization of cytoplasmic dynein with dynactin and CLIP-170 at microtubule distal ends. J. Cell Sci. 112:1437–1447.

Vaughan PS, Miura P, Henderson M, Byrne B, Vaughan KT 2002. A role for regulated binding of $p150^{Glued}$ to microtubule plus ends in organelle transport. J. Cell Biol. 158:305–319

Verhey KJ, Meyer D, Deehan R, Blenis J, Schnapp BJ, Rapoport TA, Margolis B. 2001. Cargo of kinesin identified as JIP scaffolding proteins and associated signaling molecules. J Cell Biol. 152:959-970.

Verhey KJ, Hammond JW 2009. Traffic control: regulation of kinesin motors. Nat. Rev. Mol. Cell Biol. 10, 765–777

Visscher K, Schnitzer MJ, Block SM1999. Single kinesin molecules studied with a molecular force clamp. Nature 400, 184-189.

Vissers LELM, et al. 2010. A de novo paradigm for mental retardation. Nat. Genet. 42, 1109–1112

Walker RA, O'Brien ET, Pryer NK, Soboeiro MF, Voter WA, Erickson HP, and Salmon ED 1988. Dynamic instability of individual microtubules analyzed by video light microscopy: rate constants and transition frequencies. J. Cell Biol. 107, 1437-1448.

Walter WJ, Beránek V, Fischermeier E, Diez S 2012. Tubulin acetylation alone does not affect kinesin-1 velocity and run length in vitro. PLoS ONE. 7:e42218 10.1371

Waterman-Storer CM, Karki S, Holzbaur EL 1995. The $p150^{Glued}$ component of the dynactin complex binds to both microtubules and the actin-related protein centractin (Arp-1). Proc Natl Acad Sci U S A 92:1634-1638

Watson P, Stephens DJ. 2006. Microtubule plus-end loading of p150^{Glued} is mediated by EB1 and CLIP-170 but is not required for intracellular membrane traffic in mammalian cells. J. Cell Sci. 119:2758–276

Weingarten M, Lockwood A, Hwo S, Kirschner M 1975. A protein factor essential for microtubule assembly. Proc. Natl. Acad. Sci. USA 72:18 58-62

Weisbrich A, Honnappa S, Jaussi R, Okhrimenko O, Frey D, Jelesarov I, Akhmanova A, Steinmetz MO 2007. Structure-function relationship of CAP-Gly domains. Nat. Struct. Mol. Biol.14:959–967

Weisenberg RC, Borisy GG, Taylor EW. 1968. The colchicine-binding protein of mammalian brain and its relation to microtubules. Biochemistry 7:4466–79

Weisenberg R 1972. Microtubule formation in vitro in solutions containing low calcium concentrations. Science 177:1104-5

Weiss P, Hiscoe HB 1948 Experiments on the mechanism of nerve growth. J Exp Zool 107:315-395.

West AE, Neve RL, Buckley KM 1997. Identification of a somatodendritic targeting signal in the cytoplasmic domain of the transferrin receptor J. Neurosci, 17, 6038–6047

Wickstead B, and K. Gull. 2007. Dyneins across eukaryotes: a comparative genomic analysis. Traffic. 8:1708-21.

Wilcox KS, Buchhalter J, Dichter MA 1994. Properties of inhibitory and excitatory synapses between hippocampal neurons in very low density cultures. Synapse 18:128–151.

Williams JA, Wolff J 1972. Colchicine-binding protein and the secretion of thyroid hormone. J. Cell Biol. 54: 157-165.

Witte H, Neukirchen D, Bradke F 2008. Microtubule stabilization specifies initial neuronal polarization. J. Cell Biol. *180*, 619–632.

Wong M, Munro S 2014. Membrane trafficking. The specificity of vesicle traffic to the Golgi is encoded in the golgin coiled-coil proteins. Science 346:125689

Yadav S, Linstedt AD 2011.Golgi positioning. Cold Spring Harb. Perspect. Biol. 3:a005322. 10.1101/cshperspect.a005322

Yildiz A, Tomishige M, Vale RD, Selvin PR 2004. Kinesin walks hand-over-hand Science, 303, 676–678

Zhang J, Qiu R, Arst HN Jr, Penalva MA, Xiang X. 2014. HookA is a novel dynein–early endosome linker critical for cargo movement in vivo. J. Cell Biol. 204:1009–26